Christina Rong Anfinsen

Experimental Investigation of Pressure Versus Rate Correlation for Two Phase Flow in Bead Packs

Master's thesis in Petroleum Geosciences and Engineering
Supervisor: Carl Fredrik Berg
July 2019

Master's thesis

NTNU
Norwegian University of Science and Technology
Faculty of Engineering
Department of Geoscience and Petroleum

NTNU
Norwegian University of
Science and Technology

Christina Rong Anfinsen

Experimental Investigation of Pressure Versus Rate Correlation for Two Phase Flow in Bead Packs

Master's thesis in Petroleum Geosciences and Engineering
Supervisor: Carl Fredrik Berg
July 2019

Norwegian University of Science and Technology
Faculty of Engineering
Department of Geoscience and Petroleum

NTNU
Norwegian University of
Science and Technology

Abstract

This thesis will present an experimental study of simultaneous two-phase flow, of immiscible fluids, in a three- dimensional porous medium. The scaling relation between the volumetric flow rate, Q, and the differential pressure, ΔP, is investigated during steady-state flow. The objective of this thesis is to identify one or more flow regimes, in addition to studying the transition between these regimes.

The experimental set up consists of two pumps, each pumping their respective fluid through a porous medium. The three-dimensional porous medium is a bead pack made up of glass beads in a glass tube, and the two immiscible fluids that are pumped through the bead pack, are distilled water and oil (EXXSOL D60). Flow rates were run in the range from 0.005 ml/min to 10 ml/min, and the corresponding steady-state differential pressure over the bead pack, was measured for each run. To identify different flow regimes, in addition to identifying the transition point between them, the scaling relation between the volumetric flow rate and the differential pressure. This is done by plotting the pressure drop is against the capillary number. The scaling coefficient, β, can be found from the relation $\Delta P \sim Ca^{\beta}$.

The results of this thesis are conflicting. Some results indicate two different regimes, one linear regime for the higher flow rates, and one regime that deviates from the linear trend. The non-linear regime is found at low flow rates, where capillary forces need to be accounted for. The transition between the two regimes is found at capillary number; $Ca \simeq 2 \times 10^{-5}$. Other results indicate only one linear regime. For the results indicating two different regimes, a threshold pressure, P_t, of $408.33Pa$ can be identified. The physical explanation as to why this threshold pressure and deviation from Darcy occur is discussed, but no conclusions can be drawn from this thesis. However, after accounting for this threshold pressure and investigating the relation $\Delta P - P_t \sim Ca^{\beta}$, only one flow regime was found. This regime is linear, with a scaling coefficient of $\beta \sim 1$. The results are compared to, and found to contradict, the results of a similar experiment by Sinha et al. (2017).

Keywords: Two-phase flow, porous material, steady-state, experiment.

Sammendrag

Denne masteroppgaven presenterer en eksperimentell studie av tofase-strømning, av ublandbare væsker, i et tre-dimensjonalt porøst medium. Når systemt har oppnadd likevekt undersøkes skaleringsforholdet mellom den volumetriske strømningshastigheten, Q, og differensialtrykket, ΔP. Målet med denne oppgaven er å identifisere en eller flere strømningsregimer, i tillegg til å undersøke overgangen mellom disse regimene.

Det eksperimentelle oppsett bestr av to pumper, som hver pumper deres respektive fluid gjennom et porøst medium. Det tredimensjonale porøse medium er en kulepakning bestående av glassperler i et glassrør, og de to ikke-blandbare væskene som pumpes gjennom kulepakningen, er destillert vann og olje (EXXSOL D60). Trykktapet over kulepakningen ble målt for strømningsrater i omrdet fra 0,005 ml/min til 10 ml/min. For å identifisere skaleringsforholdet mellom den volumetriske strømningshastigheten og differensialtrykket, er trykkfallet plottet mot kapillærtallet. Skalekoeffisienten, β, identifiseres fra sammenhengen $\Delta P \sim Ca^{\beta}$. Dette skaleringsforholdet brukes til å identifisere forskjellige strømningsregimer, i tillegg til å identifisere overgangspunktet mellom dem.

Resultatene fra denne masteroppgaven er motstridende. Noen resultater indikerer to forskjellige regimer, ett lineært regime for de øyere strømningshastighetene, og ett regime som avviker fra den lineære trenden. Det ikke-lineære regimet er funnet ved lave strømningshastigheter, hvor kapillære krefter må tas høyde for. Overgangen mellom de to regimene er funnet ved kapillærtallet; $Ca = 2 \times 10^{-5}$. Andre resultater indikerer bare ett lineært regime med skaleringskoeffisienten; $\beta \sim 1$. For resultatene som indikerer to forskjellige regimer identifiseres et terskeltrykk, P_t, på $408.33Pa$. Den fysiske forklaringen til hvorfor dette terskeltrykket og avviket fra Darcys ligning forekommer diskuteres, men det kan ikke trekkes konklusjoner fra resultatene fra denne masteroppgaven. Om terskeltrykket tas høyde for ved å undersøke forholdet $\Delta P - P_t \sim Ca^{\beta}$, kan bare ett strømningsregime identifiseres. Dette regimet er lineært, med en skaleringskoeffisienten $\beta \sim 1$. Resultatene er sammenlignet med, resultater fra et lignende eksperiment av Sinha et al. (2017). Resultatene i denne masteroppgaven stemmer ikke overens med hva Sinha et al. (2017) konkluderer med.

Nøkkelord: Tofasestrømning, porøst materiale, steady-state, eksperimentell studie.

Acknowledgements

This thesis was carried out at the Norwegian University of Science and Technology at the Department of Petroleum Engineering and Applied Geophysics. This thesis is written as a continuation of the specialization project submitted during the fall semester of 2018 (Anfinsen, 2018). Chapter 1-3 in this thesis will be partially identical to those same chapters in Anfinsen (2018). The thesis is submitted for the partial fulfillment of a Master Degree in Petroleum Engineering, specializing in Reservoir Engineering and Petrophysics, during the spring of 2019.

I would like to acknowledge my main supervisor Associate Professor Carl Fredrik Berg of the Department of Petroleum Engineering and Applied Geosciences (NTNU) for providing me with an interesting topic and for his guidance, advice and useful comments throughout the period of this study. I would also like to thank Roger Overå, Noralf Vedvik, and Steffen Wærnes Moen, for their assistance in helping with the experimental apparatus needed for this thesis.

Trondheim, July 2019.

Table of Contents

List of Tables

List of Figures

Nomenclature

Abbrevations

CMC	Critical micelle concentration
ID	Inner diameter
IFT	Interfacial tension
$LBP1$	Large bead pack 1
$LBP2$	Large bead pack 2
SBP	Small bead pack
SP	Single phase
TP	Two Phase

Symbols

β	Scaling coefficient
ΔP	Differential pressure/pressure drop
μ	Viscosity [Pas]
μ_i	Viscosity of the displacing fluid [Pas]
μ_o	Viscosity of the displaced fluid [Pas]
μ_p	Viscosity of phase *p* [Pas]
∇P	Pressure gradient
∇P_t	Differential pressure gradient
ϕ	Porosity [-]
ρ	Density [g/cm^3]
ρ_w	Density of water [g/cm^3]

σ	Interfacial tension $[N/m]$
A	Cross-sectional area of the flooded area $[m^2]$
Ca	Capillary number [-]
D	Inner diameter of bead pack
d	Diameter of glass beads
k	Permeability [m^2]
k_a	Absolute permeability [m^2]
k_{ri}	Relative permeability for the displacing fluid [-]
k_{ro}	Relative permeability for the displaced fluid [-]
k_{rp}	Relative permeability for phase *p* [-]
L	Length over which the pressure is measured $[m]$
L_b	Bubble diameter $[m]$
m	Mass $[g]$
m_w	Mass of water $[g]$
P_c	Capillary pressure $[Pa]$
P_t	Threshold pressure $[Pa]$
Q	Volumetric flow rate $[ml/min]$
q_o	Volumetric flow rate of oil $[ml/min]$
q_w	Volumetric flow rate of water $[ml/min]$
r_p	Pore body radius $[m]$
r_t	Throat radius $[m]$
Re	Reynolds number
Re_{min}	Minimum Reynolds Number for which Darcy's equation applies
S_p	Saturation of phase *p* in the system [-]
S_w	Water saturation [-]
S_{nw}	Non-wetting saturation [-]
S_{or}	Residual oil saturation [-]
S_{wi}	Irreducible water saturation [-]

V	Volume $[m^3]$
v	Fluid velocity $[m/s]$
V_w	Volume of water $[ml]$
V_{tot}	Volume of empty tube $[ml]$

Chapter 1

Introduction

Immiscible multiphase fluid flow in porous media play an essential role in many natural and commercial processes. This type of flow is found in a wide range of fields with both geophysical and other industrial applications (Bear, 2013). Most important for this thesis is the relevance of multiphase flow in oil reservoirs.

Over the last years, techniques for imaging and reconstructing the pore structure of porous media, like a petroleum reservoir, has developed tremendously. It is now possible to give detailed maps of the structure of porous media at the sub-pore level (Blunt et al., 2013). As a result, we know a lot about the pore structure, but on the topic of how fluids move within this porous medium, there are still unanswered questions. In the petroleum industry, Darcy's equation has traditionally been used to model fluid flow in the reservoir. To apply Darcy's law, a linear relationship between the pressure drop and the flow rate is assumed (Lage, 1998). This linear relationship exists for single-phase flow. However, simultaneous flow of two or more immiscible fluids through the same pore space creates a more complicated situation. Under certain conditions, Darcy's law cannot describe multiphase flow accurately, as the relation between the pressure drop and the flow rate has been found to deviate from the linear relation initially assumed (Xu and Wang, 2014). Thus, predicting the behavior of each fluid in multiphase flow, and their interactions at all time, gets complicated. One of the cases for which Darcy is not a good model for multiphase flow is flow at very low rates, where the relation between the pressure drop and the flow rate has been found to deviate from the linear trend (Sinha et al., 2013). This low-velocity flow is especially interesting now, in a time with extended focus on low permeability shale reservoirs, where production flow rates are low, and capillary forces are strong.

Because of its relevance to the oil industry, immiscible multiphase flow in porous media has been the subject of discussion and research for quite some time, but up until today the vast majority of work has focused on invasion processes. More specifically, the processes of either pure drainage or pure imbibition. These transient processes are found to give different displacement patterns and are further classified into capillary fingering, viscous fingering, and stable front displacement. These are non-stationary processes, and to understand them in a broader context there is a need to understand the stationary case which sets in after the initial instabilities such as viscous fingering are over in, e.g., flooding experiments. (Avraam and Payatakes, 1995) This stationary case is called steady-state, and it has received far less attention. Steady-state flow is in statistical equilibrium, although it is a dissipative process; an external energy input balances the internal energy loss to maintain the equilibrium. Thus, the average flow properties and distribution functions are invariant in time. Despite the importance of multiphase flow in porous media, there is limited pore scale experimental data available for such problems, and fundamental questions about the underlying mechanism

of multiphase fluid flow in porous media are still not adequately answered.

Recently, the relation between average volumetric flow and pressure drop across the system has been investigated both experimentally and theoretically (Tallakstad et al., 2009; Rassi et al., 2011; Sinha et al., 2017; Husøy, 2018). A way to study such flow in the laboratory is to inject the two immiscible fluids simultaneously into the porous medium. After the initial instabilities are overcome, the system reaches a state where clusters and bubbles break up and merge in such a way that the averages of macroscopic parameters remain constant, thus the system has reached a steady state regime (Tallakstad et al., 2009; Sinha et al., 2013). Numerical techniques to calculate the flow properties have also developed and branched over the years, and there are several approaches. The common goal for these techniques is to upscale the physics at the pore level to a description at scales where the porous medium may be seen as a continuum in search for better understanding of two-phase flow phenomena. This includes finding a scaling relationship between the flow rate and the pressure drop.

The current pore scale theory assumes incompressible fluids (Sinha et al., 2013). However, experimental studies have been conducted with air, which is highly compressible Sinha et al. (2017). Following Husøy (2018), this thesis will try to experimentally verify the theory by conducting the experiments using two nearly incompressible fluids, water and oil. As significant end effects were suspected in Husøy (2018) this thesis has aimed for an experimental setup minimizing the influence of end effects.

In this thesis, two-phase steady-state flow in a porous medium will be investigated experimentally. The objective is to find the relationship between the volumetric flow rate, Q, and the corresponding pressure drop, ΔP. A tube filled with glass beads makes up the porous medium, where two immiscible fluids, oil and water, will flow simultaneously. The corresponding steady state pressure drop will be measured. The main focus will be on steady-state multiphase flow at lower rates, where the object of this thesis will be to identify a transition to a lower flow regime. If this lower flow regime exists, a further goal of the thesis will be to find the scaling relationship between the volumetric flow rate and the pressure drop.

1.1 Structure of Thesis

The thesis will be structured as follows:

- Chapter 2 gives a presentation of the theory on which this project is based. The chapter also introduces numerical and experimental findings that will be compared to results from this thesis.
- Chapter 3 describes the experimental setup and procedure of the experiment.
- Chapter 4 presents the experimental results.
- Chapter 5 discusses the results presented in chapter 4. Potential sources of error will also be discussed.
- Chapter 6 makes concluding remarks based on the discussed results and presented theory. Alternative theories will also be presented.
- Chapter 7 makes recommendations on how to do further experimental research of the theory presented in chapter 2.

Chapter 2

Theory

To understand the phenomena of two-phase flow through porous media, knowledge of basic properties affecting the fluid flow is of great importance. Hence, in the following chapter, a closer investigation has been conducted on some of the fundamental properties. Related experimental studies on the topics will be presented.

2.1 Two Phase Steady State Flow

Fluid flow is often divided into two possible states of flow: single-phase flow, or multiphase flow, where several fluids flow simultaneously. When two immiscible fluids flow in a porous medium, at the macroscopic scale, the fluid flow is characterized by the relation between the flow rate, pressure drop, and fluid saturation. At the pore scale, the fluid flow is characterized by the competition of three main forces: the viscous-, capillary-, and gravitational forces (Aursjø et al., 2014; Odsæter et al., 2015). Steady-state two-phase flow is reached after initial instabilities such as viscous fingering, or invasion percolation has ended. Steady-state flow refers to the condition where the average fluid properties in the system do not change over time. For a two-phase fluid flow this means that clusters and bubbles might break up and merge, but in such a way that the averages of macroscopic parameters remain constant (Tallakstad et al., 2009). In this thesis, steady-state will be defined as the average flow variables being constant over time and can be identified when the average differential pressure is constant over a longer period of time, as illustrated in figure 2.1.

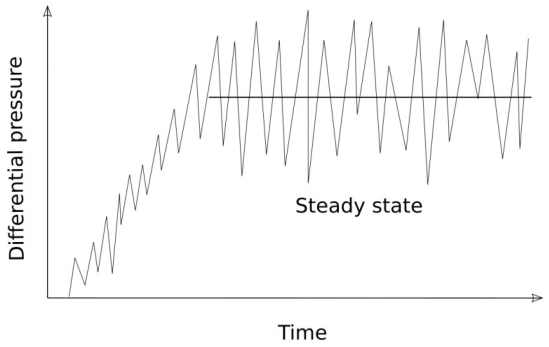

Figure 2.1: A sketch illustrating the behaviour of the differential pressure as it reaches steady state (Husøy, 2018).

The behavior and the travel pattern of the two fluids that enter the porous medium is a debated topic, and knowledge of the two-phase steady-state processes have a clear scientific value. Despite the key importance of steady-state two-phase flow, there are still large gaps in our understanding of it. To begin with, there is considerable confusion in the literature as to which system parameters besides the capillary number affect the flow and the relative permeabilities significantly, and in what way. These are parameters like viscosity ratio, flow-rate ratio, contact angle, dimensionless geometrical, and topological parameters. Such knowledge is limited, and much of the confusion in the available literature consists of which, and to what extent, different parameters have an impact on the two-phase steady state flow. Furthermore, there is a long-standing fundamental misconception concerning the nature of the flow itself, where it is assumed that the oil flows only through connected pathways, and that disconnected oil is stranded (Avraam and Payatakes, 1995)

2.1.1 Capillary Number

During steady-state flow, the processes of drainage and imbibition work simultaneously. Looking at the two processes separately will not sufficiently describe the combined process. As mentioned, there are mainly three competing forces that act during these processes. Gravity, viscous- and capillary forces. The viscous forces refer to both the viscous force of the invading fluid as well as that of the fluid being displaced. The capillary forces in the system are caused by the intermolecular forces between the two immiscible fluids (Bear, 2013; Lake et al., 1989). A variety of non-dimensional numbers can describe these forces. Most important for this thesis is the capillary number. Different expressions for capillary number can be found in literature. In this thesis, the following equation will be used:

$$Ca = \frac{\mu v}{\sigma} \tag{2.1}$$

where μ is the dynamic viscosity of the fluid, v is the velocity, and σ is the interfacial tension between the two fluid phases. This makes the capillary number the ratio of viscous forces to capillary forces. All parameters in this and subsequent equations can be found in the nomenclature on page xi.

2.1.2 Bond Number

To compare the importance of the gravitational forces to the capillary forces, the gravity number, also referred to as the Bond number, Bo, is introduced, and defined as:

$$Bo = \frac{\Delta\rho g L_b^2}{\sigma} \tag{2.2}$$

where $\Delta\rho$ is the difference in density of the two phases, g is the gravitational acceleration, L_b^2 L is the characteristic length, e.g., bubble diameter, and σ is the interfacial tension between the two fluid phases. Similar experiments as to what will be conducted in this thesis have shown that gravity will affect the fluid flow in a bead pack for given capillary numbers. Zhang et al. (2016) found that for $Bo > 0.1$ gravity cannot be neglected.

These two dimensionless numbers contribute to the characterization of whether the flow is gravity, capillary, or viscous dominated. These numbers alone will not completely characterize the fluid flow, because variations in the pore structure can lead to variations in the contribution from different forces.

2.1.3 Generalized Darcys Equation

An important pore structure descriptor is the permeability of the system. For permeability measurements, the steady state is reached when the pressure drop over the system no longer changes with time. From the flow rate and pressure, the permeability can be calculated by applying Darcy's law. Darcy's law relates the volumetric flow rate of a single fluid, Q, to the permeability, k, viscosity, μ, cross-sectional area of the porous medium, A, pressure gradient, ΔP, and the length over which the pressure is measured, L, as described in the following equation:

$$Q = \frac{-kA\Delta P}{\mu L} \tag{2.3}$$

This equation has been widely used in the oil and gas industry for a long time. Still, there are some limitations to its validity. Of relevance for this thesis is only the lower limit, Re_{min}, where Darcy's equation does not hold below this point. This flow is referred to as pre-Darcy flow. Bear (2013) states that the existence of pre-Darcy flow is attributed to non-Newtonian behavior of fluids and the fact that the streaming potential generated by the flow, particularly in fine-grained media, can produce small counter-currents along the pore walls in a direction opposite of the main flow. There is no available precise information concerning the magnitude of Re_{min}, but published data indicate that $Re_{min} < 10^{-5}$ (Fand et al., 1987). In this thesis data of this magnitude will not be included. Later, a "lower regime" will be introduced. This regime must not be mistaken for the pre-Darcy flow.

For the conditions were the Darcy's equation applies, it represents a linear relationship between the volumetric flow rate and the pressure gradient of the system and has been used to model single phase fluid flow in the reservoir. With the Darcy equation being a linear function, a plot of Q/A versus $\Delta P/L$ for different flow rates should fall on a straight line with slope equal to k/μ. Permeability can, therefore, be determined from linear regression of these data points (McPhee et al., 2015). This linear relationship is also observed for two-phase flow when the velocity is high, and the capillary forces are negligible. When the effect of capillary forces becomes comparable to the viscous forces, the volumetric flow rate and the pressure drop is found to diverge from its linear trend. This will be discussed further in this chapter.

When two or more immiscible fluids flow simultaneously in a rigid porous medium, the permeability is described by the relative permeability equations, which are considered to be the effective medium equations. The relative permeability approach views each fluid as moving in a pore space that is constrained by the other fluid. Hence, each fluid will experience a lowered effective permeability since it is now sharing the pore space with another fluid. The relative permeability of a fluid is defined as the ratio of the effective permeability of that fluid to the single-fluid permeability of the porous medium (Blunt, 2017). It is common to assume that the relative permeability depends only on the respective fluid's saturation. Increasing the saturation of one phase will lead to a decrease in the saturation of the other phase. A reduction in saturation will again lead to a reduction in the relative permeability of that phase. To account for multiple phases, Darcy's law is generalized by introducing the relative permeability, k_{rp}, of each phase p. The generalized Darcy's equation is defined as:

$$Q_p = \frac{-kAk_{rp}S_p}{\mu_p L}\Delta P \tag{2.4}$$

The concept of relative permeability is simple. However, different laboratory methods, e.g., the Penn State or the Hassler method, yield different results for the measurement (Osoba et al., 1951). This is seen as an indication that relative permeability equations do not offer a complete description of the multiphase flow.

These weaknesses have been known for a long time, and some may argue that the relative permeability approach should, and will be replaced by a better framework (Savani et al., 2017).

2.2 Related Work

As described earlier, the three primary forces that affect fluid propagation are gravity, capillary, and viscous forces. The capillary number, presented in equation 2.1, relates the capillary forces to the viscous forces and is a function of the velocity of the fluid propagation through the porous medium. As the velocity increases, the viscous force will increase. Thus, the lower rates will be dominated by capillary forces, while viscous forces will dominate the higher rates. This is followed by the assumption that capillary force can be neglected at high rates, and viscous forces can be neglected at low rates (Blunt, 2017). When two immiscible fluids are flowing simultaneously in the same porous medium, a traditional assumption is that each fluid will flow in its own interconnected pathway (Bear, 2013). If a bulk of fluid is disconnected, i.e., by snap of, it will be stranded and trapped (Avraam and Payatakes, 1995). However, lately, there have been many studies where this assumption have been questioned. Instead of the fluid flowing in continuous pathways, it has been reported to break up into discrete ganglia. These ganglia are transported by the wetting fluid, and not stranded as earlier assumed (Avraam and Payatakes, 1995; Datta et al., 2014; Aursjø et al., 2014; Sinha et al., 2017). Although some of these studies have been conducted using a two-dimensional porous medium which hardly applies to a three-dimensional situation, these results still raise the question of whether or not the assumption of interconnected pathways is correct. The ability to predict the transition in which the fluid flow changes from one flow regime to another, e.g., from capillary force dominated to viscous force dominated, is useful in a range of applications, e.g., in the upscaling of two-phase flow (Odsæter et al., 2015).

Different studies of two-phase steady state flow have been conducted to get a better understanding of fluid behavior at different flow rates. The goal of these studies is to be able to predict the fluid's behavior at different flow rates, and to identify the point of transition between the different flow regimes, but the results of these experiments vary greatly. In the following, the varying results of some of the different experiments will be presented. The execution of the experiments is different, but a common goal is the identification of the transitions zone between flow regimes when two immiscible fluids are flowing simultaneously.

Experiments by Avraam and Payatakes (1995) identified four different types of fluid flow patterns that changed with the change of flow rate. The results of this study showed that at a lower flow rate and saturation the fluid flowed as large ganglia that had the size of several pores. The authors referred to this as large ganglion dynamics. The size of the ganglia decreased with increasing flow rate until the ganglia were the size of a single pore. This was referred to as small ganglion dynamics. These two types of ganglion dynamics were observed for capillary numbers in the range 1×10^{-8} to 1×10^{-5}. At even higher flow rates, the third type of flow was observed. At this point, most of the oil was flowing in disconnected droplets with approximate sizes of diameter to that of the pore throat. The authors referred to this type of flow as drop- traffic flow. At the highest flow rates, it was observed that both phases started flowing through separate and uninterrupted pathways, which was referred to as connected pathway flow. This fluid flow regime was reported for capillary numbers at $Ca > 5.01 \times 10^{-6}$.

Tallakstad et al. (2009) conducted six steady-state experiments where they studied the flow patterns of two immiscible fluids flowing simultaneously through a horizontal two-dimensional model. The model of the porous medium consisted of a single layer of glass beads with a diameter of 1 mm between transparent plates. They used a glycerol-water solution as the wetting phase, and air as the non-wetting phase. This

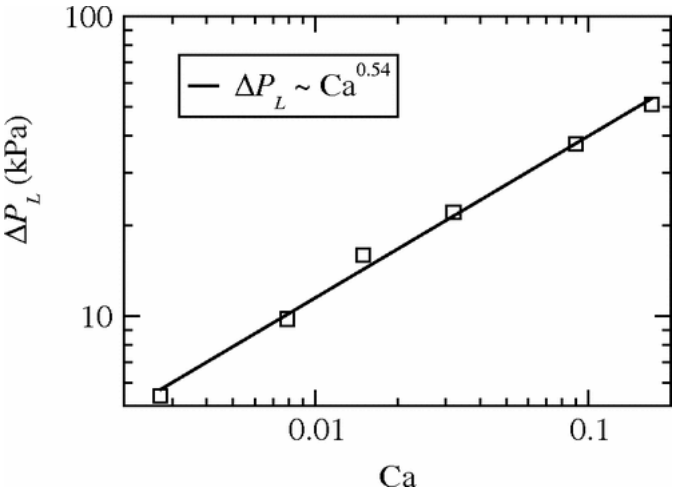

Figure 2.2: Results from the experiment conducted by Tallakstad et al. (2009). Mean pressure difference, ΔP_L, during steady state as a function of Ca. A power law dependence is found, with exponent $\beta = 0.54 \pm 0.08$ (Tallakstad et al., 2009).

resulted in a large viscosity ratio. The fractional flow was kept fixed by simultaneous injection of the two phases. The results of this experiment showed a power law relationship between the steady state pressure gradient and the capillary number. The scaling was corresponding to $\Delta P \sim Ca^{\beta}$, where β was found to be 0.54 ± 0.08. The results can be seen in figure 2.2. Tallakstad et al. (2009) conducted a more recent micromodel study, where the authors observed ganglion movement in the viscous flow regime. This was found at capillary numbers greater than 1×10^{-3}, which is lower than the transition found by Avraam and Payatakes (1995). Note that Tallakstad et al. (2009) used a different definition of the capillary number than what will be used in this thesis. He defines it as:

$$Ca = \frac{\mu_w Q_w a^2}{\gamma \kappa_0 A}$$

where μ_w is the viscosity of the glycerol-water solution, Q_w is the flow rate of the wetting phase, γ is the surface tension, κ_0 is the absolute permeability, and $A = Wa$ is the cross-sectional area, where W is the width of the porous model frame.

Rassi et al. (2011) conducted a study where they researched the scaling relationship between the differential pressure, ΔP, and the capillary number, Ca, similar to what Tallakstad et al. (2009) had done earlier. For the two immiscible fluids, that were flowing simultaneously, Rassi et al. (2011) used water and air. The results of the experiment gave a correspondence to $\Delta P \sim Ca^{\beta}$, where β was ranging from 0.30 to 0.45, depending on the saturation. These results can be seen in figure 2.3. Unlike Tallakstad et al. (2009), Rassi et al. (2011) conducted the experiment using a 3D bead pack as the porous medium. Rassi et al. (2011) used the same definition of capillary number as defined in equation 2.1, i.e. a different definition than what Tallakstad et al. (2009) used. Thus the experiments are not directly comparable.

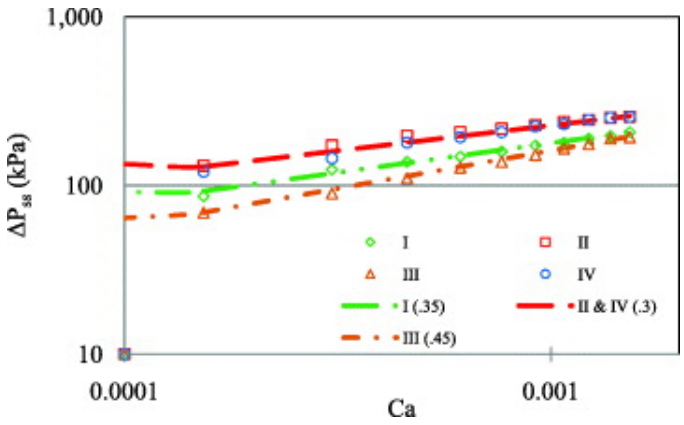

Figure 2.3: Plot of the steady state pressure difference and the corresponding capillary pressure presented by Rassi et al. (2014). Average steady-state pressure drop versus corresponding capillary number. The straight lines show the power-law fits for each repetition: I; $\beta = 0.35$, II;$\beta = 0.3$, III; $\beta = 0.45$ and IV; $\beta = 0.3$.

Unlike the previously mentioned studies, Rassi et al. (2011) investigated the effect of saturation on the system, and looked at the non-wetting saturation fraction, S_{nw}, as a function of the capillary number. The results of this study can be seen in figure 2.4. Three years after the article was published, a corrigendum of the study was published. The corrigendum, (Rassi et al., 2014), states that the horizontal axes for Ca in figure 2.4 should be divided by a factor of 27.70, and hence range from 3.61×10^{-6} to 7.22×10^{-5}. This does not impact any of the discussion or the conclusions drawn in the original publication. Thus this figure is included in this thesis as the conclusions to the relationship between saturation and the capillary number drawn from the figure are still valid.

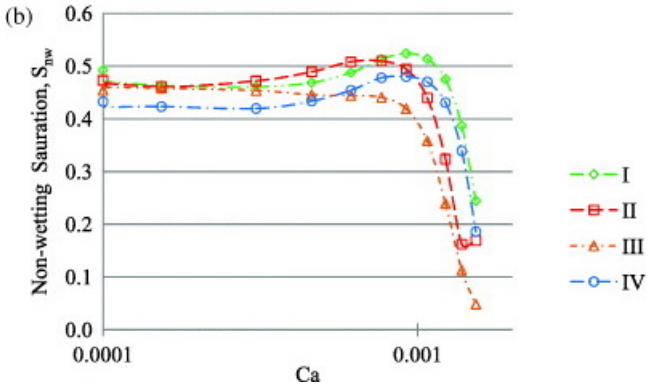

Figure 2.4: Non-wetting saturation in the bead pack as a function of capillary number (Rassi et al., 2011).

In 2011, Grøva and Hansen (2011) conducted a numerical study simulating a system that was similar, but not identical to the Tallakstad et al. (2009) experiment. Grøva and Hansen (2011) defined what they called the freezing transition. Below the freezing transition, Grøva and Hansen (2011) observed only one phase was mobile, while the other was trapped and immobile. They scaled the effective permeability of the non-wetting phase to the capillary number with the scaling relation $|K_{eff}| \sim Ca^{\beta}$ and found that β was varying from 0.53 to 0.80 depending on the saturation. This support Tallakstad et al. (2009) in their assumption that the scaling coefficient is dependent on saturation. Grøva and Hansen (2011) also tested the effect of the mobility

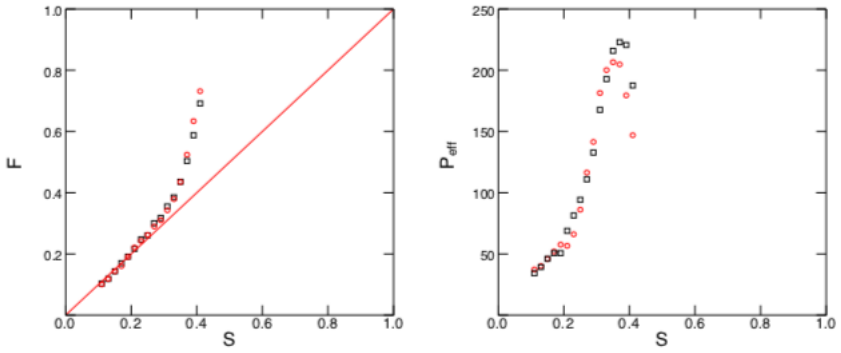

Figure 2.5: Fractional flow versus saturation (left) and effective permeability versus saturation (right) for the simulations by Grøva and Hansen (2011). Black squares symbolizes a mobility ratio at M=1, while red circles is $M = 1 \times 10^{-4}$.

ratio, and ran their simulation with two different ratios; $M = 1$ and $M = 1 \times 10^{-4}$, where the latter is consistent with the mobility ratio of the Tallakstad et al. (2009) experiment. A plot of fractional flow vs. saturation and k_{eff} vs. saturation for the two mobility ratios can be seen in figure 2.5. The figure indicates low sensitivity to the mobility ratio.

In a study conducted by Datta et al. (2014), the transition from continuous fluid flow to ganglia displacement was investigated. The objective of this study was to find the transition zone for when the non-wetting fluid breaks up into ganglia, and hoe the transition zone is dependent on the flow rate. For low flow rates, both fluids are believed to flow through continuous paths, while they for larger flow rates are believed to start to break into discrete flowing ganglia (Datta et al., 2014). When increasing the flow rate, the pressure gradient increases, and the pore-scale arrangement of fluids will be altered. This makes the flow rate, Q, a critical parameter when describing the fluid flow patterns. For their experiment Datta et al. (2014) used a 3D porous medium consisting of glass beads. They proposed that the transition zone would occur when the sum of the viscous forces from the two immiscible fluids surpass the capillary forces acting on the pore scale. A capillary number threshold described the transition zone for both the wetting and non-wetting fluid. They reported values for the critical capillary numbers that define the transition between the two flow regimes were $Ca_w = 7 \times 10^{-4}$ and $Ca_{nw} = 5 \times 10^{-3}$.

Like Tallakstad et al. (2009), Aursjø et al. (2014) also conducted an experiment were they flowed two immiscible fluids simultaneously through a two-dimensional porous medium. As the porous medium Aursjø et al. (2014) used a Hele-Shaw cell, with a layer of randomly distributed borosilicate glass beads. The two immiscible fluids were grade oil and water-glycerol solution, with a mobility ratio of M = 1.3. Initially, the water-glycerol mix was left behind in clusters, but after reaching steady-state, the two fluids were both flowing in interconnected pathways from inlet to outlet. The scaling coefficient between the pressure drop and the flow rate was found to range from 0.67 to 0.74. This scaling exponent is somewhat higher than those reported in similar studies like Tallakstad et al. (2009). Aursjø et al. (2014) explained this with the fluids, to a certain degree, was flowing side by side.

The theory of interconnected pathways for each fluid during steady-state two-phase flow was again questioned by Reynolds et al. (2017). As the porous medium, a permeable sandstone was used. The two

immiscible fluids flowing were nitrogen and brine. Both capillary number and saturation were kept constant. The tests were run with a low capillary number with the range $Ca_w = 7.0 \times 10^{-7}$ to 3.5×10^{-5} and $Ca_{nw} = 2.27 \times 10^{-8}$ to 1.13×10^{-6}. For observations, they used x-ray imaging at pore scale to track the fluid pathways. From this, they found a new type of flow, which they referred to as dynamic connectivity. During this type of flow, the fluids were flowing through pathways that were periodically reconnected. Reynolds et al. (2017) observed that the pores filled with the non-wetting fluid were not necessarily connected. They stated that the transition from the dynamically connected flow regime to the flow regime where no pathways were connected could be described by the capillary number of the wetting phase and non-wetting phase, similar to the study by Datta et al. (2014). From the results of this experiment the critical capillary numbers were estimated to $Ca_w = 4.5 \times 10^{-6}$ and $Ca_{nw} = 8.5 \times 10^{-8}$.

While the results from some of the aforementioned studies align and support similar theories, there are clearly also conflicting results. Thus a conclusion to the behavior of simultaneous two-phase immiscible flow in porous media cannot be drawn. The amount of available literature on experiments on three-dimensional models is lacking and does not give a satisfactory answer to many of the lingering questions on the topic. A recent study published by Sinha et al. (2013) claims to explain some of the varying results. The experiments and theory by Sinha and Hansen (2012); Sinha et al. (2013, 2017), serve as a foundation for the work in this project.

The abovementioned studies have investigated both flow regimes and scaling relation between volumetric flow rate and pressure drop, but have not devoted much time to the physical explanation behind it. In 2012 Sinha and Hansen (2012) presents a theory regarding this. In their study, Sinha and Hansen (2012) investigated the scaling between the pressure and the flow rate through numerical simulations and mean field calculations. This was used to derive a generalized Darcy equation for steady-state immiscible two-phase flow of Newtonian fluids. They found that for the capillary dominated regime at low capillary number, the barriers created by the capillary pressure at the interfaces between the fluids, created what they call a yield threshold. This yield threshold is the pressure needed for the two immiscible fluids to start flowing. These capillary thresholds will be randomly distributed throughout the system, and by introducing a probability distribution for the yield thresholds, a global threshold pressure that corresponds to the minimum sum among all such possible paths can be derived. Sinha describes the threshold pressure as follows: Along a continuous flow path throughout a porous medium, the threshold pressure is defined as the sum of all the thresholds along this path. The global threshold pressure for the system will then be the minimum sum of all the thresholds along all the possible flow paths. Just above this threshold pressure, there only exists one possible flow path, but as the pressure in the system starts to rise, more and more paths will open up, until all of them are open and the flow rate, Q, becomes linear with the differential pressure, ΔP (Sinha and Hansen, 2012). An overall threshold pressure was thus introduced in their work and calculations, defined as ΔPc. There are different ways to calculate the threshold pressure. One method is to measure the differential pressure as the flow rate approaches zero, $Q = 0$, by plotting the pressure versus flow rate, and then finding the intersect at the y-axis which will then represent the threshold pressure. The logarithm of the differential pressure minus the threshold pressure, $\Delta P - \Delta Pc$, is plotted versus the logarithm of the capillary number, Ca. The scaling relation between the pressure and the corresponding capillary number was proposed to be $\Delta P - \Delta Pc \sim Ca^{\beta}$. (Sinha et al., 2017).

Sinha and Hansen (2012) investigated two different situations. One with constant saturation and the other with fluctuating saturation. For each situation, they plotted the differential pressure, including the threshold pressure, versus the capillary pressure. The results of this experiment can be seen in figure 2.6, with

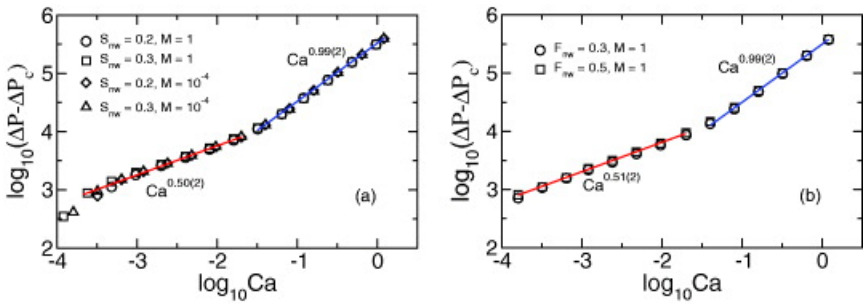

Figure 2.6: Scaling of excess pressure drop to capillary number from numerical simulations by Sinha et al. (2017). Two different flow regimes can be observed. A lower regime with a scaling coefficient of $\beta = 0.5$, and a linear upper regime of $\beta \simeq 1$.

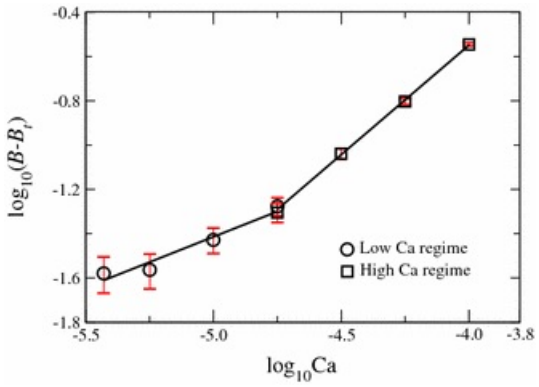

Figure 2.7: Plot of dimensionless excess pressure drop ($B - B_t$) as a function of the capillary number, Ca, from the experimental study by (Sinha et al., 2017). Two different flow regimes can be observed. The scaling of these regimes corresponds to the numerical simulations.

constant saturation to the left, and fluctuating saturation to the right. These plots show that there exists at least two flow regimes, one for the lower, and one for the higher flow rates. For the low flow rates some of the thresholds blocking the fluid flow are shut, and the flow is found to be quadratically dependent on the differential pressure, giving $\beta = 0.5$ for the scaling relationship $(|\Delta P| - \Delta Pc) \sim Ca^{\beta}$. When the flow rate increases, more and more of the barriers created by the capillary pressure at the interface of the two fluids are overcome. As the capillary pressure barriers are overcome and all paths are opened up, the flow becomes linearly dependent on the differential pressure. This is consistent with a β of 1. This regime can be seen as the blue section in figure 2.6. In this situation, the overall threshold pressure is negligible compared to the differential pressure, and the fluid flow can be represented with the well-known Darcy equation 2.3 (Sinha and Hansen, 2012; Sinha et al., 2013). Moreover, Sinha and Hansen (2012) found ΔP_c to be independent of the viscosity ratio, and claim this is strong support of what they call an intuitive physical description of the threshold pressure. In their report, they state that: "As ΔP_c is related to the sum of capillary thresholds (p_c) over connecting paths and p_c does not depend on the viscosities, ΔPc also should not and that is what we found" (Sinha and Hansen, 2012).

The authors Sinha et al. (2013) believe that the varying results of the previous mentioned studies by Rassi et al. (2011), Tallakstad et al. (2009) and Grøva and Hansen (2011) can be explained by introducing the yield threshold pressure. Both Rassi et al. (2011) and Grøva and Hansen (2011) used the scaling relationship

$\Delta P \sim Ca^{\beta}$. Rassi et al. (2011) found that β was varying from 0.30 to 0.45 depending on the saturation, while Grøva and Hansen (2011) saw this same effect as a visible curvature in the scaling plots. Sinha et al. (2013) claims this indicates a non-zero ΔP_c that has been ignored. When the experiment by Rassi et al. (2011) is reanalyzed using $\Delta P - \Delta Pc \sim Ca^{\beta}$ instead of $\Delta P \sim Ca^{\beta}$, β is found to be ~ 0.5. In the experiment by Tallakstad et al. (2009), β is found to be 0.54 ± 0.08 using the scaling relation $\Delta P \sim Ca^{\beta}$. Sinha et al. (2013) states this is due to the fact that one of the fluids was percolating in their system, making $\Delta P_c = 0$, and their results will be correct even without accounting for the threshold pressure.

Some years later, the same authors, Sinha et al. (2013) conducted a new study to quantify the dependency of the flow rate to the differential pressure. Again they presented both a numerical and an experimental study. For the experimental study, they used two immiscible Newtonian fluids flowing simultaneously, in av overall vertical direction, in a three-dimensional porous medium consisting of glass beads to find the relation between the pressure difference and the volumetric flow rate during steady state. The results can be seen in figure 2.7, where the flow rate is plotted against the dimensionless pressure. Also here two different flow regimes are observed. The transition between flow regimes was observed for a capillary number of $1 \times 10^{-4.75}$. For capillary numbers higher than the transition point, the capillary number scaled close to linearly with the pressure drop, giving a scaling exponent of $\beta = 0.99$. For capillary numbers lower than the transition point the scaling exponent $\beta = 0.46$. For the numerical simulations, the scaling coefficients were found to be $\beta =\sim 0.5$ and $\beta =\sim 1$, for the lower and upper regime, respectively. The transition point between the zones was found at Ca = $1 \times 10^{-1.5}$.

In 2018 it was attempted to test the theory presented by Sinha and Hansen (2012) experimentally. This was done at the Norwegian University of Science and Technology by June Katrin Husøy resulting in the master thesis (Husøy, 2018). The theory was tested by flowing two immiscible fluids through a three-dimensional porous medium and finding the scaling relation between the volumetric flow rate, Q, and the differential pressure, ΔP, during steady-state flow. From this scaling relationship, the transition point between the flow regimes could be identified. The transition point can be seen as the change in the gradient where the scaling coefficient changes from ~ 1 to a lower scaling coefficient.

The experimental set up consisted of two pumps, each pumping their own fluid, distilled water and oil (EXXSOL D60) through porous media. Two different porous media were tested, one containing glass beads of size 1 mm and one containing glass beads of 0.2 mm in diameter. Steady-state differential pressure was measured for different flow rates. For the porous medium containing the 1 mm diameter glass beads, a transition between two different flow regimes was observed for a capillary number, Ca, of 1×10^{-5}. For the highest flow rates, in the viscous dominated regime, the scaling coefficient was close to 1, implying a linear relationship. When decreasing the flow rate, a transition towards a more capillary dominated flow regime was observed, with a scaling coefficient of approximately 0.47. These results imply a transition zone between flow regimes for a given capillary number. It was questioned whether or not this change in slope can be attributed to inlet/outlet effects. For the porous medium containing the 0.2 mm diameter glass beads, no such transition point towards a non-linear regime was observed. Further details about the experiment can be found in Husøy (2018).

The experiment by Husøy (2018) was further researched by Anfinsen (2018) as a specialization project during the autumn semester of 2018. Like the thesis by Husøy (2018), the specialization project presented an experimental study of simultaneous two-phase flow, of immiscible fluids, in a three-dimensional porous medium. The objective of the project was to find the scaling relation between the volumetric flow rate, Q,

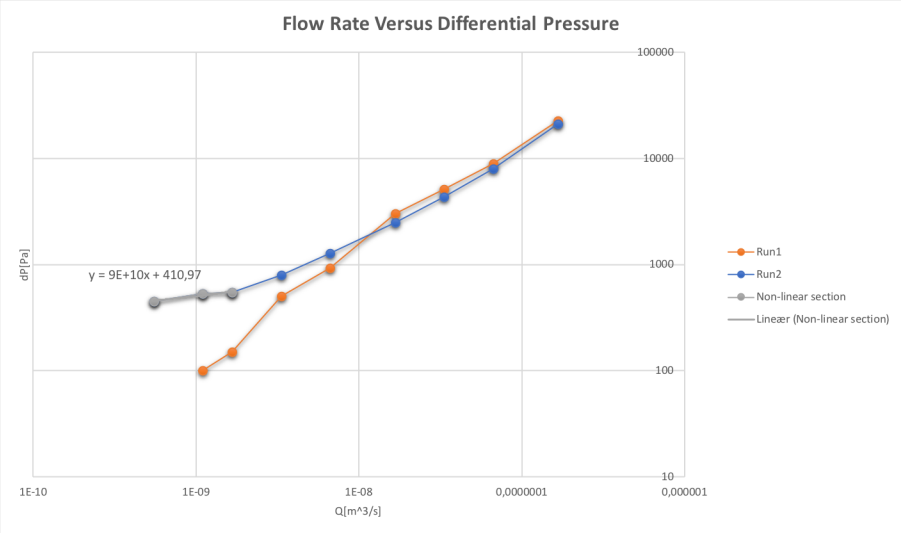

Figure 2.8: Scaling relationship between the volumetric flow rate, Q, and the differential pressure, ΔP, during steady state flow by Anfinsen (2018). When measured data points are plotted, the results of run 2 indicate two different flow regimes.

and the differential pressure, ΔP, during steady-state flow. The three-dimensional porous medium was a bead pack made up of glass beads in a teflon tube, and the two immiscible fluids that are pumped through the bead pack, are distilled water and oil (EXXSOL D60). Flow rates were run in the range from 0.005 ml/min to 10 ml/min, and the corresponding steady-state differential pressure over the bead pack was measured for each run. Some modifications were made to the experimental setup, to avoid end effects affecting the flow. The pressure drop versus the capillary number was plotted to find the scaling coefficient, β, from the relation $\Delta P \sim Ca^{\beta}$. The results indicated two different regimes. One linear regime for the higher flow rates and one regime that deviates from the linear trend. The non-linear regime is found at low flow rates, where capillary forces need to be accounted for. The transition between the two regimes is found at capillary number; $Ca = 1.64 \times 10^{-5}$. However, after accounting for a threshold pressure, ΔP_c, created by the capillary pressure at the interfaces between the fluids in a pore throat as introduced by Sinha et al. (2013), only one regime was found. This regime is linear, with a scaling coefficient of $\beta \sim 1$. The plotted results can be seen in i figure 2.8 and 2.9. Ultimately the results by Anfinsen (2018) contradict the theory by Sinha et al. (2013), but with limited data, the validity of the results need to be questioned.

This thesis will be a continuation of the specialization project by Anfinsen (2018). Additional modifications were made to the experimental set up in an attempt to either test the findings by both Husøy (2018) and Anfinsen (2018). The modifications will be further explained in chapter 3.

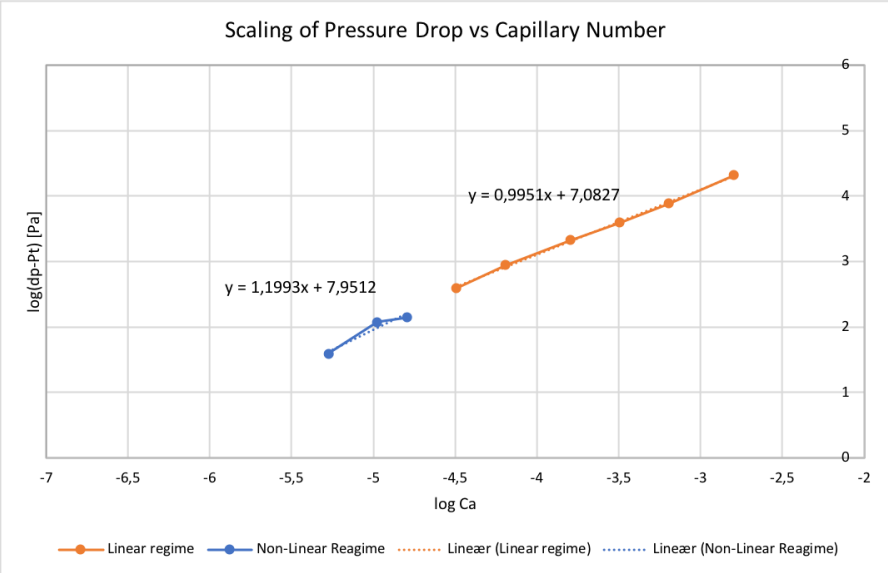

Figure 2.9: Scaling relationship for run 2 by Anfinsen (2018). After accounting for threshold pressure, the data from run 2 no longer indicate two different regimes.

2.3 Pore schematics and the interplay between forces

The abovementioned studies raise questions about flow regimes, and especially about the existence of a lower flow rate regime dominated by capillary forces, that deviates from the linear relationship known from the Darcy equation. The physical explanation as to why this regime exists, if it does, is not known. What is observed is that in the cases where this regime is identified, it is found to have a lower scaling coefficient than that of the Darcy regime. In practice, this means that more energy is used in the lower flow rate regime. The total energy loss of fluids flowing in a porous material can be divided into two categories.

$$E_{total} = E_c + E_v \tag{2.5}$$

where E_v refer to viscous dissipation of energy, while E_c represent all other energy dissipation. Thus, energy dissipation due to fluid redistribution induced by capillary forces is included in E_c. At high velocities, E_v dominates, and the relation between rate and pressure gradient is given by Darcy's law. The question that will be attempted answered in this thesis is how the energy is lost to E_c, i.e. how the fluids move in the capillary dominated regime in order to use more energy, causing a lower scaling coefficient, also considering whether or not the scaling of this regime constant and possible to predict. A normal assumption has been that in multiphase flow, each fluid move in its interconnected path, but lately several studies are challenging this assumption, as presented earlier in this chapter.

In his book Blunt (2017) reports that for a capillary number lower than 1×10^6 the fluid flow will depend on capillary forces. For this lower flow regime, the fluid distribution, and thereby the relative permeability of the fluid, will not be dependent on the viscosity or flow rate of the fluid. If the capillary number is increased beyond 1×10^3, a viscous controlled regime is reached, and the viscous forces start to dominate at the pore scale. At this point, trapped droplets of the non-wetting fluid will be mobilized and begin to flow as discontinuous bulks of fluid. These bulks of non-wetting fluid are referred to as ganglia. It has been reported ganglion movement in systems where there is an overall similarity in the pore throat size and pore body size. Thus, the difference in capillary pressure needed to mobilize a ganglion is believed to be small (Blunt, 2017). Blunt (2017) is introducing a different view on how the fluids move that differs from the theory of interconnected paths, but this theory is not extended to the capillary dominated regime.

The theory of ganglion movement presented by Blunt (2017) is consistent with the theory presented by Sinha et al. (2013) that was introduced earlier in this chapter. In addition to describing ganglion movement when viscous forces are high enough, the theory by Sinha et al. (2013) also describes a lower flow regime. Sinha et al. (2013) believes the pressure gradient to be lower in this regime because of a threshold pressure in each pore throat that needs to be overcome before both phases can flow through as ganglions. Figure 2.10 illustrates a ganglion trapped between pore throats. The threshold pressure is, as described earlier, connected to the interface between the two phases in the pore throat. Sinha et al. (2017) reports the scaling of this regime to be consistent with $\beta = 0.5$. According to Sinha et al. (2013) the transition to the upper flow regime will be consistent with the mobilization of ganglions.

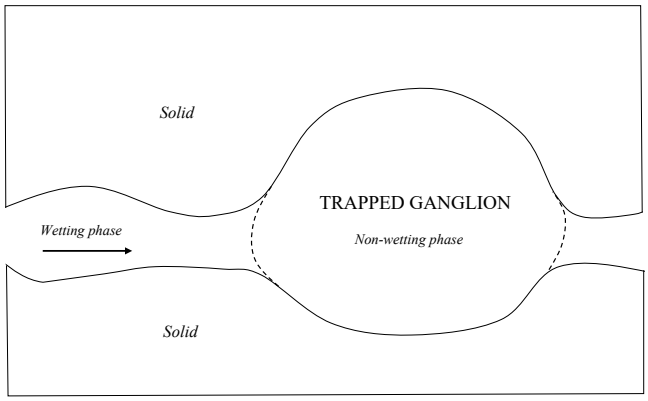

Figure 2.10: An illustration of a trapped ganglion, caused by a large difference in radius between the pore throat and pore body.

As introduced earlier in this section, deviation from Darcy's equation at lower rates indicates that energy is used on something else than moving the fluids. As this is in the capillary dominated regime, it is natural to assume this use of "extra" energy is connected to capillary forces. If it is not connected to ganglion movement as Sinha et al. (2013) states, another possibility is that the extra energy used in this regime is moving the interface between oil and water back and forth. An illustration of this can be seen in figure 2.11. When viscous forces are small, the energy lost to the movement of the interface could be enough to affect the pressure gradient to deviate from the linear regime, and lead to a lower scaling coefficient.

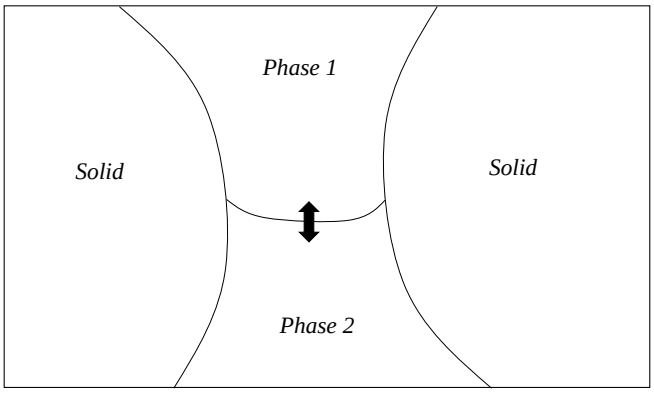

Figure 2.11: Illustrates the back and forth movement of the interface between oil and water in a porous media.

Chapter 3

Experiment - Materials and methods

In the following chapter, the experiments will be described in detail. Information about equipment and materials is found in this chapter.

3.1 Experimental Apparatus

As the object of this thesis is to identify flow regimes during steady state, the experimental setup needs to be constructed so that steady state flow can occur. Husøy (2018) reported that the filters at inlet and outlet of the bead pack caused boundary effects where the fluids were flowing as larger droplets. These boundary effects are causing the differential pressure to fluctuate, and steady-state as defined in section 2.1 is not achieved. To avoid these boundary effects, some modifications from the set up used by Husøy (2018) were made to increase the chance of reaching steady-state flow. By measuring the pressure at a distance after the inlet filter, and before the outlet filter, the end effects caused by the filter are reduced, and the measured pressure is believed to be at steady state. An illustration of the experimental set up can be found in figure 3.1 and 3.2, for single-phase flow and two-phase flow, respectively. The experiment was conducted first for a horizontal overall flow direction, then for a vertical overall flow direction. The experimental set-up for both cases was essentially the same but tilted 90°for vertical flow. The actual experimental set-up used in the lab can be seen in figure 3.3a and 3.3b on page 19.

To measure the pressure drop, pressure transducers were installed, as seen in figure 3.1 and 3.2, to monitor the pressure over the middle part of the bead pack where end effects are believed to be reduced. The outlet and inlet tubing was placed in the same reservoir, making the system a closed loop. This way, the fluid level in the reservoir is kept constant, which is essential to ensure correct pressure measurements. If the outlet tube were to be placed in a separate reservoir, the fluid level would rise over time, and the pressure would increase with the rising fluid column. Thus the pressure transducers would measure an increasing pressure and not a stabilized steady state pressure.

As the two fluid are immiscible with different densities, they separate in the reservoir. The two inlet tubes were placed in the center of their respective columns, to avoid potentially re-injecting contaminating particles that will gather either at the bottom or the top of the reservoir depending on its density. The outlet tube was placed in the middle of the two phases, making the segregation easier as well as avoiding interference from the outlet fluids to the inlet tubes. The reservoir can be seen in figure 3.4.

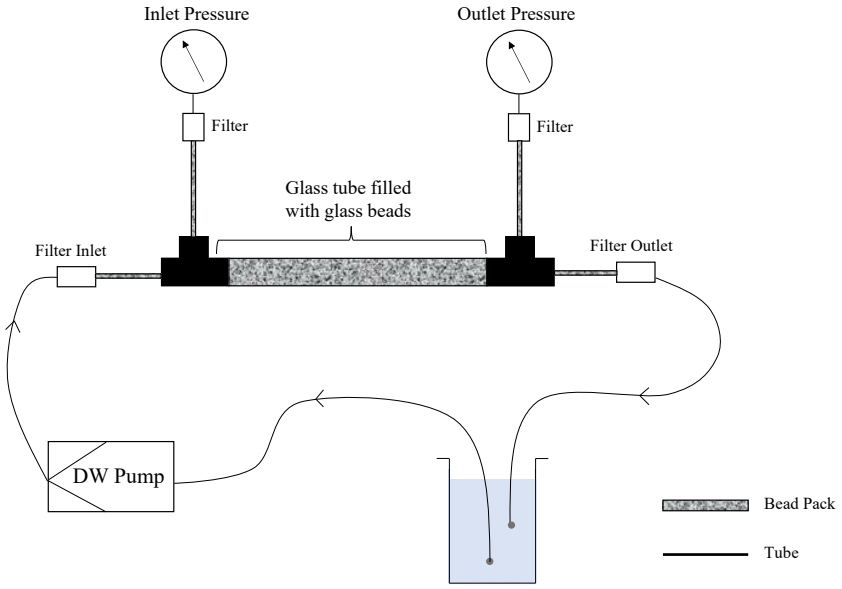

Figure 3.1: Illustration of experimental set-up for single phase flow.

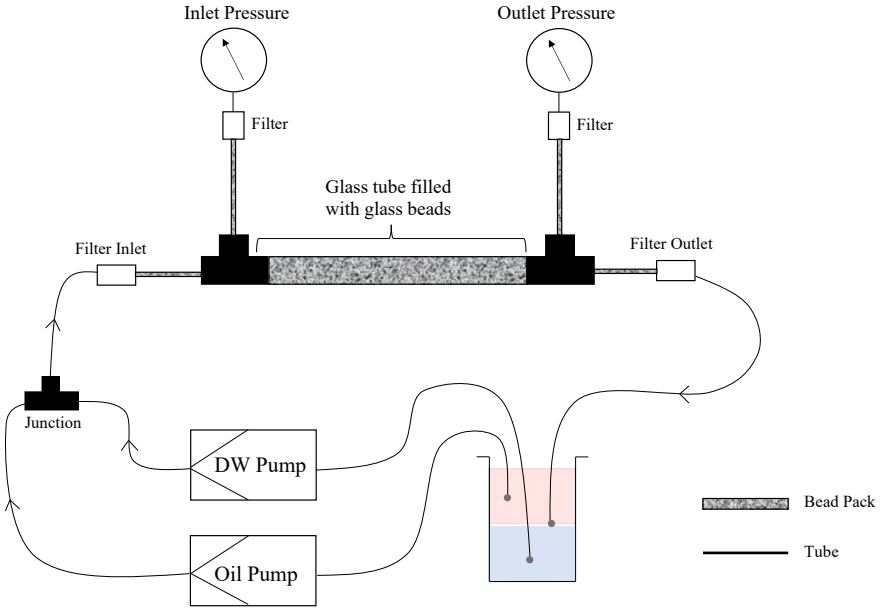

Figure 3.2: Illustration of experimental set-up for two phase flow.

Figure 3.4: Oil-water reservoir. Inlet tubes placed in the center of their respective fluid columns, and outlet tube placed in the middle of the two phases.

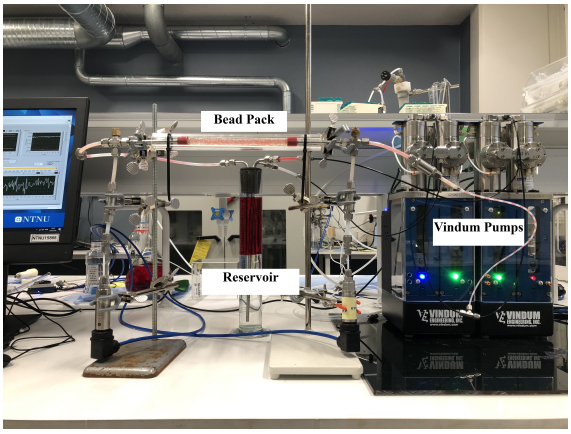

(a) Set-up for horizontal flow.

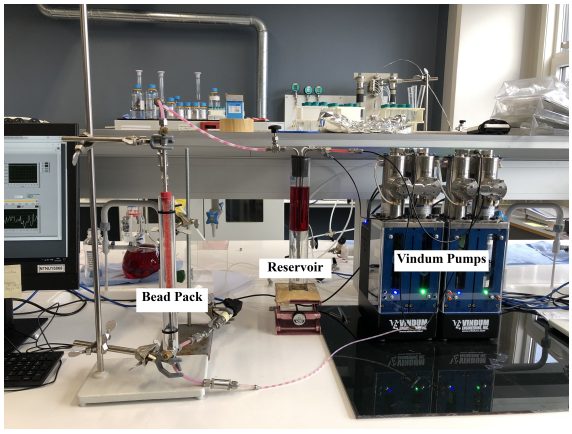

(b) Set-up for vertical flow.

Figure 3.3: Experimental set-up. The set-up in these two pictures are essentially the same, but in figure 3.3b the set-up is tilted 90°for flowing vertically through the glass bead pack.

3.1.1 Glass tube

For the tube between the pressure transducers, a glass tube was used. The tube consisted of two standard glass tubes welded together and was custom made by Astrid Salvesen, glassblower at NTNU. The glass tube was connected to the rest of the experimental set up by threaded couplings in glass. Thus the set up could not withstand high pressures.

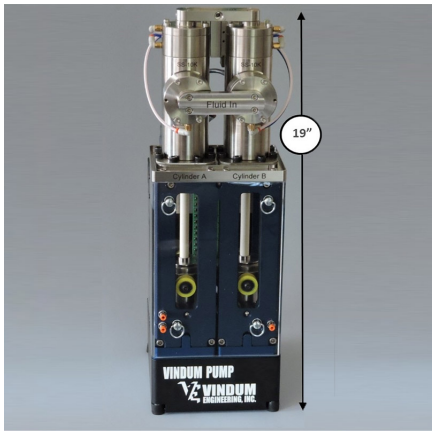

Figure 3.5: The Vindum 12k pump (VindumEngineering, 2018). Two of these pumps ere used in the experiment.

3.1.2 Tubing, Filters, and Valves

The remaining experimental set-up consisted of transparent teflon tubes and stainless steel fittings from Swagelok. For both inlet and outlet, the "Stainless Steel In-Line Particulate Filter" from Swagelok was used. The inner diameter of the filter was corresponding to the inner diameter of the tubes. The screen had a 90 Micron Pore Size, preventing even the smallest beads of 0.2mm from escaping (Swagelok, 2018).

3.1.3 Pump Specifications

The two pumps used in the experiment were Vindum 12K pumps. The pump can be seen in figure 3.5. These pumps are dual-piston metering pumps that offer ultra-precise pulse-free, continuous flow in either constant-pressure and constant-rate modes, making the delivery and retracting amount of fluid very accurate (VindumEngineering, 2018). The pump has a delivery flow rate that ranges from 0.0001 to 29 ml/min. The pulse-free fluid flow is made possible because of a return rate multiplier. The return rate multiplier ensures that when one of the cylinders is delivering fluid, the other cylinder prepares to deliver fluid at the same pressure as in the active cylinder by always retracting more fluid than what is being delivered. Choosing a return rate multiplier of 2 means that the retracting cylinder will retract twice the amount of fluid as the active cylinder is delivering. It will, therefore, have time to equilibrate the pressure across the cylinders constant before changing from one cylinder to the other.

3.1.4 Pressure Transducers

Two different pressure transducers were installed to monitor the pressure drop throughout the system. For the first runs, UNIK 5000 was used, see figure 3.6a. These sensors have a range from 0-250 mBar, with an accuracy of 0.2% of full scale. These were later replaced by a differential pressure transmitter by Keller, type PRD-33X. See figure 3.6b. The differential pressure transmitter has a maximum range of 40 bar abs and 350 mBar diff. The accuracy of the PRD-33X by Keller is 0.1% of full scale, which makes this more accurate than the UNIK 5000 sensors.

The pressure data were acquired by using National Instruments LabVIEW. The data output was programmed to give the pressure at P_1 and P_2, as well as the differential pressure across the sphere pack, ΔP, which was given as $\Delta P = P_1 - P_2$. The code can be found in Appendix A.

(a) UNIK 5000 pressure transducers.

(b) PRD-33X Keller differential pressure transducer.

Figure 3.6: Showing the pressure transducers used in the experiments.

3.2 Porous Media and Fluid Properties

3.2.1 Sphere Pack

When the tubes are filled with glass beads, it is referred to as a bead pack. The experiments were conducted using two different sizes of glass beads. One sphere pack consisting of 1mm beads, and the other consisting of 0.2mm beads. These sphere packs will further be referred to ass large bead pack (LBP), and small bead pack (SBP) respectively. As the first LBP was damaged, a new one had to be made for the experiments using a surfactant. The large bead packs will further be referred to as LBP1 and LBP2. Details about the porous media can be found in table 3.1, and the different sizes of glass beads can be seen in figure 3.7.

In similar experiments like Husøy (2018) and Anfinsen (2018), teflon tubes had been used as the confining media in the sphere packs. For this thesis, the teflon tube between the transducers was replaced by a glass tube. For a further explanation as to why the teflon tubes needed to be replaced, see Anfinsen (2018).

The glass beads were added to the system by using a funnel. To pack the glass beads in the tubes, the system was flooded with distilled water at the maximum rate, using the Vindum pump. The valves were opened one by one to control the water flow, and thereby control the movement of the glass beads. This ensured that the system was properly packed in all of the tubes, filters, and junctions. An illustration of this set-up used for packing the sphere packs can be seen in figure 3.8. Additional glass beads were added to the system until no movement was spotted while flooding the system with water.

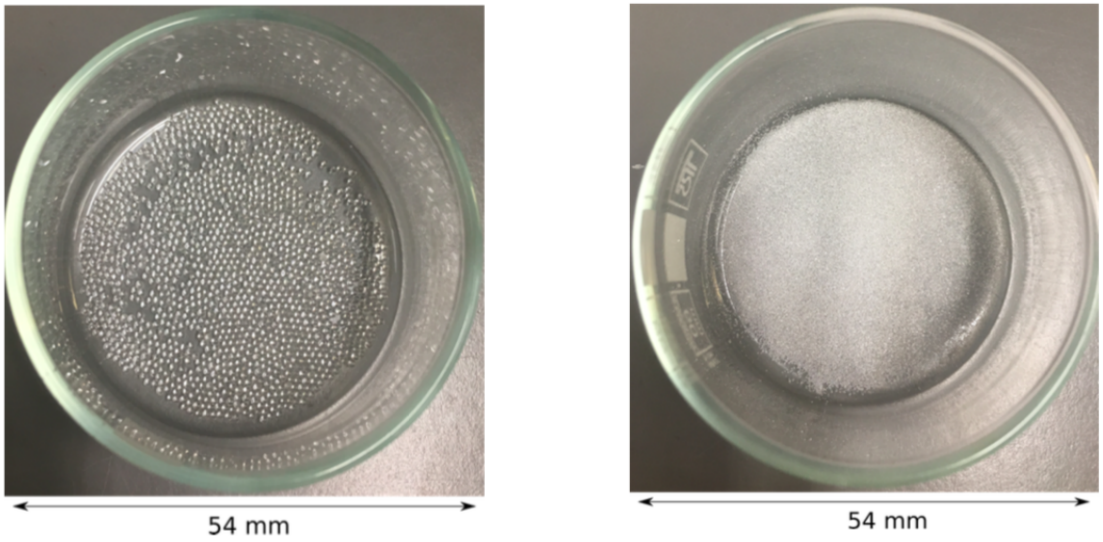

(a) 1.0 mm beads

(b) 0.2 mm beads

Figure 3.7: Showing the two different size of glass beads used in the experiment. Figure 3.7a is showing the 1mm beads used for the LBP, and figure 3.7b is showing the 0.2mm beads used for the SBP. Pictures are taken from Husøy (2018) as the same type of beads are used in this experiment.

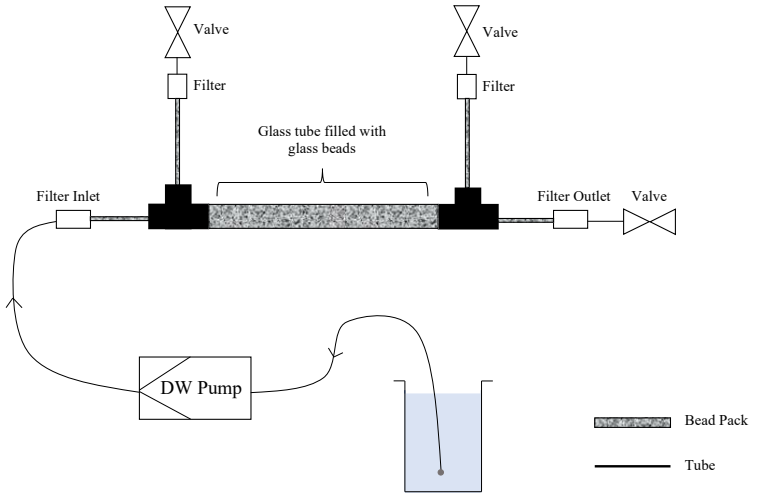

Figure 3.8: Illustration of the set-up used when packing the teflon tubes with glass beads.

The porosity in the glass tube was estimated by filling a glass tube, identical to the one used in the experiment, with dry glass beads and measuring its dry weight. Next, the bead pack was filled with water and weighed again. The difference in weight of the two samples is then equal to the weight of the water in the pore space. By applying the following equations, the porosity of the glass bead pack could be found. This porosity was

assumed to be equal to the porosity of the system. As the porosity was assumed to be constant throughout the system, this value was used for all further calculations.

$$V = \frac{m}{\rho} \tag{3.1}$$

$$\phi = \frac{V_p}{V_t} \tag{3.2}$$

Table 3.1: Properties for experimental set-up.

Property	**Large bead pack**	**Small bead pack**
Glass bead diameter $[mm]$	1	0.2
Inner diameter of glass tube $[mm]$	9	9
Bead pack length $[mm]$	200	200
Porosity	0.377	0.334
Cross sectional area $[mm^2]$	23.98	21.25

3.2.2 Fluid properties

The two immiscible fluids used in the experiment were distilled water and EXXSOL D60 oil. These fluids are nearly incompressible. By using two nearly incompressible fluids we are removing one of the uncertainties associated with the experiment conducted by Sinha et al. (2017), as his theory is based on two incompressible fluids, but his experiment was conducted using air, which is highly compressible.

For visual purposes, a coloring agent was added to the clear EXXSOL D60. For this, the" Oil Red O" from Alfa Aesar was used. The coloring agent was added to make it possible to tell the oil and the water apart while flooding the two fluids through the bead packs. The process of dyeing the oil red was carried out by first adding the pigment to a small amount of the oil. This oil was then stirred and filtered before adding more EXXSOL D60, and the process was repeated. The final product was filtered several times to avoid containment from any excess color agent particles in the experimental system. For the clear EXXSOL D60, the density and viscosity are $790kg/m^3$ and $1.43mPas$, respectively (Lindberg, 2005). These same values were used for the dyed red EXXSOL D60, as adding a small amount of "Oil Red O" does not change the density or the viscosity significantly. For the distilled water, the density and viscosity are $1000kg/m^3$ and $1.79mPas$, respectively. As the two fluids used in this thesis were the same as the fluids used by Husøy (2018), with equal density and viscosity, the interfacial tension measured by Husøy (2018) is used for further calculations. This interfacial tension between EXXSOL D60 oil and distilled water was measured to $30.98mN/m$.

3.2.3 Surfactants

Two different surfactants were used in the experiment, Zalo Ultra and Sodium dodecyl sulfate [SDS]. Zalo Ultra is a liquid hand dishwashing soap consisting of 15-30% anionic surfactants and 5-15% Nonionic surfactants (Orkla, 2016). The Sodium dodecyl sulfate used in the experiment was a 98.5% SDS solution with a molecular weight of $288.372g/mol$. For SDS the critical micelle concentration is at $9.5 \times 10^{-3}mol/dm^3 = 0.0095mol/liter$. Above this point, the surface tension remains relatively constant with concentration.

3.3 Experimental Procedure

To avoid contamination in the system, all equipment had to be cleaned before the experiment could start. Tubes, filters, and the glass beads had never been used before and were therefore not considered a significant source of contaminating particles. Nevertheless, everything was cleaned with distilled water to remove dust from its surface. A filter was used to wash the glass beads. After the system was cleaned, mounted, and packed with glass beads, the experiments could start. First, all the measurements needed for the single phase experiment was sampled. This because once the oil is introduced to the system, the system will be contaminated.

After the system was flooded, air bubbles were observed trapped in the sphere pack. The best way to remove these was to close the valve at the outlet and continue pumping fluid from the pump to build up the pressure in the sphere pack. The sphere pack was then closely monitored, and when the air bubbles were fully dissolved in the water, the outlet valve was opened, creating a substantial pressure drop over the system. This led to the air bubbles moving towards the outlet. The process was repeated until no air clusters were observed in the sphere pack.

3.3.1 Selection of Data

To decide whether or not the measured data was reliable, the background noise of the measurements had to be analyzed. Before starting the experiments, the pressure was measured over the bead pack without flow. This was done to gather information about the background noise, as noise from pressure transducers had been a problem in earlier experiments (Husøy, 2018; Anfinsen, 2018).

When starting experiments, the system was flooded, and the differential pressure was measured over the system, using pressure transducers and lab View, as explained in section 3.1.4. The pressure of interest is the pressure drop over the system at steady state flow, defined as in 2.1. To acquire this pressure, the transducers were placed at a distance from both inlet and outlet of the bead pack, to avoid end-effects from the filters that would disturb the steady state flow, as explained in section 3.1.

To identify the steady-state regime, the measured pressure drop was plotted against time to find when it stabilized, and thus reached the steady state, as defined in section 2.1. From visual inspection of this plot, a starting time for the steady state was chosen. An example of this can be seen in figure 3.9 for horizontal two-phase flow at $Q = 0.02$ in LBP1 run 1 . The red line in the plot indicates the chosen steady-state region. All measured pressure drop values within this region were used to calculate the average pressure drop that was used for further calculation and analysis. All values from this stable section of the plot were used to calculate the differential pressure for that given flow rate. For some flow rates, spikes in pressure were observed in the otherwise stable regime. These spikes were observed to correlate with the change of cylinder in the pumps and could be overlooked when choosing a steady state section. To avoid altering the average value with these spikes, three times the standard deviation was set as a cut off value. See Appendix B for differential pressure versus time plots for all flow rates.
As mentioned earlier, two different pressure transducers were used. Unik 5000 was used for single phase run LBP1, horizontal flow in LBP1 run 1-2 and vertical flow in LBP1 run 1-2. PRD-33X by Keller was used for single-phase run LBP2 and SBP, vertical flow in LBP1 run 3-4, vertical flow in SBP run 1-2 and LBP2 with surfactant run 1-2.

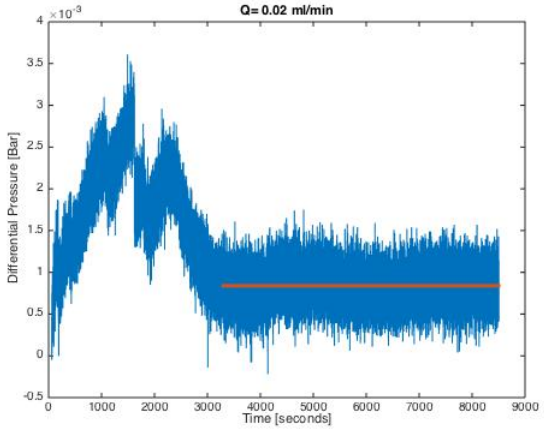

Figure 3.9: ΔP versus time was plotted for every flow rate to identify a steady state region and calculation the average pressure drop for that given flow rate. This figure show the referenced plot for horizontal two phase flow at $Q = 0.02$ in LBP1 run 1.

3.3.2 Single Phase Experiment

Three single phase experiments were conducted, one for each bead pack. Only distilled water was used for these experiments. The water was flooded at different rates, and the corresponding pressure drop was measured. An illustration of the single-phase experiment can be seen in figure 3.1. The average differential pressure, ΔP was found as described in section 3.3.1, and Darcy's equation could be used to calculate the permeability of the system. All single phase experiments were conducted before any oil was introduced to the system. Results for these experiments can be found in table 4.2 to 4.3, and plots for all rates can be found in Appendix A.

3.3.3 Two Phase Experiment

For the two-phase flow, six experiments were conducted. Two using the LBP1 and flowing horizontally. Two using the LBP1 and flowing vertically. As well as two using the SBP and flowing horizontally.

To get a simultaneous flow of the two phases, both pumps were started simultaneously and at equal rate. The individual flow rate from each pump is defined as q, while the total flow rate flowing through the bead pack is defined as Q. This gives the relationship $q_o + q_w = Q$, where $q_o = q_w$.

As the filters were placed at the start and the end of the bead pack, both inlet and outlet of the filter fitted the 4.2 mm diameter tube. Because the fluids were pumped through a 1.8 mm tube from the pump, this tube was connected to a 4.2 mm tube before connected to the filter. When the fluids were flowing from the pump through the 1.8 diameter tubes, they were flowing as droplets of oil and water in a steady flow of equally small droplets. When the fluids entered the larger tube before the filter, the oil accumulated into larger slugs. As a consequence of this, the fluids entered the bead pack in large slugs. To avoid this, a small tube was connected to the filter. This was done by filling the larger tube with glue, pushing the smaller tube through the glue, and connecting this glued tube to the filter. This way, the fluids could move directly from the smaller tube, through the filter, and into the bead pack. The glued tube can be seen in figure 3.10. There were not observed leakage of fluids during the experiment. Note that this modification was made after air bubbles

were removed from the bead pack by increasing the pressure. Thus the glued tubes were never exposed to high pressures. This modification to the original set-up was used for all two-phase experiments.

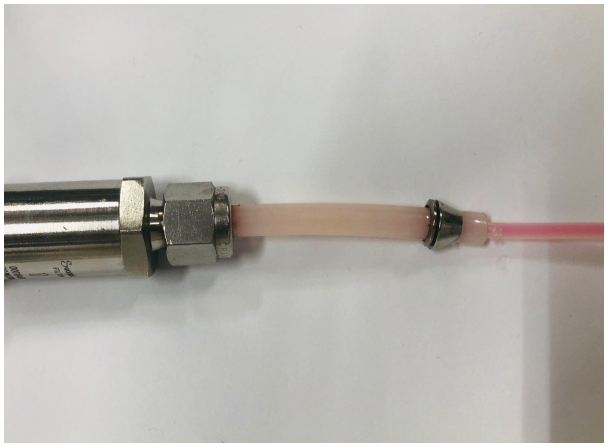

Figure 3.10: The glued tubes.

The steady state region was found following the procedure described in section 3.3.1. The saturation of the system was assumed to be constant. Thus the only varying parameter was the flow rate. Results form the two-phase experiments can be found in tables 4.4 to 4.9. The relative permeability of the system was found following the same procedure as for single phase, assuming that the saturation of the system was 50/50 oil and water. Two runs were completed for each experiment. The first run is starting at the lowest flow rate and increasing until the maximum flow rate is reached. The next run is starting at the maximum flow rate and decreasing for each measurement until reaching the lowest flow rate again. If the properties of the bead pack have remained the same within the experiment, the results of these two runs should be somewhat equal. Thus overlapping results support the validity of the measurements.

The main objective of the two-phase flow experiments was to find the scaling relationship between the flow rate and the pressure drop. To find this, the differential pressure values for the two-phase fluid flow was plotted against the capillary number or the corresponding flow rate. This will be further explained in chapter 5.

3.3.4 Surfactant Experiment

To determine the effect of the interfacial tension, four experiments were conducted using two different surfactants. The first one used zalo as a surfactant, and the second used sodium dodecyl sulfate, further referred to as SDS, as a surfactant. Zalo was added to the distilled water, making a 1% solution. For the SDS solution, the intent was to create a weaker surfactant. 2.74 grams of SDS was added to 1 liter distilled water making a solution at critical micelle concentration.

The intent of adding a surfactant was to decrease the surface tension between the to immiscible fluids, but still have to separate phases. By reducing the surface tension, the capillary number will increase, following equation 2.1. For these experiments, the LBP2 was used, and the flow was vertical.

Chapter 4

Results

In this chapter, all measured results will be presented and plotted. Starting with results from the single-phase experiments, followed by two-phase experiments without surfactant, and finishing with results from the surfactant experiments. For analysis and discussion of results, see chapter 5.

4.1 Porosity

The porosity of the LBP1 was found as described in section 3.2.1.

$$m_w = 4.78g$$

because $\rho_w = 1.0g/cm^3$ at $20°C$ this leads to

$$V_w = 4.78ml$$

From table 3.1 we find

$$V_{tot} = (4.5mm)^2 * \pi * 200mm = 12.723ml$$

This gives the porosity for the LBP; ϕ_{LBP}.

$$\phi_{LBP} = \frac{V_w}{V_{tot}} = \frac{4.780ml}{12.723} = 0.377 = 37.7\%$$

Same procedure gives ϕ_{SBP} = 33.4% for the SBP. The porosity of LBP2 is assumed to be similar to that of LBP1. As porosity calculations are not decisive for the interpretation of the results, $\phi_{LBP1} = \phi_{LBP2}$ will be used for all further calculations.

4.2 Results for Single Phase Experiments

Initially, two single phase experiments were conducted - one for the LBP1 and one for the SBP. Table 4.1 and 4.2 presents the flow rates with corresponding measured differential pressure for these tests. A plot of flow rate to pressure drop can be seen in figure 4.1.

Table 4.1: Single Phase Fluid Flow Data- LBP1.

Q $[ml/min]$	Q $[m3/s]$	ΔP $[Pa]$	Q/A $[m/s]$	$\Delta P/L$ $[Pa/m]$
5.000	8.333E-08	1560	3.4745E-03	7800
2.000	3.333E-08	570	1.3898-03	2850
1.000	1.667E-08	320	6.9492-04	1600
0.500	8.333E-09	170	3.4746E-04	850
0.200	3.333E-09	68.89	1.3898E-04	344.45

Table 4.2: Single Phase Fluid Flow Data- SBP.

Q $[ml/min]$	Q $[m3/s]$	ΔP $[Pa]$	Q/A $[m/s]$	$\Delta P/L$ $[Pa/m]$
1.000	1.667E-08	8440	6.9492-04	42200
0.500	8.333E-09	4220	3.4746E-04	21100
0.200	3.333E-09	1710	1.3898E-04	8550
0.100	1.667E-09	850	6.9492E-05	4250
0.050	8.333E-10	420	3.4746E-05	2100

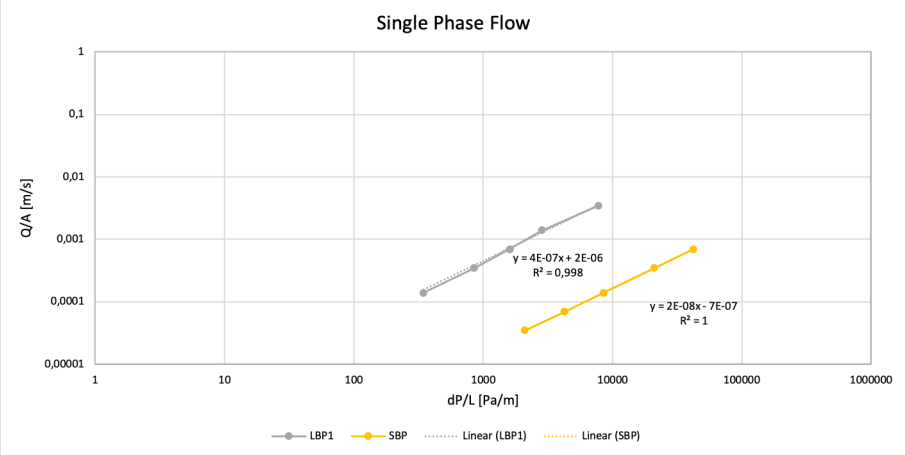

Figure 4.1: Q/A versus $\Delta P/L$ for LBP1 and SBP, with the corresponding linear trend lines for each case.

A new large bead pack (LBP2) had to be made for the surfactant experiments after the first one was damaged. Being of the same materials, with the same dimensions as LBP1, the new bead pack is expected to have properties somewhat equal to LBP1. A single phase experiment is still conducted using the LBP2, as permeability can be strongly dependent on the packing of the glass beads. Results from the LBP2 single phase experiment is presented in table 4.3 and the data is plotted together with the other single phase experiments in figure 4.2.

Table 4.3: Single Phase Fluid Flow Data - LBP2.

Q $[ml/min]$	Q $[m3/s]$	ΔP $[Pa]$	Q/A $[m/s]$	$\Delta P/L$ $[Pa/m]$
5	8,333E-08	860	0,003474582	4300
2	3,333E-08	310	0,001389833	1550
1	1,667E-08	150	0,000694916	750
0,5	8,333E-09	70	0,000347458	350

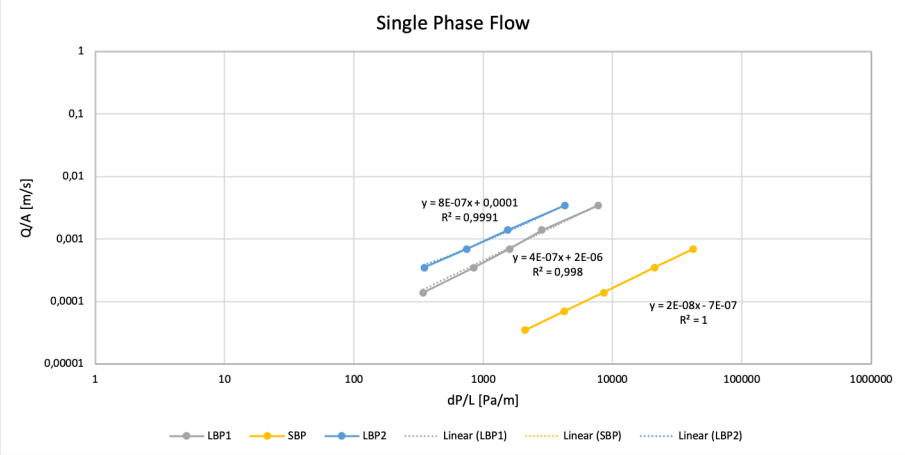

Figure 4.2: Q/A vs. $\Delta P/L$ for all single-phase experiments, with corresponding linear trend lines for each case. LBP1 $\neq$ LBP2.

From the plot in figure 4.2 the permeability of the bead packs could be found. Knowing the flow rate, viscosity, length, and the cross-sectional area of the bead pack, Darcys relation, 2.3, can be used to calculate the permeability of a system. The plotted data show linear trends, and the slope of this line, s, will then be defined as the permeability divided by the viscosity of the flowing fluid. Thus, the permeability can be found using the following relation.

$$s = \frac{k}{\mu_w} \qquad [\mathrm{m}^2\,\mathrm{Pa}^{-1}\,\mathrm{s}^{-1}]$$

$$k = s * \mu_w \qquad [\mathrm{m}^2]$$

Applying this relation to the LBPs and SBP, the effective permeability of the system is the only unknown parameter. This permeability was found to be $k = 716$ Darcy for LBP1, $k = 1432$ Darcy LBP2, and $k = 35.8$ Darcy for SBP.

4.3 Results of Two Phase Experiments

Six experiments were conducted for two-phase flow - two with horizontal flow and four with vertical flow. For the vertical flow experiments, two were conducted using the LBP, and two were conducted using the

SBP. The setup was similar to the setup for the single phase experiment, with the only difference being the junction mixing the two phases before entering the bead pack. See figure 3.2 on page 18 for experimental set-up. As earlier described the setup for the vertical flow experiment is the same as for the horizontal, but tilted 90°. In the following chapter, the measured results will be presented. Flow rate versus corresponding differential pressure will be plotted for each run.

4.3.1 Horizontal Flow

The following tables present the result for the two-phase horizontal flow. These results are plotted in figure 4.3. Values marked * are not considered sufficiently stable or is outside the range and accuracy of the pressure transducers. These values will not be used for further analysis, but are presented here as it can contribute to indicate the trend better.

Table 4.4: Two Phase Horizontal Fluid Flow Data - LBP1 Run 1.

Q $[ml/min]$	Q $[m^3/s]$	ΔP $[Pa]$	Q/A $[m/s]$	$\Delta P/L$ $[Pa/m]$
22.000	3.667E-07	15450	1.5288E-02	77250
20.000	3.333E-07	12500	1.3898E-02	62500
10.000	1.667E-07	5170	6.9492E-03	25850
5.000	8.333E-08	2530	3.4746E-03	12650
2.000	3.333E-08	1150	1.3898E-03	5750
1.000	1.667E-08	600	6.9492E-04	3000
0.500	8.333E-09	380	3.4746E-04	1900
0.200	3.333E-09	210	1.3898E-04	1050
0.100	1.667E-09	130*	6.9492E-05	650
0.050	8.333E-10	35.76*	3.4746E-05	178.8
0.020	3.333E-10	82.651*	1.3898E-05	413.25
0.010	1.667E-10	18.9*	6.9492E-06	94.5
0.005	8.333E-11	47.1*	3.4746E-06	235.5
0.002	3.333E-11	100*	1.3898E-06	500

Table 4.5: Two Phase Horizontal Fluid Flow Data - LBP1 Run 2.

Q $[ml/min]$	Q $[m^3/s]$	ΔP $[Pa]$	Q/A $[m/s]$	$\Delta P/L$ $[Pa/m]$
22.000	3.667E-07	15430*	1.5288E-02	77150
20.000	3.333E-07	13400	1.3898E-02	67000
10.000	1.667E-07	5730	6.9492E-03	28650
5.000	8.333E-08	2710	3.4746E-03	13550
2.000	3.333E-08	1120	1.3898E-03	5600
1.000	1.667E-08	620	6.9492E-04	3100
0.500	8.333E-09	290	3.4746E-04	1450
0.200	3.333E-09	62.99	1.3898E-04	314.97
0.100	1.667E-09	55.05*	6.9492E-05	275.26
0.050	8.333E-10	14.59*	3.4746E-05	72.96
0.020	3.333E-10	-0.375*	1.3898E-05	-72.95
0.010	1.667E-10	44.54*	6.9492E-06	222.695
0.005	8.333E-11	43.85*	3.4746E-06	219.26
0.002	3.333E-11	82.493*	1.3898E-06	412.46

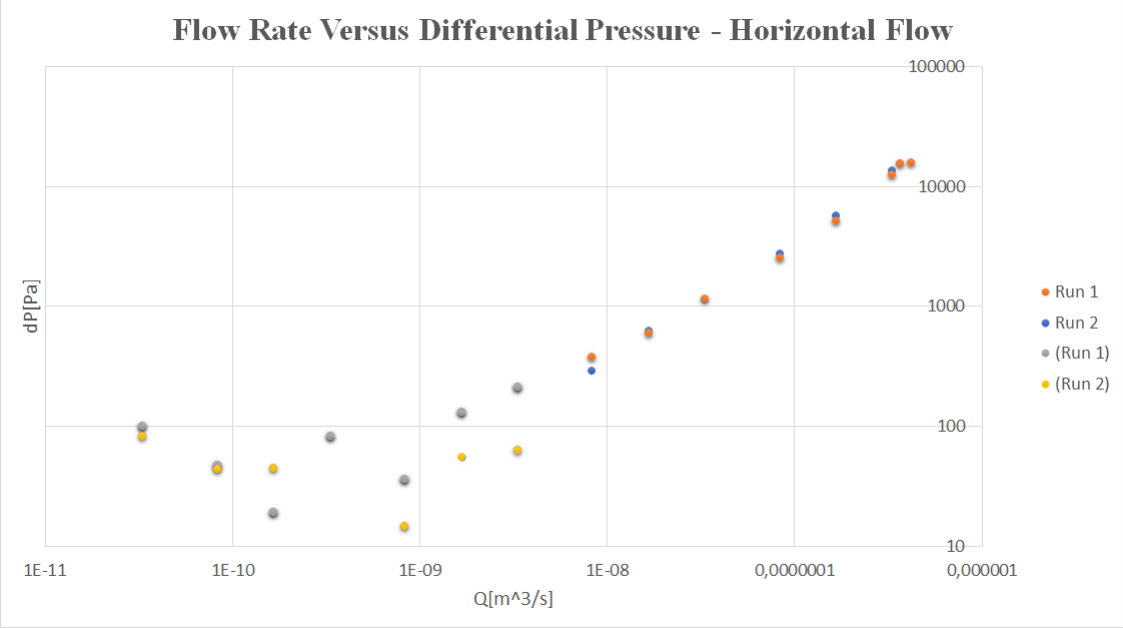

Figure 4.3: ΔP vs. Q for two phase horizontal flow.

All measurements below $Q = 0.2ml/min$ was found to be outside the accuracy of the pressure transducers and cannot be included when further analyzing the results. These results are marked in yellow and grey in figure 4.3. For the remaining results, the data points from the two runs overlap well. An average between the two runs will, therefore, be used for further discussion.

Observations in Horizontal Flow

As the two flowing phases are immiscible, they entered the filter to the bead pack as evenly distributed bubbles. The size of the bubbles is decreasing with increasing flow rate. This can be seen in figure 4.4, where bubble distribution is shown for $Q = 4.0$ ml/min and $Q = 10.0$ ml/min. From this figure, it can also be observed that the teflon tube is oil-wet. For the highest flow rates, the lengths of the bubbles were between 3 to 4 mm, while for the lower flow rates the bubbles were approximately 10 mm. For all flow rates, the bubbles were evenly distributed. When the fluids reached the glass tube they appeared to be flowing simultaneously and side by side. The slugs that had been observed in the teflon tube could no longer be observed in the bead pack. With the glass tube being water-wet, the oil would no longer cling to the surface as it had done in the teflon tube. This made visual observations easier and results more reliable. The glass bead pack had a larger diameter than the teflon tube, and throughout the bead pack, the fluids were found to segregate due to gravitational effects. Because of its lower density, the oil was flowing along the top of the bead pack, while the distilled water was flowing along the bottom. This effect can be seen in figure 4.5. Ganglion movement is first observed at 10 ml/min. Some ganglion movement is observed at the higher rates, but the fluids are mainly flowing in interconnected paths. After some time, the ganglion movement can no longer be observed, and the two phases seem to find their interconnected path. On the second run, when starting at the maximum flow rate and decreasing for each measurement, the ganglion movement is no longer observed at any flow rates. After finding the path of least resistance, the respective fluids seem to stick to that path.

Shortly after starting the experiment, gravitational forces were observed to impact the flow. The difference in density between the fluids led to a gravitational segregating of the fluids. At the top of the bead pack, oil saturation became higher, while water saturation increased at the bottom of the bead pack. This effect can be seen in figure 4.5. The gravitational segregation was more dominant at the lowest rates, as the fluids need time to separate.

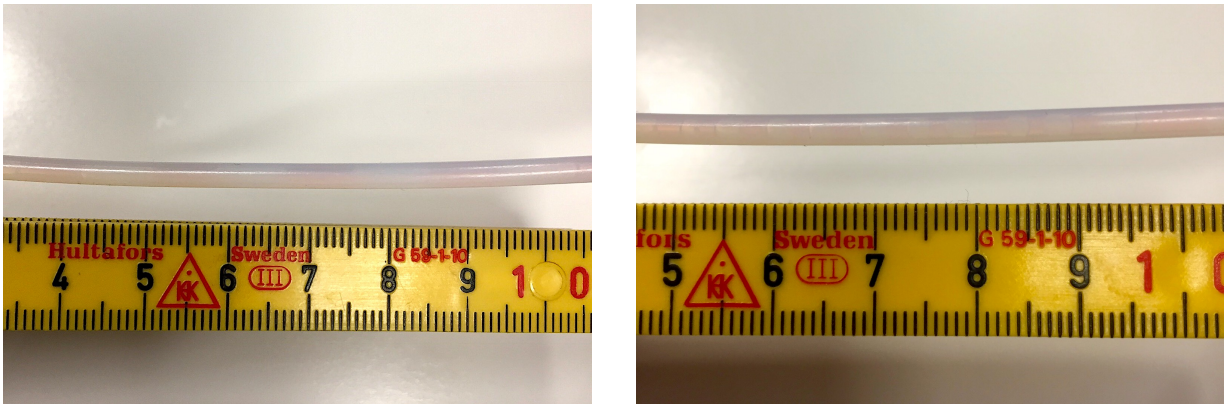

(a) Q = 4.0 ml/min. **(b)** Q= 10.0 ml/min.

Figure 4.4: The size of the droplets in inlet tube is evenly distributed, and decrease with increasing flow rate.

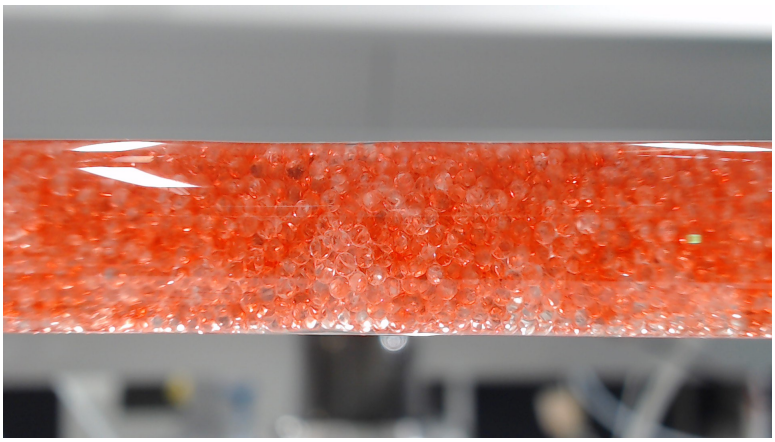

Figure 4.5: During horizontal flow, gravity is affecting the flow by separating the fluids according to density. This effect could be observed at all flow rates. This figure is showing the effect at $Q = 0.2ml/min$.

4.3.2 Vertical Flow

Vertical flow in Large Bead Pack

The following tables present the result for the two-phase vertical flow in the LBP. These results are plotted together with the results from the SBP in figure 4.6.

Table 4.6: Two Phase Vertical Fluid Flow Data - Run 1, LBP1.

Q $[ml/min]$	Q $[m^3/s]$	ΔP $[Pa]$	Q/A $[m/s]$	$\Delta P/L$ $[Pa/m]$
22.000	3.667E-07	14200*	1.5288E-02	71000
20.000	3.333E-07	12690	1.3898E-02	63450
15.000	2.500E-07	8550*	1.0423E-02	42750
10.000	1.667E-07	4820	6.9492E-03	24100
5.000	8.333E-08	2300*	3.4746E-03	11500
2.000	3.333E-08	930	1.3898E-03	4650
1.000	1.667E-08	720	6.9490E-04	3600
0.750	1.250E-08	640	5.2120E-04	3200
0.5000	8.333E-09	560	3.4750E-04	2800
0.4000	6.667E-09	530	2.780E-04	2650
0.3000	5.000E-09	490	2.0850.E-04	2450

Table 4.7: Two Phase Vertical Fluid Flow Data - Run 2, LBP1.

Q $[ml/min]$	Q $[m^3/s]$	ΔP $[Pa]$	Q/A $[m/s]$	$\Delta P/L$ $[Pa/m]$
20.000	3.333E-07	13700*	1.3898E-02	68500
15.000	2.500E-07	8250	1.0423E-02	41250
10.000	1.667E-07	4860	6.9492E-03	24300
5.000	8.333E-08	2500	3.4746E-03	12500
2.000	3.333E-08	1180	1.3898E-03	5900
1.000	1.667E-08	730	6.9490E-04	3650
0.750	1.250E-08	630	5.2120E-04	3150
0.5000	8.333E-09	540	3.4750E-04	2700
0.4000	6.667E-09	490	2.780E-04	2450
0.3000	5.000E-09	500	2.0850.E-04	2500

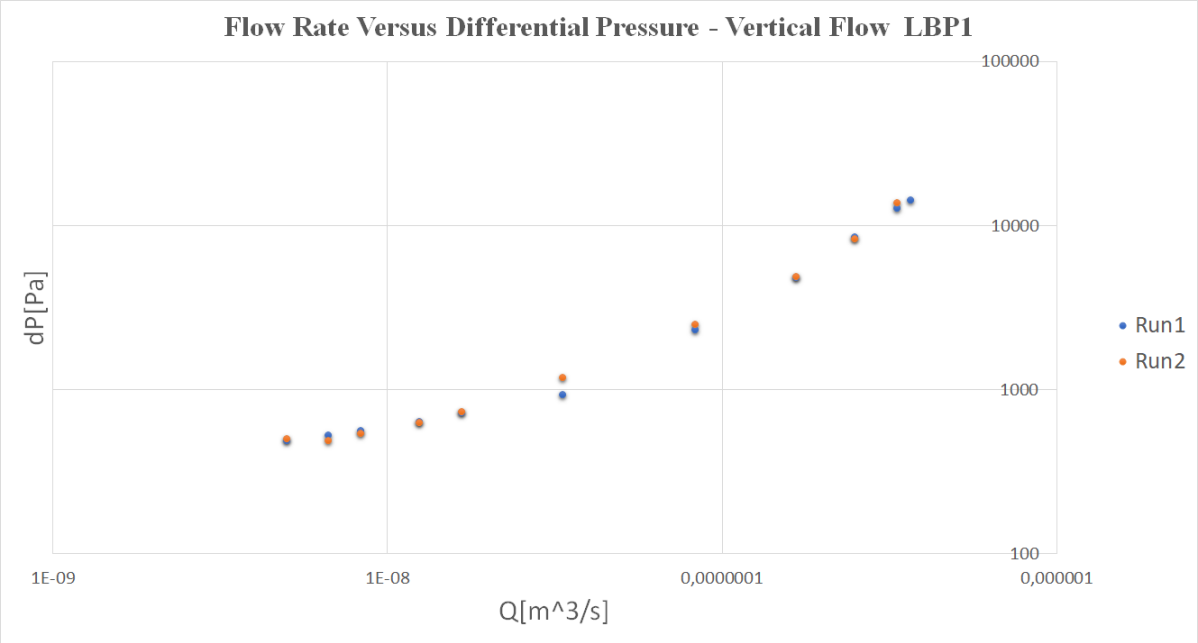

Figure 4.6: ΔP vs. Q for two phase vertical flow in LBP.

All data points from the two runs overlap well. An average between the two runs will thus be used for further discussion.

Vertical flow in Small Bead Pack

The following tables present the result for the two-phase vertical flow in the SBP. These results are plotted together with the earlier presented results from the LBP in figure 4.7.

Table 4.8: Two Phase Vertical Fluid Flow Data - Run 1, SBP.

Q $[ml/min]$	Q $[m^3/s]$	ΔP $[Pa]$	Q/A $[m/s]$	$\Delta P/L$ $[Pa/m]$
2	3.33333E-08	47340*	0.001568763	236700
1	1.66667E-08	29360*	0.000784382	146800
0.5	8.33333E-09	15330	0.000392191	76650
0.2	3.33333E-09	7490	0.000156876	37450
0.1	1.67E-09	2840	7.84382E-05	14200
0.05	3.33333E-10	1290	1.56876E-05	6450
0.02	8.33333E-10	1170*	3.92191E-05	5850
0.01	1.66667E-10	1110	7.84382E-06	5550

Table 4.9: Two Phase Vertical Fluid Flow Data - Run 2, SBP.

Q $[ml/min]$	Q $[m^3/s]$	ΔP $[Pa]$	Q/A $[m/s]$	$\Delta P/L$ $[Pa/m]$
0.5	8.33333E-09	12230	0.000392191	61150
0.2	3.33333E-09	4960	0.000156876	24800
0.1	1.66667E-09	2650	7.84382E-05	13250
0.05	8.33E-10	1660	3.92191E-05	8300
0.04	6.66667E-10	1290	3.13753E-05	6450
0.02	3.33333E-10	900*	1.56876E-05	4500
0.015	2.5E-10	1000*	1.17657E-05	5000

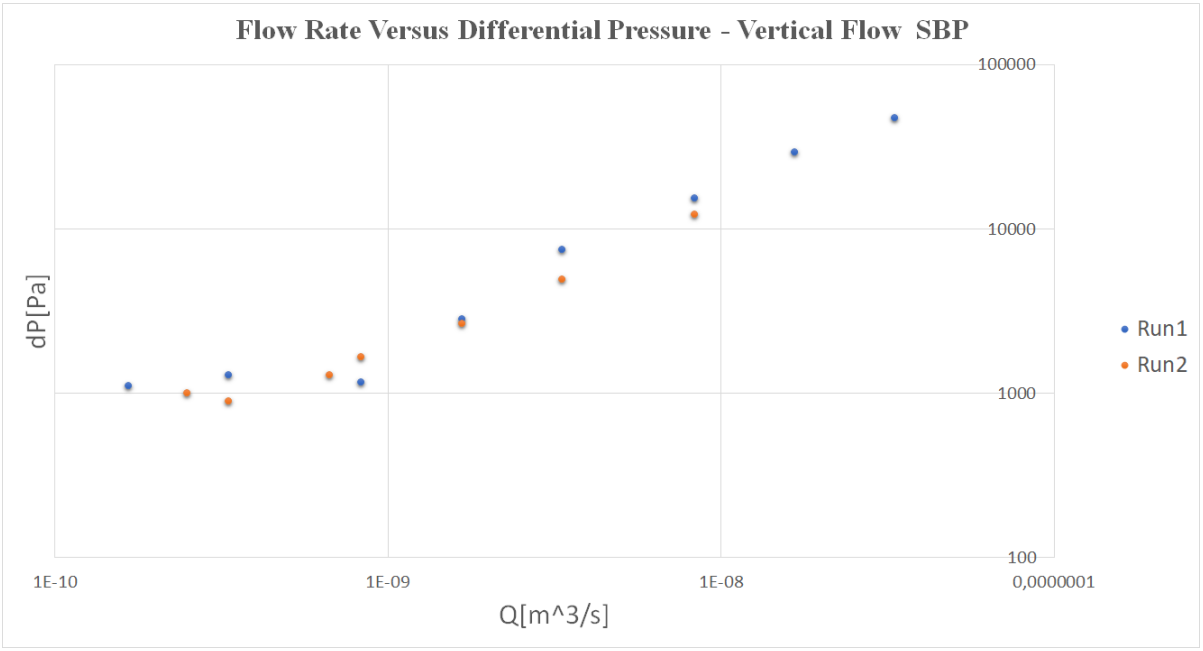

Figure 4.7: ΔP vs. Q for two phase vertical flow in SBP.

All upper data points from the two runs overlap well. An average between these point in the two runs will be used for further discussion. Within the lower data points, there are greater variations, and these are believed to be outside the accuracy of the transducers. This data will not be used for further analysis.

Observations in Vertical Flow

At the inlet to the bead pack, the two fluids are observed to behave similarly as to how they behaved for the horizontal flow where they entered the filter to the bead pack as evenly distributed bubbles. The size of the bubbles decreased with increasing flow rate. For all flow rates, the bubbles were evenly distributed.

During the horizontal flow experiment gravitational effects were found to impact the flow by segregating the fluids so that oil saturation was higher at the top of the bead pack while water saturation was higher at the bottom. During this experiment, the wettability of the bead pack seems to have changed. When the direction

of flow is changed to vertical flow, and gravity no longer affects the flowing patterns, both phases are found to still follow the same path as they did during the vertical flow experiment. Evenly distributed saturation is not achieved and may impact the flow patterns of the fluids. Ganglion movement is not observed for any rates during the vertical flow.

At the outlet of the bead pack, the fluids occasionally flow simultaneously side by side, which substantiates the assumption that both phases are flowing simultaneously in the bead pack. Occasionally the fluids are leaving the outlet filter as larger clusters. This does not necessarily mean that the fluids are flowing as large droplets in the bead pack, as there is room in the filter for accumulation of fluids. Thus we can not determine how the fluids move at the outlet of the bead pack.

4.4 Results for Surfactant Experiment

4.4.1 Two Phase Flow - with Zalo as Surfactant

The following tables present the result for the two-phase vertical flow with zalo in the water phase. These experiments were run in the LBP2. The results are plotted in figure 4.8.

Table 4.10: Two Phase Vertical Fluid Flow Data with Zalo - Run 1, LBP2.

Q $[ml/min]$	Q $[m^3/s]$	ΔP $[Pa]$	Q/A $[m/s]$	$\Delta P/L$ $[Pa/m]$
15	2,500E-07	5870	0,010423745	29350
10	1,667E-07	3960	0,006949163	19800
5	8,333E-08	2770	0,003474582	13850
2	3,333E-08	1880	0,001389833	9400
1	1,667E-08	1370	0,000694916	6850
0,75	1,250E-08	1270	0,000521187	6350
0,5	8,333E-09	1040	0,000347458	5200
0,4	6,667E-09	920	0,000277967	4600
0,3	5,000E-09	880	0,000208475	4400

Table 4.11: Two Phase Vertical Fluid Flow Data with Zalo - Run 2, LBP2.

Q $[ml/min]$	Q $[m^3/s]$	ΔP $[Pa]$	Q/A $[m/s]$	$\Delta P/L$ $[Pa/m]$
15	2,500E-07	4800	0,010423745	24000
10	1,667E-07	3700	0,006949163	18500
5	8,333E-08	3300	0,003474582	16500
2	3,333E-08	1970	0,001389833	9850
1	1,667E-08	1400	0,000694916	7000
0,75	1,250E-08	1150	0,000521187	5750
0,5	8,333E-09	930	0,000347458	4650
0,4	6,667E-09	850	0,000277967	4250
0,3	5,000E-09	700	0,000208475	3500

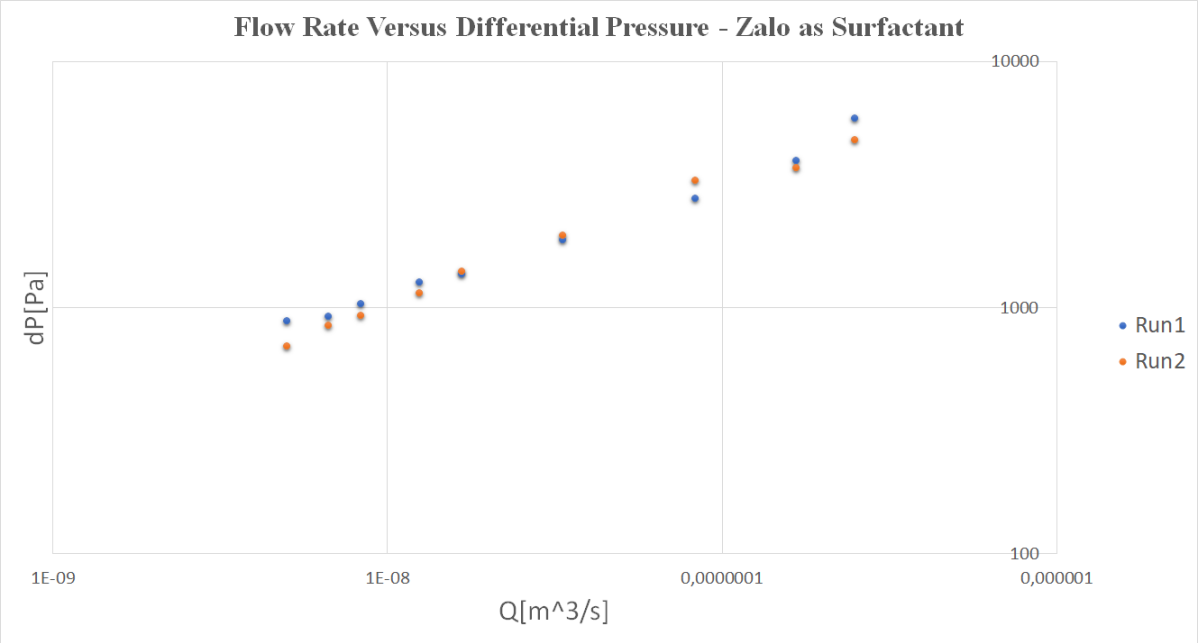

Figure 4.8: ΔP vs. Q for two phase vertical flow in LBP, with zalo as a surfactant.

All data points from the two runs overlap well. This validates the results of the experiment. An average between the two runs will, therefore, be used for further discussion.

Observations in Zalo Experiment

At the highest rates, the two phases are behaving as an emulsion throughout the system. They are mixed in the reservoir, see figure 4.12a, and entering the bead pack as one phase. For flow rates below 2 ml/min, this problem decreases, as water and oil start separating in the reservoir. Two phases are observed to enter the bead pack, but both phases seem to be emulsions. One containing more oil, and one containing more water, but both oil and water appear to be present in both phases. Through the bead pack, the two phases fully mix and exit the bead pack as one emulsion. This effect is consistent for all flow rates tested.

In the bead pack, the oil is observed to be moving as small droplets within the water phase. The surfactant seems to make the oil droplets small enough to move through the same pore throats as the water does. Even if the rate is low enough for the oil and water to enter the bead pack as two phases, they leave the bead pack as an emulsion.

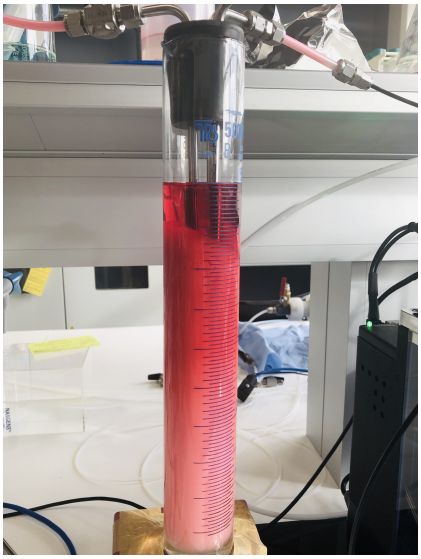

(a) Reservoir at high rates with oil and water in an emulsion.

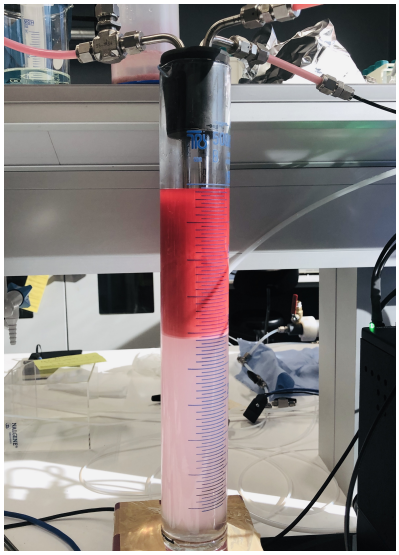

(b) Oil and water separate in different phases at lower rates. Both phases still contains both oil and water.

Figure 4.9: Showing the effect of adding Zalo to the reservoir.

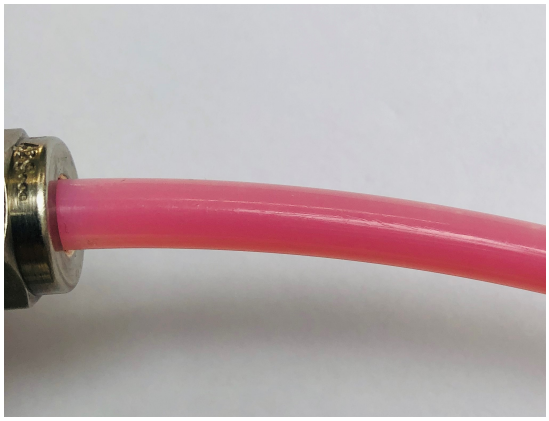

Figure 4.10: Oil and water is observed as an emulsion at the outlet of the bead pack.

4.4.2 Two Phase Flow - with Sodium Dodecyl Sulfate as Surfactant

The following tables present the result for the two-phase vertical flow with SDS in the water phase. These experiments were run using the LBP2. The results are plotted in figure 4.11.

Table 4.12: Two Phase Vertical Fluid Flow Data with SDS - Run 1, LBP.

Q $[ml/min]$	Q $[m^3/s]$	ΔP $[Pa]$	Q/A $[m/s]$	$\Delta P/L$ $[Pa/m]$
15	2,500E-07	10100	0,010423745	50500
10	1,667E-07	8400	0,006949163	42000
5	8,333E-08	6080	0,003474582	30400
2	3,333E-08	3890	0,001389833	19450
1	1,667E-08	2870	0,000694916	14350
0,75	1,250E-08	3300	0,000521187	16500
0,5	8,333E-09	3500	0,000347458	17500
0,4	6,667E-09	3370	0,000277967	16850
0,3	5,000E-09	2870	0,000208475	14350

Table 4.13: Two Phase Vertical Fluid Flow Data with SDS - Run 2, LBP.

Q $[ml/min]$	Q $[m^3/s]$	ΔP $[Pa]$	Q/A $[m/s]$	$\Delta P/L$ $[Pa/m]$
15	2,500E-07	10500	0,010423745	52500
10	1,667E-07	8500	0,006949163	42500
5	8,333E-08	5900*	0,003474582	29500
2	3,333E-08	3900	0,001389833	19500
1	1,667E-08	2900	0,000694916	14500
0,75	1,250E-08	2600	0,000521187	13000
0,5	8,333E-09	2300	0,000347458	11500
0,4	6,667E-09	2200	0,000277967	11000
0,3	5,000E-09	2100	0,000208475	10500

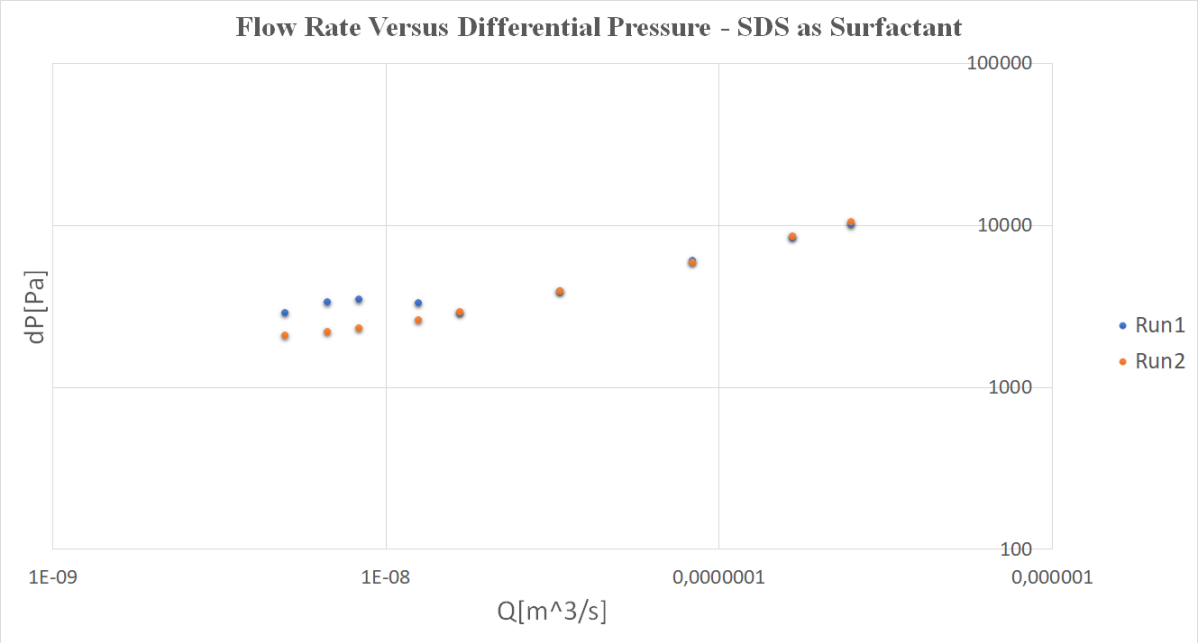

Figure 4.11: ΔP vs. Q for two phase vertical flow in LBP, with SDS as a surfactant.

All upper data points from the two runs overlap well. This validates the results of the experiment. The lower points do not overlap but show the same trend. An average between the two runs will thus be used for further discussion.

Observations in SDS Experiment

Observations verify that SDS is a weaker surfactant than zalo. The fluids are behaving as two phases in the reservoir and into the bead pack for flow rates below 10 ml/min. Through the bead pack, the two phases are mixed and exit the bead pack as an emulsion. For flow rates above 10 ml/min, the fluids are behaving as an emulsion throughout the system. See figure 4.12.

In the bead pack, the observations are similar to those of the zalo experiment during low flow rates. In the bead pack, the oil is observed to be moving as small droplets within the water phase. The surfactant seems to make the oil droplets small enough to move through the same pore throats as the water does. Even if the two phases enter the bead pack as two phases, they leave the bead pack as an emulsion.

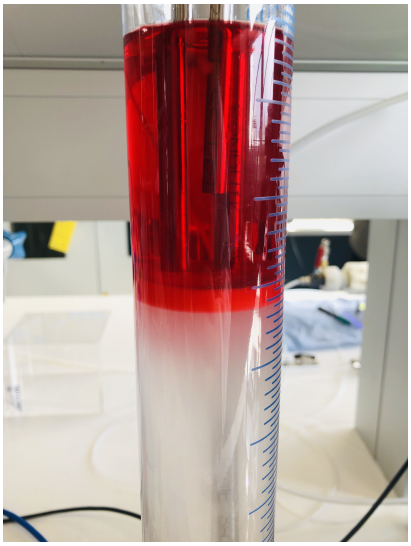

(a) Emulsion in reservoir when $Q = 10ml/min$.

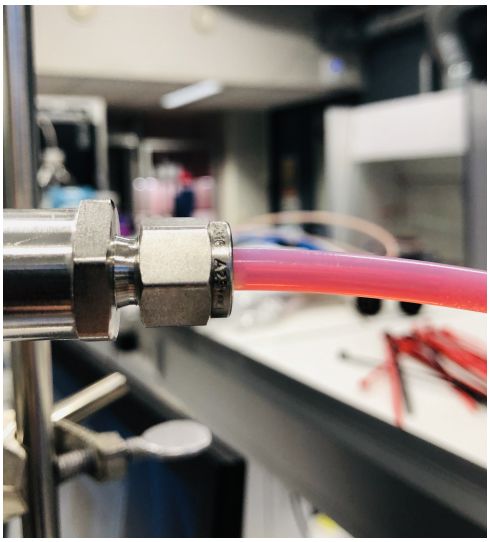

(b) The fluids are observed to flow as an emulsion at the outlet of the bead pack. This effect is observed for all flow rates.

Figure 4.12: Showing emulsions in the system during Sodium Dodecyl Sulfate experiment.

Chapter 5

Discussion

In this chapter, the validity of the measured data will first be discussed. Further, the steady-state results presented in chapter 4 will be discussed and interpreted, as well as compared to results from similar experiments. Last, potential sources of error will be considered.

5.1 Data Validity

5.1.1 Overlap

For each experiment, there were conducted two runs. One was increasing the flow rate up to the maximum rate, and one was decreasing the flow rate back to the initial starting point. Each measured flow rate should produce about the same pressure drop for both runs, given that all other factors are kept constant. In the plotted results presented in chapter 4, this is seen as overlapping data points. When hysteresis is low, the overlapping data points are considered valid data, and these can be used for further analysis. If the data does not overlap, it is not considered as valid results, and thus will be omitted during analysis. Many of these data points are found at the lower rates. This is believed to be because the pressures are outside the accuracy range of the pressure transducers.

5.1.2 Serial Correlation

Serial correlation, or autocorrelation, is the relationship between a variable and a lagged version of itself over various time intervals. Repeating patterns often show serial correlation when the level of a variable affects its future level (Shumway and Stoffer, 2017). Serial correlation is thus often used in signal processing as a mathematical tool for finding repeating patterns. If a background noise exists, this needs to be accounted for before analyzing the results. Therefore, the serial correlation of the no-flow case is checked. This is done by plotting the autocorrelation function, C, defined in equation 5.1. When the function drops to zero, or within a given significance limit, there is no longer any serial correlation between the data points. The autocorrelation for the noise in the no-flow case, for both pressure transducers, are plotted in figure 5.1. Notice that after < 10 time steps, where one timestep is 0.1 second, there is no longer any correlation between the data. This noise can thus be considered as random and insignificant. As long as the data point lies within the accuracy of the transducers, the data is deemed to be adequate. A cutoff value is implemented to the MATLAB code, to remove extreme values before calculating the average.

$$C = \frac{\frac{1}{n}\sum(p(t) - p(\bar{t})(p(t + \Delta t) - p(\bar{t}))}{\frac{1}{n}\sum(p(t) - p(\bar{t}))^2} \tag{5.1}$$

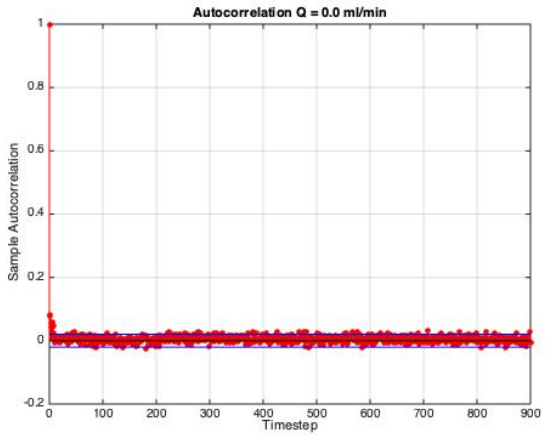

(a) Serial correlation of background noise using the UNIK 5000 pressure transducers.

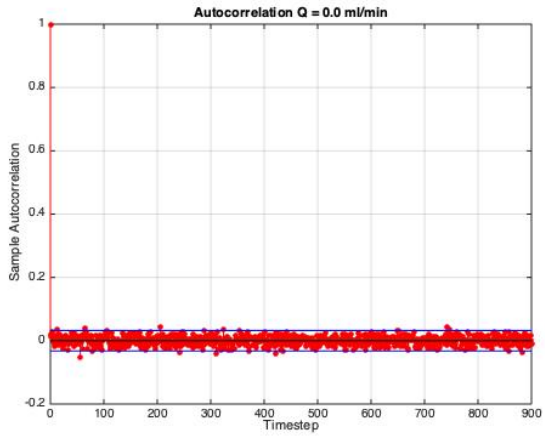

(b) Serial correlation of background noise using the Keller PRD-33X pressure transducer.

Figure 5.1: Serial correlation for the no flow cases indicates no correlation between the data. This noise is considered random and insignificant.

Background noise with a repeating pattern would be beneficial to account for using a filter, but seeing that there is little to no repeating noise in the measured data, a filter is considered unnecessary. The largest spikes of the background noise are of about $0.006bar$ and will not significantly affect the results. The measured background noise can be found in Appendix B.

5.2 Permeability

In section 4.2, the absolute permeability of the bead packs were calculated and presented. When a second fluid is introduced to the system, the effective permeability of the fluids will decrease, as mentioned in section 2.1.3.

The relation between the single-phase permeability and the two-phase permeability can be illustrated when the flux is plotted against the pressure gradient for both single-phase and two-phase. In figure 5.2, the lines representing the two-phase experiments are shifted more to the right than in the results from the single-phase experiments for the same bead pack. This is consistent with the theory of relative permeability. All measured data show a good fit to the linear trend, indicating valid measurements

The relative permeability can be calculated using the same relation as presented in section 4.2 for the single phase experiment. The viscosity has been estimated by assuming a 50/50 oil/water saturation. This estimated viscosity is used when calculating the permeability. All permeabilities are presented in table 5.1. The single phase permeabilities are the same as presented in 4.2.

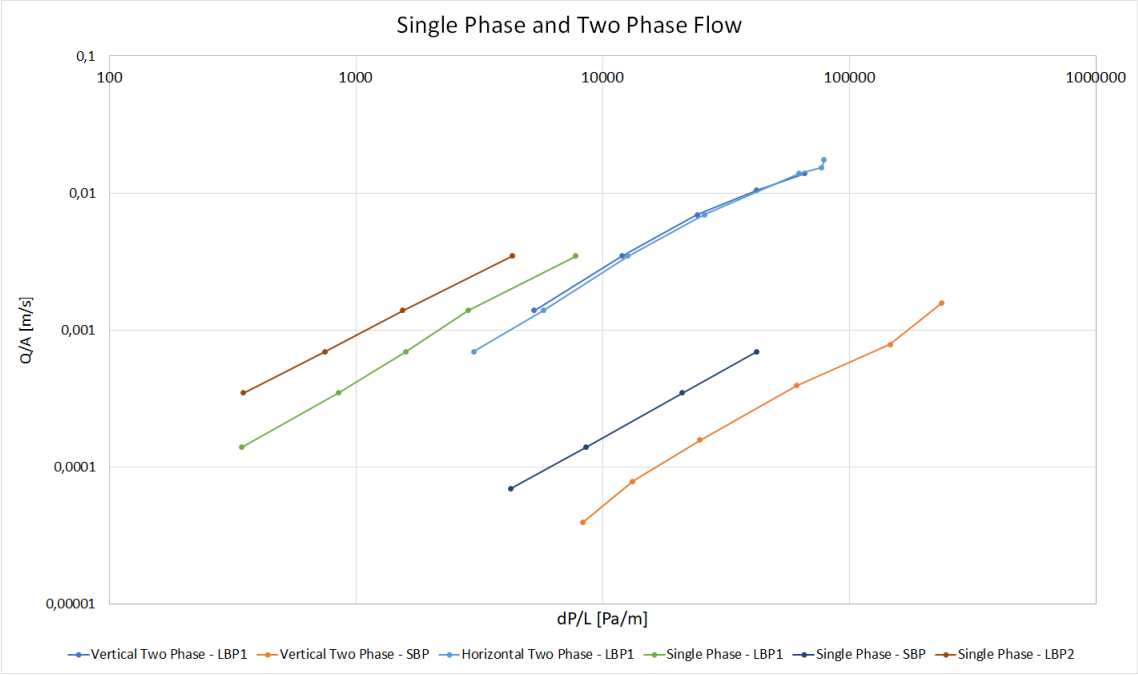

Figure 5.2: Flux versus pressure gradient for single and two phase flow experiments.For each experiment, only the upper data point that indicate a linear regime is used in this plot.

Table 5.1: Relative permeability for single phase (SP) and two phase(TP) experiments. For the SP experiments $k_e = k_a$.

$Experiment$ [$-$]	s [$m^2/Pa * s$]	k_e [$mDarcy$]
SP-LBP1	4.00E-07	716
SP-LBP2	8.00E-07	1432
SP-SBP	2.00E-08	35.8
TP-Hor-LBP1	2.00E-07	322
TP-Ver-LBP1	2.00E-07	322
TP-Ver-SBP	6.00E-09	9.66

Notice that the permeabilities of the SBP are significantly lower than those of the LBP1 and LBP2. This corresponds to the pore structure of small beds where the pore space between beads is smaller. Both horizontal and vertical flow in LBP1 give the same relative permeability, for the upper data point as the direction of flow does not affect the relative permeability, when in the same flow regime. Also, note that the permeability of the two LBPs does not overlap even if the dimensions of the tube and materials are similar. Thus, the packing of the beads seems to be critical for permeability.

5.3 Identification of Flow Regimes and Scaling relationship

In the following sections, the results presented in chapter 4 will be interpreted and discussed. For each case, the results concerning the threshold pressure will first be addressed, before going into detail about the observed flow regimes and scaling relations, comparing the results to the findings by Sinha et al. (2017), Husøy (2018) and Anfinsen (2018).

5.3.1 Horizontal Flow

By visual analysis of the results plotted in figure 4.3, all valid data points appear to follow the same linear trend. From this, there cannot be identified two distinct flow regimes for horizontal flow as predicted by Sinha et al. (2013).

However, according to Sinha et al. (2013), a threshold pressure need to be identified and accounted for before different regimes can be identified. Considering the threshold pressure is identified as the pressure required for the flow to start, this threshold pressure is found by extrapolating the trend line to the point where it intersects with the y-axis, in the plot of Q vs. ΔP. Applying this to the results of the horizontal flow experiment yields a somewhat negative threshold pressure. This is a mathematical solution, not a physical. A threshold pressure cannot be negative. Thus we consider the threshold pressure to be zero, or non-existing, for the horizontal flow case, i.e., $\Delta P_t = 0$.

To investigate possible scaling relationships, the pressure is plotted against the capillary number. This is presented in figure 5.3, where results are plotted together with results form Husøy (2018) for comparison. As $\Delta P_t = 0$ this does not need to be accounted for, and the result is still comparable to results by both Husøy (2018) and Sinha et al. (2017). An average between measured values of run 1 and run 2 has been used for this analysis.

Table 5.2: Two Phase Horizontal Fluid Flow Data - Average values.

Q [ml/min]	Q [m3/s]	Ca [-]	ΔP [Pa]	log Ca [-]	log(ΔP) [-]
22	3.6667E-07	7.95E-04 6	15440	-3.100	4.1886
20	3.3333E-07	7.22E-04	12950	-3.141	4.1120
10	1.6667E-07	3.61E-04	5450	-3.442	3.7358
5	8.3333E-08	1.81E-04	2620	-3.743	3.4180
2	3.3333E-08	7.22E-05	1135	-4.141	3.0550
1	1.6667E-08	3.61E-05	610	-4.442	2.7853

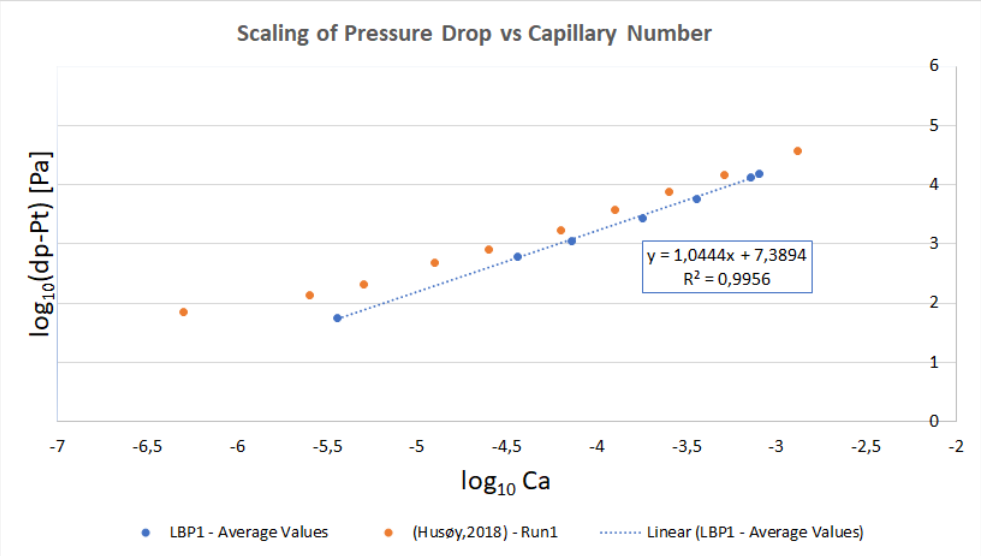

Figure 5.3: Logarithmic plot of capillary number versus differential pressure. Only one flow regime is observed, and the slope is $\beta = 1.0444 \simeq 1$.

For $\Delta P \sim Ca^{\beta}$, the scaling relationship of $\beta \sim 1$ corresponds to the upper regime reported by Sinha et al. (2017). Following the theory by Sinha et al. (2017), the transition to the upper regime should correspond to when ganglion movement is first observed. Some ganglion movement was observed during the horizontal flow, but these were first observed at $Q = 10ml/min$. The ganglion movement was a transitory effect, and during steady-state, the fluids flowed in interconnected paths. Thus the results of the horizontal flow experiment do not support the theory presented in Sinha et al. (2017).

In figure 5.3 the results from Husøy (2018) is plotted together with the results from this thesis. Husøy (2018) did identify a deviation from the linear regime at low flow rates when flowing horizontally through a bead pack of the same dimensions as the LBP1. In the experiment by Husøy (2018) the pressure has been measured directly at inlet and outlet of the bead pack. If the two phases are not entering the porous medium simultaneously but in separate bulks of fluid, it is possible that only one phase is moving at the time at the inlet of the porous media. This will cause a higher use of energy as varying velocities are more energy-intensive than moving at a constant rate. This effect will be diminishing following the principle of diffusivity, and the two phases will flow simultaneously after some time. For this thesis, modifications were made to the experimental setup, and the pressure drop was measured at a distance from both inlet and outlet of the bead pack. This resulted in only one identified regime, and thus substantiates the assumption that the lower regime found by Husøy (2018) is due to boundary effects, and not the threshold pressure that Sinha et al. (2013) presents.

Even if a lower regime cannot be observed in figure 5.3 for the results from this thesis, the existence of a lower flowing regime cannot be dismissed. At lower flow rates, the measured data points presented in figure 4.3 are varying, assumably because of inaccuracy in the pressure transducers. As the accuracy of the pressure transducers is not sufficient for measuring these low pressures, a lower regime might exist, but cannot be found from these result. Ideally, there should be more data points in the lower regime to identify the threshold pressure with more accuracy.

During the conduction of the horizontal flow experiment, the fluids were observed to segregate due to gravity effects. Gravitational forces had not been accounted for earlier during the experiment. To check the effect of gravity, the bond number was calculated. The size of an oil droplet inside the tubing must be smaller than the diameter of the tubing itself. Assuming a diameter of $d = 1.8mm$, which is the diameter of the smaller tube leading into the bead pack, and using $g = 9.81m/s^2$, we get a bond number of 0.215, from equation 2.2. This indicates that the initial assumption of neglecting gravitational forces was not correct. The segregation of the two phases corresponds to the findings of Zhang et al. (2016), who states that gravity will affect the flow for $Bo > 0.1$. The segregation of the two phases facilitates interconnected flow paths. Thus the experiment is comparable to the experiments by Husøy (2018) and Anfinsen (2018), where interconnected paths were facilitated by a difference in wettability within the bead pack.

To better compare the experiment to Sinha et al. (2017) it was decided to rotate the experimental set-up 90°and flow in a vertical direction, as this is done in the experiment by Sinha et al. (2017).

5.3.2 Vertical Flow

For the large bead pack vertical flow experiment, the LBP1 was used. This is the same bead pack as used in the horizontal flow experiment. When starting the vertical flow experiment, the wettability of the bead pack was observed to have changed. The fluids still followed the same interconnected paths as in the horizontal flow experiment, were gravity effects had segregated the fluid. Results from the vertical flow experiment are found to differ from the horizontal flow experiment. Among else, it indicates a threshold pressure.

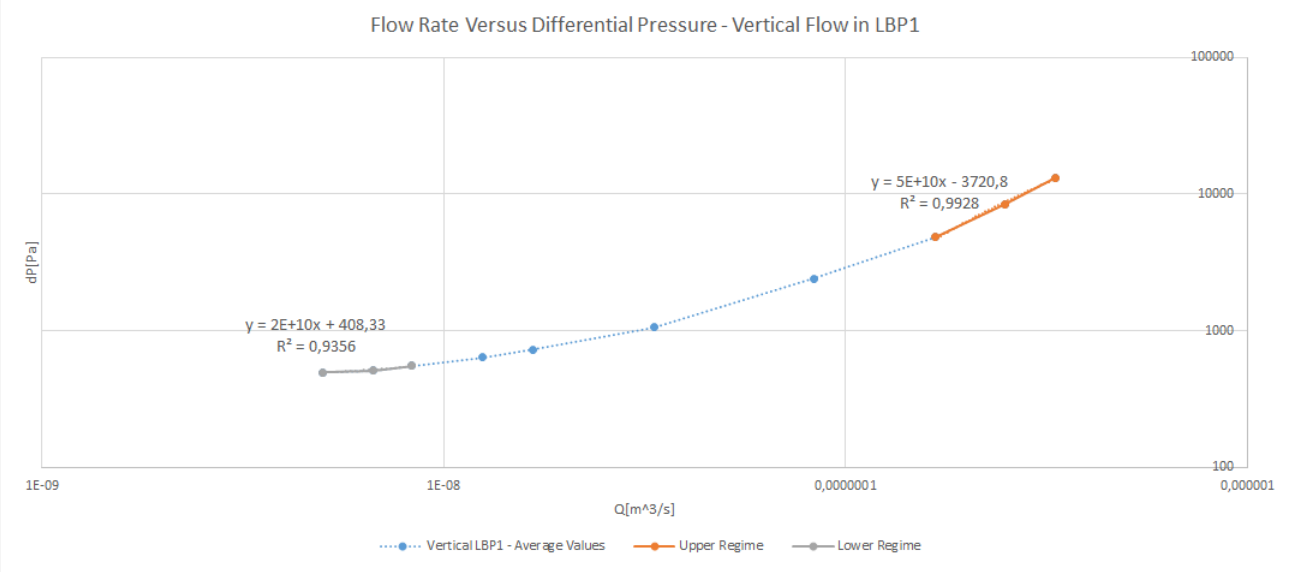

Figure 5.4: A transition between two distinct flow regimes can be observed in the LBP1. A threshold pressure was calculated from the trend line of the lower regime. The constant describing the upper regime yield a quite large negative number. This number is very sensitive to small deviations in the measured data, and can thus be overlooked.

From the plotted result from the vertical flow in LBP1, a transition between two flow regimes is observed. The average of these results is are plotted in figure 5.4, and the two possible flow regimes are indicated. The upper flow regime follows the same trend as that identified in the horizontal flow, but for lower rates, the

slope takes a non-linear turn and seems to extrapolate to a non-zero value. This non-zero value is defined as the threshold pressure, P_t as discussed in section 2.2 and reported by Sinha et al. (2017). By extrapolating the trend line of the lower regime, the threshold pressure is found to be $408.33Pa$. The transition zone between flow regimes is found at a flow rate of approximately $3.33 \times 10^{-8} m^3/s$, which corresponds to approximately $Ca = 2 \times 10^{-5}$. This is somewhat consistent with both Sinha et al. (2017) and Husøy (2018), who found a transition point at $Ca \approx 10^{-4.75}$ and $Ca \approx 10^{-5}$, respectively. However, this result differs from what was found in the numerical simulations of Sinha et al. (2017). In their paper, the authors point out that the transition point between phases might depend on different factors, like pore space geometry, saturation and viscosity ratio, and thus might vary with different experiments.

As presented in section 4.3, the two different regimes seen in the LBP1 cannot be observed for the SBP. For the SBP, the results are similar to the results of the horizontal flow, with only one linear regime, indicating a non-existing threshold pressure, i.e., $\Delta P_t = 0$. These results match the results by Husøy (2018). The flow regime detected in the SBP seems to be corresponding to the upper regime identified in the LBP. In her thesis, Husøy (2018) indicated that the transition to a lower regime might be found at lower flow rates for the SBP and that by investigating even lower rates one might be able to identify a second flow regime. This theory does not match the theory by Sinha et al. (2013). Sinha et al. (2013) suggests that the threshold pressure is created by capillary forces at the interface between two fluids in the pore throat. Thus, stronger capillary forces should lead to a higher threshold pressure. According to Sinha et al. (2013) the flow changes from the lower to the upper regime when all thresholds are overcome and the two phases are flowing as ganglions in all pore throats. Following this theory, as the capillary forces are stronger in the SBP, the change of flow regimes should be observed more to the right for the SBP than the LBP. As this is not the case for the SBP, this can indicate that the theory behind the ganglion movement described by Sinha et al. (2013) cannot be applied to this experiment.

As the two flow regimes can only be observed in the vertical flow experiment, it is natural to think the effect is related to gravitational forces, as all other properties are identical to those in the horizontal flow experiment. Remember that the bond number was estimated to around 0.215 and that gravitational segregation was clearly observed during the horizontal flow experiment. For the vertical flow experiment, gravitational forces will affect the flow even more, and gravitational segregation must be accounted for when analyzing the result. During gravitational segregation, the relative permeability will vary through the bead pack, as oil saturation will be higher at the top of the bead pack, while the bottom of the bead pack will have a higher water saturation. The relative permeability of oil, k_{ro} will be lower at the bottom of the bead pack where S_w is high, while k_{rw} will be low at the top of the bead pack where S_w is low. A varying relative permeability will yield a lower effective permeability than that for a constant saturation. This leads to a larger ΔP, where more energy is used, and we get a lower scaling coefficient; $\beta < 1$.

In their experiment, Sinha et al. (2013) choose to ignore the effect of gravitation in their analysis based on the bond number, which they calculate to be approximately 0.001. As introduced in chapter 2 the bond number is defined as:

$$Bo = \frac{\Delta \rho g L_b^2}{\sigma}$$

Comparing the bond number of Sinha et al. (2017) to that of this thesis, we see that $\Delta\rho$ is larger by a factor of three, while σ is larger by a factor of two. This means that the low bond number calculated by Sinha et al.

(2017) solely depends on L_b^2 that they choose to be around $100\mu m$. Based on the results of this thesis, where gravitational forces are found to affect the result of the vertical flow experiment, it is reasonable to belie that gravitational forces should not have been ignored by Sinha et al. (2017). If gravitational segregation occurs, the effect is strongest at lower rates because the phases need time to segregate. Thus, the lowest relative permeability in the bead pack is found at the lowest flow rate. If gravitational segregation occurred during the experiment by Sinha et al. (2017) this could describe the deviation from the linear regime at low flow rates, without implying a threshold pressure.

The results of the vertical flow in the SBP neither support nor contradict this theory. A lower regime was not identified, but the stronger capillary forces can counteract the gravitational segregation. Thus, even lower rates would need to be investigated to identify it.

To interpreter the transition between flow regimes, and compare results to the results from other experiments as done for the horizontal flow case, the logarithm of the pressure drop minus the threshold pressure was plotted as a function of the logarithm of the capillary number. Table 5.3 and 5.4 presents the the average values used for both the LBP1 and SBP. Plotted results can be seen in figure 5.5 and 5.6.

Table 5.3: Two Phase Vertical Fluid Flow Data - LBP1.

Q [m$^3/s$]	ΔP [Pa]	log($\Delta P - P_t$) [Pa]	Ca [-]	log Ca [-]
5E-09	495	2.0397	1.08342E-05	-4.9652
6.66667E-09	510	2.0902	1.44456E-05	-4.8403
8.33333E-09	550	2.2159	1.80571E-05	-4.7434
1.25E-08	635	2.3973	2.70856E-05	-4.5673
1.66667E-08	725	2.5310	3.61141E-05	-4.4423
3.33333E-08	1055	2.8182	7.22282E-05	-4.1413
8.33333E-08	2400	3.3037	0.000180571	-3.7434
1.66667E-07	4840	3.6488	0.000361141	-3.4423
2.5E-07	8400	3.9038	0.000541712	-3.2662
3.33333E-07	13195	4.1072	0.000722282	-3.1413

Table 5.4: Two Phase Vertical Fluid Flow Data - SBP.

Q [m$^3/s$]	ΔP [Pa]	log($\Delta P - P_t$) [Pa]	Ca [-]	log Ca [-]
2.5E-10	1000	2.7887	6.11453E-07	-6.2136
3.33333E-10	900	2.7115	8.15271E-07	-6.0887
6.66667E-10	1290	2.9565	1.63054E-06	-5.7877
8.33333E-10	1660	3.1054	2.03818E-06	-5.6908
1.66667E-09	2650	3.3550	4.07635E-06	-5.3897
3.33333E-09	4960	3.6604	8.15271E-06	-5.0887
8.33333E-09	12230	4.0735	2.03818E-05	-4.6908
1.66667E-08	29360	4.4620	4.07635E-05	-4.3897
3.33333E-08	47340	4.6717	8.15271E-05	-4.0887

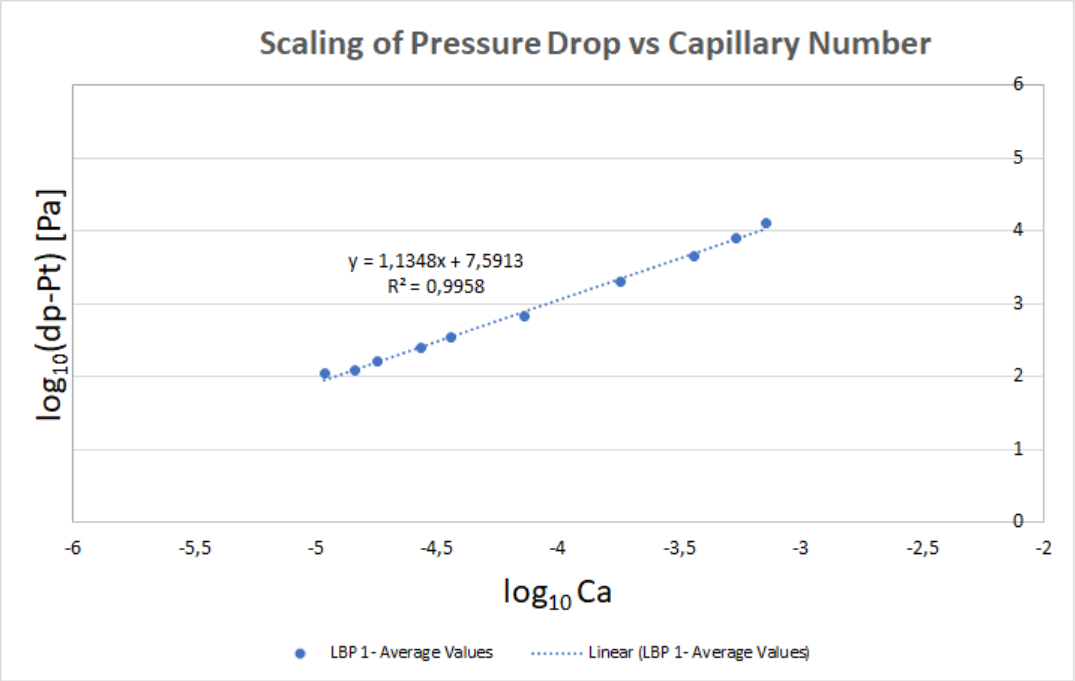

Figure 5.5: Scaling of Pressure drop versus capillary number for two phase vertical flow in LBP1. A transition point to a lower regime is no longer detectable. Only one flow regime is observed, with a slope of $\beta = 1.1348$. This β is slightly larger than that of the upper regime by Sinha et al. (2017) where $\beta \simeq 1$.

When accounting for the threshold pressure, the two regimes earlier observed in figure 5.4 for LBP1 can no longer be observed. All data points can be seen as part of the same regime, following a linear trend, with a scaling coefficient of $\beta = 1.1348$. The results are now similar to the SBP where $\beta = 0.9594 \approx 1$. The results from the SBP corresponds well to what Sinha et al. (2017) identifies as the upper regime. For the LPB1 the scaling is a bit larger than what Sinha et al. (2017) classify as the upper regime. This scaling is very sensitive to measured value of the upper data points, and can thus deviate slightly from the true scaling. In contrast to the theory by Sinha et al. (2013), who states that ganglion movement should occur during this flowing regime, the phases were flowing as interconnected fluids and not as ganglion during the vertical flow experiment. This observation contradicts the theory of a threshold pressure connected to ganglion movement presented by Sinha et al. (2013).

The results also do not match the results of Tallakstad et al. (2009), Rassi et al. (2011), Grøva and Hansen (2011) or Aursjø et al. (2014), who all point to a lower scaling relation of $\beta < 1$. When comparing results to the experiments mentioned above, one must remember that these studies did not account for the threshold pressure, ΔP_t. As stated by Sinha et al. (2017), including the threshold pressure is crucial for the consistency of the results. If the assumption that this threshold pressure exists is correct, this causes the comparison of the scaling relations to be inconsistent and not comparable.

With the results indicating only one linear regime after accounting for the threshold pressure, the results are supporting the presumption that the two regimes found in the LBP by Husøy (2018), occurred due to end-effects, not capillary forces. For the SBP Husøy (2018) found that there was no transition to a capillary dominated regime with a lower scaling coefficient. This corresponds well to the results in this thesis, but is

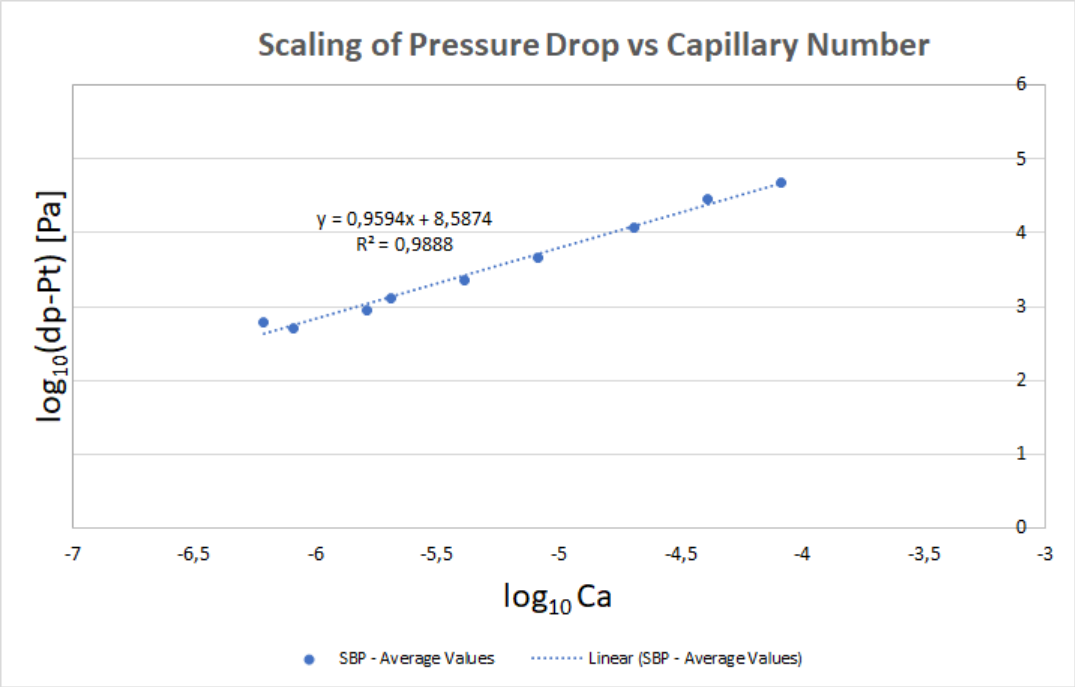

Figure 5.6: Scaling of Pressure drop versus capillary number for two phase vertical flow in SBP. When accounting for the threshold pressure, only one flow regime is observed, with a slope of $\beta = 0.9594 \simeq 1$.

still not considered a good comparison, as the lack of a lower flow regime can occur if the transition point is outside the spectrum of studied capillary numbers and flow rates.

Note that the uncertainty of the lower data points measured by Sinha et al. (2017) is high. An omega PX409 differential pressure transducer was used to measure these pressures. When checking the accuracy of these transducers, it is found to be lower than that of the transducers used for this thesis, with an accuracy of $4.9psi$. This implies that the transducers are accurate down to about $0.34bar$. The PRD-33X by Keller used in this study is accurate down to $0.035bar$. Thus, it is possible that the lowermost data points by Sinha et al. (2017) are outside the accuracy of the transducers, generating the transition to the lower regime.

Another important aspect of this discussion is what definition of the capillary number to use. The capillary number presented in this project does not take into account the effect of the grain size, and thereby the pore size of the system. The same definition of capillary number was used in the experiment by Sinha et al. (2017). The experiment by Sinha et al. (2017) used glass beads of diameter 0.098 mm and a confining medium with an inner diameter of 5.0 mm. As these beads are a lot smaller than the ones used in this project, of ~ 1 mm, accounting for this in the definition of the capillary number can be of importance when comparing results. In a porous medium, bigger pores generally yield smaller capillary forces. This would indicate that the capillary forces in this experiment will be smaller than those used in the Sinha et al. (2017) experiments. By including the diameter of the beads, d, a capillary number can be defined as:

$$Ca_{new} = \frac{Q\mu d}{\sigma A}$$

Accounting for grain size would make the capillary number of the Sinha et al. (2017) experiment even

smaller compared to the capillary numbers in this thesis. A smaller capillary number indicates that the fluid flow is more capillary dominated. Thus, a possible explanation as to why the lower flowing regime is not detected in this thesis can be that the pressure has not been measured for capillary numbers small enough. Disregarding grain size, and comparing the investigated capillary numbers of this thesis to those of Sinha et al. (2017) we find that for the small bead pack the range of capillary numbers includes the transition to a lower flow regime found by Sinha et al. (2017). Meanwhile, for the large bead packs, the investigated capillary numbers seem to all lie within what Sinha et al. (2017) identifies as the upper regime.

Pressure Gradients

If the transition to a lower regime is to be detected, the right flow rates need to be investigated. To check whether or not the range of measured data is comparable to both regimes found by Sinha et al. (2017), the pressure gradient of the system is calculated. The pressure gradient is used because this number accounts for the different dimensions of the bead packs used in the different studies, and thus makes for a good comparison. Pressure gradients from Sinha et al. (2017), Husøy (2018), and this thesis is plotted against capillary number in figure 5.7. A table containing all plotted values can be found in Appendix C .

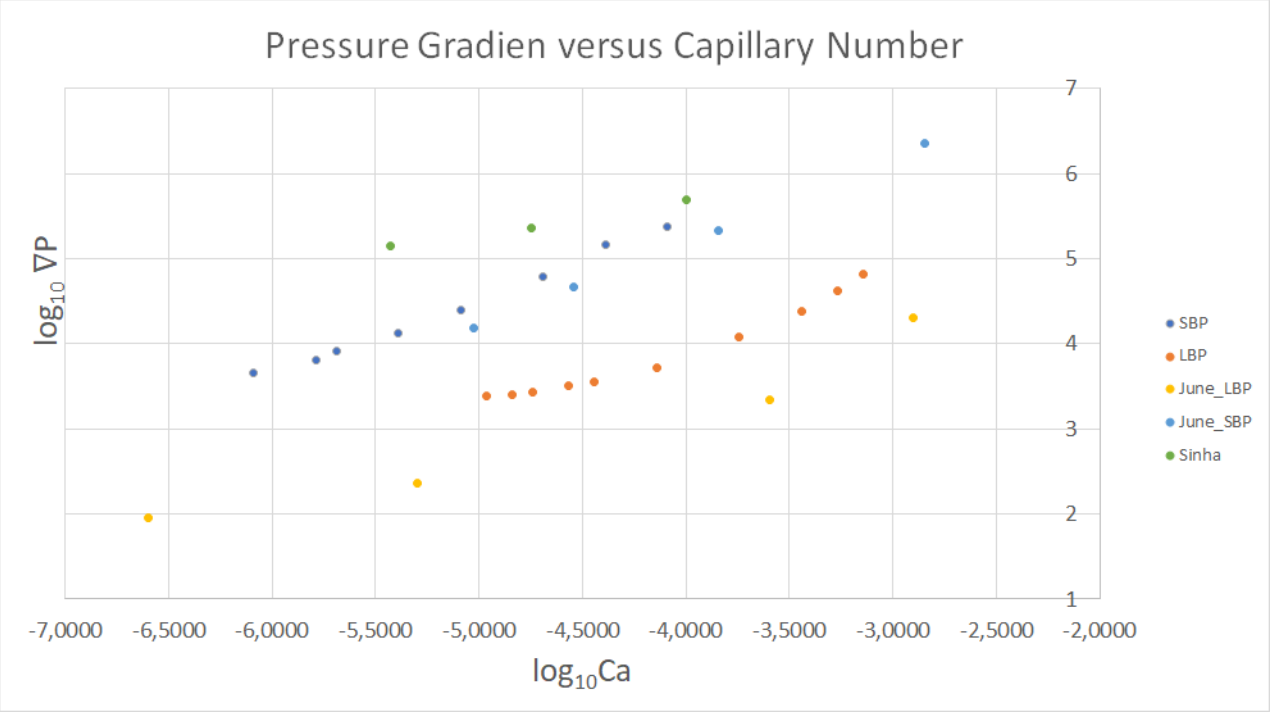

Figure 5.7: Pressure gradients from Sinha et al. (2017), Husøy (2018), and this thesis is plotted against capillary number. The figure illustrates that the range of pressure gradients tested during this thesis is covering the two regimes indicated by Sinha et al. (2017). Not all measured data is included, but values for both maximum and minimum rate is plotted.

From figure 5.7 we find that pressure gradients corresponding to both the upper- and lower regime identified by Sinha et al. (2017) are measured for this thesis. The lower regime identified by Sinha et al. (2017) has a pressure gradient of $\nabla P = 142857 Pa/m$. During this thesis gradients down to $\nabla P = 2475 Pa/m$. was tested. Sinha et al. (2017) found the transition to the upper flow regime at $\nabla P = 228571 Pa/m$,

and data is measured up to a pressure gradient of $\nabla P = 500000 Pa/m$. During this thesis gradients up to $\nabla P = 236700 Pa/m$ was tested. This gradient is within what Sinha et al. (2017) defines as the upper regime. From this, it is reasonable to believe that the data collected in this thesis should indicate the transition to a lower flow regime, if this regime were to exist. By using a longer bead pack, Husøy (2018) managed to test a larger range of pressure gradients than what has been done during this thesis. The gradients tested in this thesis are still believed to be of a large enough range, as they cover what Sinha et al. (2017) define as the transition point between the flow regimes.

If we then assume that a large enough range of flow rates have been tested, it is interesting to see that most results indicate only one flow regime and that this regime corresponds to the upper regime found by Sinha et al. (2017). Sinha et al. (2017) states that during the upper regime, the fluids will move as ganglion. Visual observations contradict this theory, as no ganglion movement is observed during any of the experiments. The one experiment that did show a deviation from the linear regime was the two-phase vertical flow in LBP1. This deviation might be caused by gravitational segregation of the fluids, as explained earlier in this chapter. Also, if accounting for the threshold pressure as Sinha et al. (2017) does, only one linear regime can be identified. Thus all results of this thesis contradict the theory presented by Sinha et al. (2013)

5.3.3 Vertical Flow with Surfactant

To test whether or not the deviation from the linear regime is connected to interfacial tension between the two phases, as Sinha et al. (2017) suggested, the two-phase experiment was rerun with surfactants. The goal was only to reduce IFT, and still keep two separate phases. This way, if the scaling of the two regimes still indicated two regimes, this would substantiate that the deviation from the linear regime is not connected to interfacial tension between the phases. Identification of two separate regimes would thereby contradict the theory presented by Sinha et al. (2013).

In figure 5.8 the results from the two surfactant experiments are plotted together with the results from the ordinary two-phase flow experiment. The figure shows that when introducing a surfactant to the system, only one regime can be observed. This regime is not consistent with the upper regime, as found in the SBP and horizontal flow experiment, but scales more similar to the lower regime found in the two-phase flow experiment.

As the surfactant experiment does not move towards zero as $Q \to 0$, it is possible to determine a threshold pressure. This is done by extrapolating the lines, and finding their intersection points, as seen in figure 5.9. The threshold pressures are found to be $P_t = 1755.3 Pa$ and $P_t = 512.68 Pa$, for SDS and zalo experiment respectively.

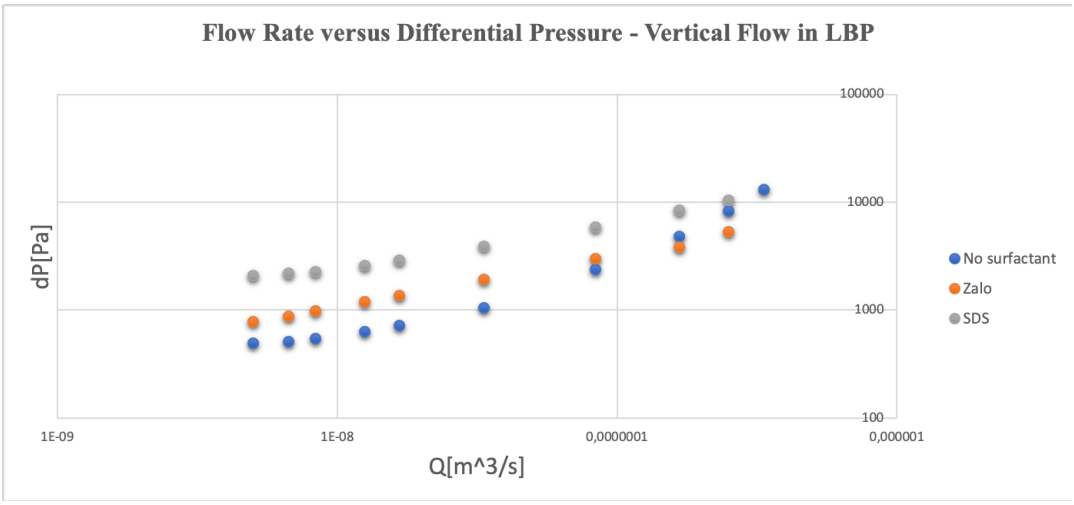

Figure 5.8: Results from both surfactant experiments plotted together with results from the two-phase vertical flow experiment in LBP1. The results of the surfactant experiments are indicating one linear regime.

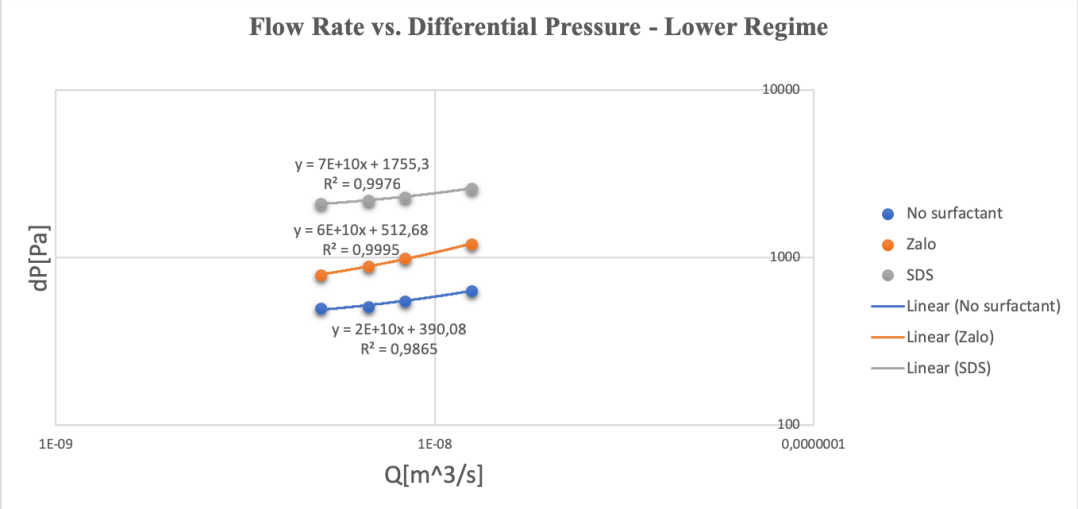

Figure 5.9: Threshold pressure is found from trend lines of the lowermost data points.

To properly compare the results of the surfactant experiments to the other experiments, the logarithm of the pressure drop minus the threshold pressure is again plotted as a function of the logarithm of the capillary number. This is seen in figure 5.12. In this plot, it becomes clear that only one regime can be identified, as all data points follow a linear trend. The scaling coefficients is found as $\beta = 0.7$ for $|\Delta P - \Delta P_t| \sim Ca^{\beta}$ for both the SDS and zalo experiment. To compare with the results by Sinha et al. (2017), this is somewhat in the middle of the two regimes found in their experiments.

Both single-phase flow and two-phase flow at higher rates should follow Darcy's equation. Thus, it would be natural to think that the surfactant experiment should move towards a scaling coefficient of $\beta \sim 1$. An answer to why these results do not indicate this might be because the two phases are made into an emulsion throughout the bead pack. Some of the energy in the two phases goes into making the emulsion, leading to a lower scaling coefficient. It is natural to think that if higher flow rates were tested, and the two phases would

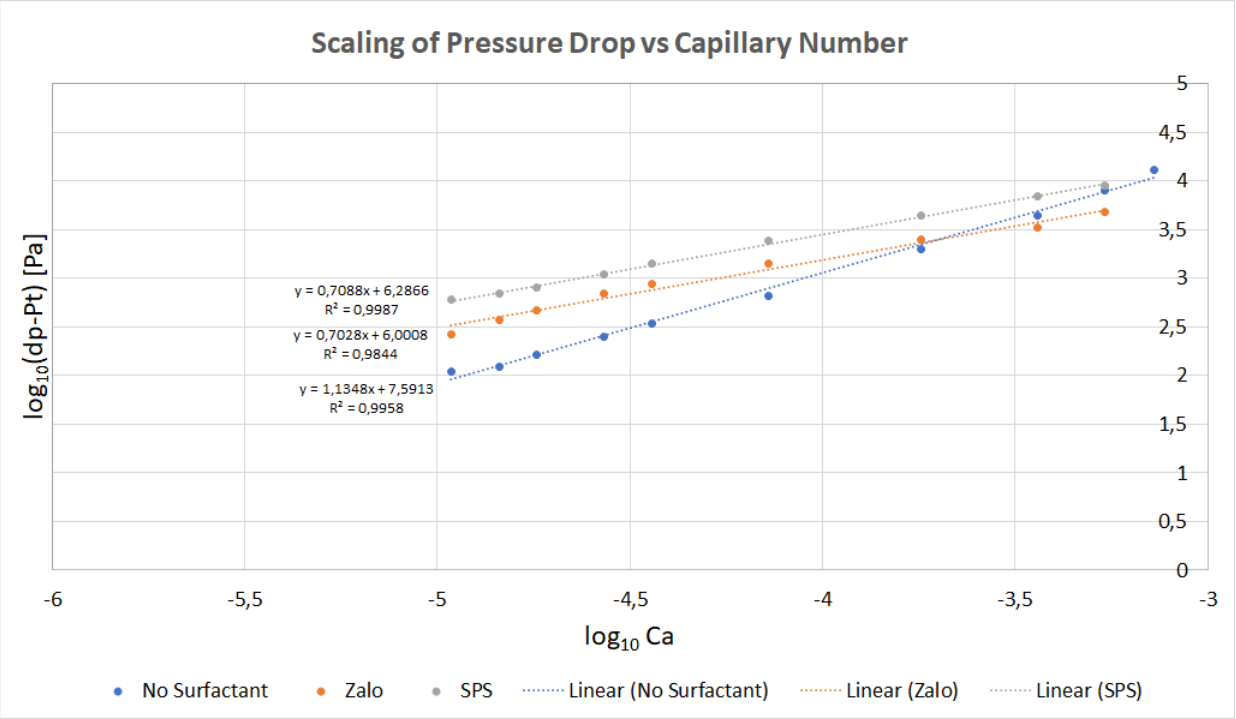

Figure 5.10: Threshold pressure is accounted for, and the results are plotted against capillary number to find the scaling coefficients of $\Delta P - \Delta P_t \sim Ca^{\beta}$.

move as an emulsion throughout the bead pack, the results would be similar to the result of the single-phase flow experiment. Higher rates were not tested, as the identification of a lower flow regime was the object of this thesis.

In figure 5.11, the results from the surfactant experiments are plotted together with the other experiments. The surfactant experiments can be seen not following the same trend as the other experiments. Here, a linear regime cannot be identified, and thus, no effective permeability can be calculated for the systems. This is believed to be because the fluids are mixing into an emulsion with increasing rates, and thus, the fluid properties constantly change.

Because of the emulsion of the two phases, the experiment cannot be considered a two-phase experiment. Thus there is no basis for comparing the results to the results from the original two-phase experiment. Therefore we can neither conclude, nor exclude, that the deviation from the linear regime governed by Darcy's equation correlates to the IFT between the two phases. To check if the phases are behaving as a single phase, the results are plotted together with the results from the single-phase experiment, in figure 5.12. Here, the upper part of the surfactant results can be seen to move towards the linear trend of the single-phase experiment. This supports the claim that the two phases are made into an emulsion at higher rates. If the experiment were to be re-conducted, it would be beneficial to use a weaker surfactant.

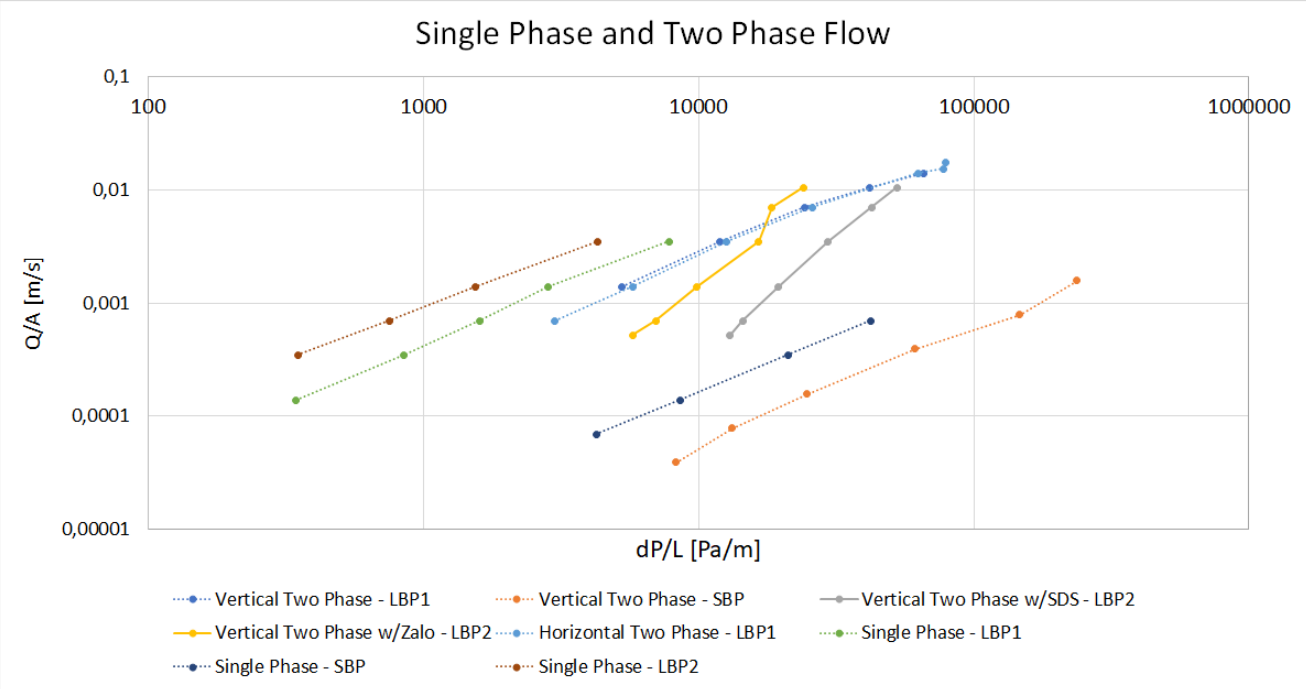

Figure 5.11: Flux versus pressure gradient for all runs, including surfactant experiments. A linear trend cannot be identified from the surfactant experiments, as the grade of emulsion is constantly changing throughout the experiment.

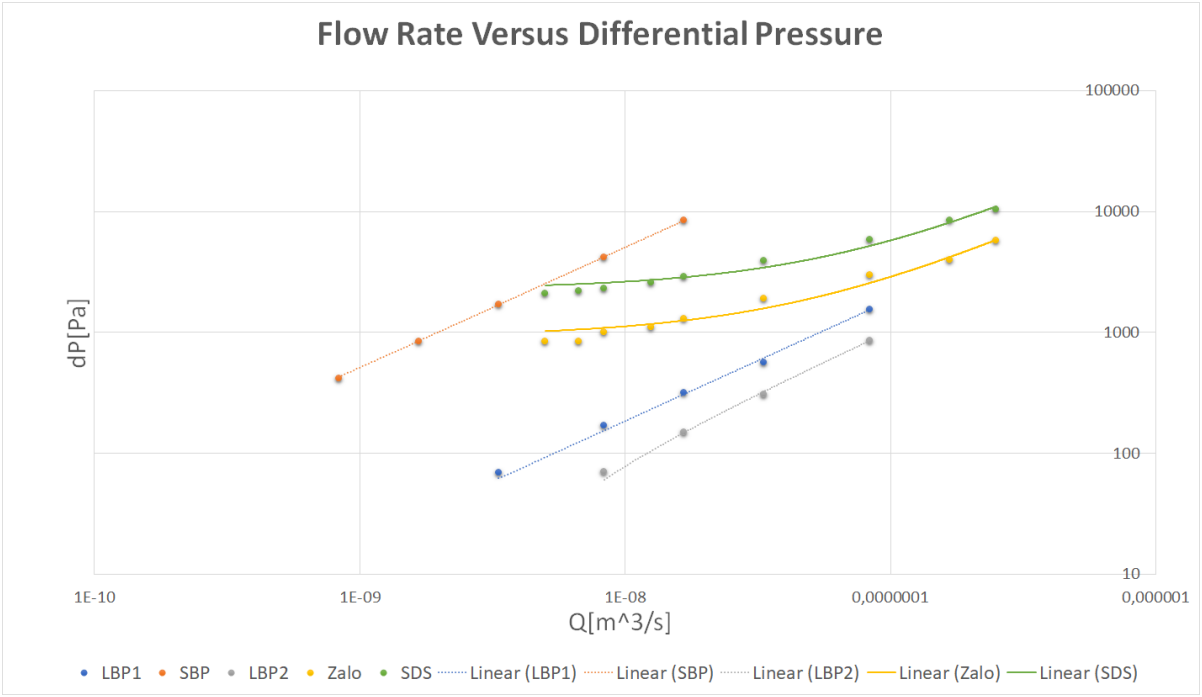

Figure 5.12: Results of surfactant experiment plotted together with the results of the single-phase experiments. The plot indicates that the two phases are behaving as an emulsion at higher rates.

Adding a surfactant strongly affects the capillary number. From equation 2.1, it is clear that a decrease in IFT will lead to an increase in capillary number. As mentioned earlier, the deviation from the linear regime is expected to exist in a capillary dominated regime, i.e., at low capillary numbers. Thus, when adding a surfactant, the pressure drop should be measured at even lower rates. This was not done during the experiment. Therefore a second flow regime cannot be ruled out based on the result from the surfactant experiments.

From the results presented and discussed in this chapter, it is hard to conclude on the existence of the lower flowing regime. Most results do not indicate this regime, but the regime might exist outside the investigated capillary numbers. What all results do indicate, is that if the lower regime exists, it is most likely not caused by a threshold pressure in the pore throats caused by IFT between the phases as Sinha et al. (2013) suggests.

5.4 Fluid Propagation Pattern

An essential difference between the experiments conducted in this thesis and those of Sinha et al. (2017) and Husøy (2018) is that the middle part of the experimental setup was made of glass. This enables visual observations. No ganglion movement was observed in the bead pack, infact the immiscible fluids were flowing in interconnected paths for all flow rates. Although ganglion movement has been visually observed in other experiments, as presented in chapter 2, this has all been in two-dimensional experiments. In a two-dimensional medium, the number of possible fluid propagation patterns are significantly more limited than in a three-dimensional medium. Thus, ganglion movement will occur at lower flow rates. The visual observations in this thesis all indicate that the existence of a lower flow regime is not connected to ganglion movement.

Another possible explanation to the existence of a lower flow regime is the theory of back and forth movement, or vibrations, of the interfaces between the immiscible phases, as presented in chapter 2. The theory states that energy is lost to the movement of the interface, leading to a lower scaling coefficient. Based on the results of this thesis, this is not a reasonable explanation. This theory should not be affected by the direction of flow. Given that the lower flow regime is only identified when flowing vertically, it is reasonable to believe its existence is connected to gravitational forces. Furthermore, no movement is visually observed between the two phases in the bead pack. This also contradicts the theory of vibrating interfaces.

Thus, we are left with the theory of gravitational segregation as the most likely explanation to the existence of a lower flowing regime during vertical flow. During gravitational segregation, the relative permeability will vary through the bead pack, as a consequence of the varying difference in saturation between the top and the bottom of the bead pack. A varying relative permeability will yield a lower effective permeability than that for a constant saturation. This leads to a larger ΔP, where more energy is used and we get a lower scaling coefficient; $\beta < 1$. In this scenario, the fluids still flow in interconnected paths.

Except in the case of gravitational segregation, the results of this thesis do not indicate a lower flow regime. Still, it is possible that the regime exists outside the investigated capillary numbers. What all results do indicate, is that if the lower regime exists, it is most likely not caused by a threshold pressure in the pore throats caused by IFT between the phases as Sinha et al. (2013) suggested.

5.5 Sources of error

Conducting an experimental study, a vast range of error sources may contribute to errors in the results. Small sources of error are often negligible, while others make a more significant impact on the results, and needs to be taken into account when concluding the experiment. In the following section, potential sources of error will be presented, and their impact on the results briefly discussed.

Filters and valves

As the inner diameter of both the filter and valves were the same as that of the tubes, the impact of both filters and valves on the fluid flow is expected to be small. It was of concern that the oil would accumulate into larger slugs at the filter and that the phases would enter the bead pack sequentially in large slugs. With the bead pack being made of glass the fluid propagation could to some degree be observed. Some accumulation was observed at the filters, but the phases seemed to flow simultaneously when reaching the bead pack.

Gravity

As discusses earlier in this chapter, gravity needs to be considered a source of error during the horizontal flow experiment, as this induces vertical segregation of the fluids, that again affect the flow patterns in the bead pack. The bond number need to be considered to decide whether or not gravity will affect the flow.

Aging of columns

A possible source of error that has been reported by both Aursjø et al. (2014), Sinha et al. (2017) and Husøy (2018) is aging of the columns. This aging occurs when the strongly water-wet glass beads are altered towards a more oil-wet condition. This altering of wettability can occur when the water-wet beads are flooded with oil over a long period of time. If the wettability is changed, the saturation of the system will change, and this results in changing of the threshold pressure. As a consequence of this, two measurements under otherwise identical conditions, but with some time between, can yield varying results. The effect of aging was tested by Husøy (2018) on bead packs similar to the ones used in this experiment. Husøy (2018) found that the aging effect was negligible for measurements obtained within a week. Observations during this thesis contradict the findings by Husøy (2018), and change in wettability of the bead pack need to be considered a possible source of error.

Discontinuous flow

When the pump changes from delivering fluid from one cylinder to the other, a pulse is detected in the flow rate. This can be observed as a change of pressure in the system. This is mostly a problem at and at very high rates, above 10 ml/min, because the system does not have time to stabilize before the pump changes cylinder again.

At very low rates this is also believed to be a problem, although the extent of this problem has not been measured as the pressure transducers do not give accurate measurements at these rates. In this thesis, the measurements at the lowest rates have not been accounted for, because of the inaccuracy in the pressure transducers.

Inconstant pressure in system

The pump mechanism also induces another possible source of error. The retracting of fluids into the pump is not at a constant rate equal to the delivery rate. When the inactive cylinder is filling up with fluids, the rate of the retracting fluid is higher than the pumps delivery rate. Because of this, the fluid level in the reservoir is not kept constant. The fluid level will drop about 1 cm when the pump is retracting fluid, before slowly rising to the initial fluid level. At the very low pressures of interest in this experiment, this change of fluid level will affect the pressure readings.

Air bubbles trapped in the system

As mentioned in section 3.3, air bubbles were observed to be trapped in the bead pack during the initial flow with distilled water. Large trapped air bubbles would change the characteristics of the system considerably. The bubbles were attempted removed as explained in section 3.3, but due to the low-pressure tolerance of the system, some bubbles remained in the system and may have affected the results.

Contamination in the system

Fine dust was observed on the surface of the beads. As explained in section 3.3, the beads were cleaned, but some particles may have been left on the beads. If so, the introduction of small contamination particles to the system could lead to clogging of filters over time. After running the experiment a couple of times, some contaminating particles were observed in the reservoir. These particles accumulated in the intersection between the fluid phases. To avoid unwanted particles to re-enter the system, the inlet tubes of both water and oil was placed in the center of their respective reservoir. Due to these adjustments, contamination from the small dust particles was not considered to be a significant source of error.

Another possible source of contamination in the system can come from the particles used to dye the oil red. If larger excess particles get into the system, this could also lead to clogging of filters. To avoid this, the oil was filtered through a filter before introduced to the system. When dismantling the system, some accumulation of darker particles were observed in both inlet and outlet of the glass bead pack. This may have affected the flowing pattern of the fluids in the bead pack. No end effects were observed during conduction of the experiments; the impact of these particles is thus considered to be small. The contamination found when dismantling the system can be seen in figure 5.13.

Environmental factors

The most relevant environmental factor in this experiment is temperature. The accuracy of the pressure transducers used to measure the excess pressure drop over the bead pack can be affected by a change in temperature. Still, this is not considered to be of great impact on the results, as any change in temperature is believed to affect both sensors similarly. Thus, as we are only interested in the pressure drop over the system, a similar small change in both measured pressures will not affect the results.

The viscosity of the oil is also affected by a change in temperature, as the viscosity decreases with increasing temperature. The temperature in the lab has been measured to vary with approximately 10°C between night and day, from 15°at night to a maximum of 25°midday. Within these temperatures of relevance, the change of viscosity to temperature is close to linear. Where the change in viscosity is about 3% and 2.5% pr. 1°C, for water and EXXSOLD60 respectively (Paar, 2019; Lindberg, 2005).

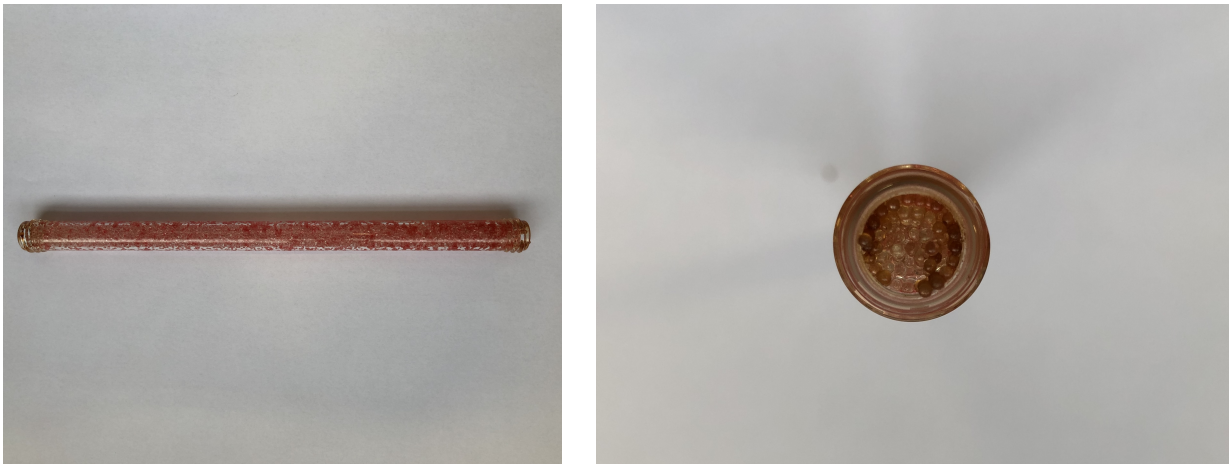

Figure 5.13: A darker color is observed at inlet and outlet of the bead pack. This is believed to be an accumulation of the red particles used to dye the EXXSOL D60.

Looking at Darcy's equation 2.3, a 3% change in viscosity will result in a 3% increase of velocity. This changes the lowest flow rates from 0.300 ml/min to 0.309 ml/min, which will affect the results considerably. Some measurements lasted more than 12 hours and were conducted during the night. During these measurements, the temperature is considered a possible source of error.

Chapter 6

Conclusion

The objective of this thesis has been to identify flow regimes during steady state flow of two immiscible fluids, where the main focus have been on the lower flow rates. The scaling relation between the pressure drop and the volumetric flow rate has been found. This relation was used to investigate the existences of a lower flow regime.

Modifications has been made to the experimental setup, believing to minimize the significant influence of end effects suspected in Husøy (2018). By using two incompressible fluids, one of the uncertainties associated with the experiment by Sinha et al. (2017) has been removed in this thesis. Thus this thesis better reflects the current pore scale theory which is assuming incompressible fluids (Sinha et al., 2017).

For the horizontal flow experiment, only one linear flow regime is observed. When scaling $\Delta P \sim Ca^{\beta}$, β is found to be 1.0444. The threshold pressure is not observed, and the scaling corresponds to the upper regime found by Sinha et al. (2017). The results substantiate the assumption that the lower regime found by Husøy (2018) is due to boundary effects, and not the threshold pressure that Sinha et al. (2013) presents.

For the vertical flow experiment in LBP1, a deviation from the linear regime was found for the lowest rates. At $Ca = 2 \times 10^{-5}$ the slope takes a non-linear turn, indicating a threshold pressure and two different flow regimes. The threshold pressure is found to be $408.33Pa$. The deviation from the linear trend can be explained by gravitational segregation of the two phases. This leads to oil saturation being higher at the top of the bead pack, while the bottom of the bead pack will have a higher water saturation. Such varying saturation will lower the relative permeability of the bead pack. A varying relative permeability will yield a lower effective permeability than that for a constant saturation. This leads to a larger ΔP, where more energy is used, and we get a lower scaling coefficient; $\beta < 1$.

The experiment by Sinha et al. (2017) also tested vertical flow, but the impact of gravitational forces were ignored. Based on the results of this thesis, where gravitational forces are found to affect the result of the vertical flow experiment, it is reasonable to belie that gravitational forces should not have been ignored by Sinha et al. (2017). If gravitational segregation occurs, the effect is strongest at lower rates because the phases need time to segregate. Thus, the lowest relative permeability in the bead pack is found at the lowest flow rate. If gravitational segregation occurred during the experiment by Sinha et al. (2017) this could describe the deviation from the linear regime at low flow rates, without implying a threshold pressure in the pore throats.

For the SBP only one linear regime is observed. This corresponds to the theory of gravitation segregation as capillary forces are stronger, and flow rates are higher in the SBP. Thus, segregation of the fluids would take more time in the SBP.

If accounting for the threshold pressure, the two regimes observed for vertical flow in LBP1 can no longer be observed. Only one regime can be identified, with a scaling coefficient of $\beta = 1.1348$. The results indicate the same regime as found in the SBP where $\beta = 0.9594$.

Visual observations confirmed that the fluids were flowing in interconnected paths for all measured flow rates. No ganglion movement was observed. The theory by Sinha et al. (2013) states that ganglion movement should occur when the fluids enter the linear regime. Observations from this thesis contradict this theory, and thus also challenge the theory of a lower flow regime caused by a threshold pressure created by the capillary pressure at the interface of the two fluids.

Although ganglion movement has been observed in experiments with similar fluid velocities as investigated in this thesis, all these experiments have been using two-dimensional media. When using two-dimensional media, ganglion movement is expected to occur at lower rates due to a limited choice of flow paths. Observations from this thesis substantiate this, as some ganglion movement have been observed for the maximum flow rate. This indicates that ganglion movement will occur when the flow rate is high enough, but the transition zone between a lower regime and the linear regime is not connected to the mobilization of ganglion.

The results of this thesis imply that the existence of a lower flow regime is unlikely, but cannot be ruled out completely. What all results do indicate, is that if the lower regime exists, it is most likely not caused by a threshold pressure in the pore throats caused by the capillary pressure at the interface of the two fluids as Sinha et al. (2013) suggested.

A surfactant was added to the vertical LBP1 to test if the transition to the non-linear regime was affected by a change of IFT. As the surfactant caused an emulsion we were unable to draw any conclusions from this experiment. This experiment should be retested with a weaker surfactant.

Chapter 7

Recommendations for further research

Based on the observations made during the process of writing this thesis, some recommendations for further work are presented in the following.

Only two runs have been conducted for each experiment in this thesis. This is because experiments with real data are usually very time consuming, requiring even days to finish a single run. Thus, acquiring a larger amount of data was not possible during the given period of time. The limited amount of data makes the collected data less reliable. Hence, the first thing needed in further research is to collect more data. The scaling relationship, $\Delta P \sim Ca^{\beta}$, needs to be verified by more three-dimensional studies before drawing any conclusion to the value of the scaling coefficient, β. Further research is needed. Apart from repeating the same tests to acquire more data, other modification's could be made to the experiment to expand our understanding of steady-state two-phase flow. The following ideas could be tested:

1. A closer study of the low flow rates. To identify the different regimes, it would be valuable with more data with even lower flow rates than what was investigated in this project. This is especially interesting for the SBP and the surfactant experiments where lower capillary numbers need to be tested to accurately compare the results to other similar studies. Measuring the pressure drop for such low flow rates requires specially designed pressure transducers.

2. Running a new surfactant experiment with a weaker surfactant, i.e. a surfactant with a lower CMC. Ideally, the surfactant should reduce the IFT, but not to a point were emulsion is made. If a two-phase experiment with altered IFT is achieved, it would be possible to determine whether or not a deviation from the linear regime is connected to interfacial tension between the two phases in a pore throat, as Sinha et al. (2017) suggests. An experiment like this needs to be conducted with lower rates to obtain the desired capillary numbers.

3. Another interesting topic to study closer is the scaling coefficients dependency on other parameters. Especially interesting is the effect of saturation and mobility ratio. A suggestion would be to run the same experiments using other fluids with a more significant difference in viscosity, e.g., distilled water and air, or EXXSOL D60 oil and glycerol. Running the experiment at different fixed saturations would also be of great interest. Another perspective of interest would be further testing of bead packs with other dimensions than presented in this thesis.

4. An alternative to doing more experiments could be to do simulations. Based on the different theoretical

approaches, simulations could be conducted. If the simulations were to indicate the same trends as found during the experiments, this would strongly substantiate the theory.

If experimental studies on this topic were to be continued, it would be beneficial to limit the potential sources of error. A pump that can deliver a constant flow rate at both high and low rates would avoid the problem of discontinuous flow. This is crucial for the flow to stabilize at steady state. Each experiment should be completed during the shortest possible time frame to limit the wettability change of the bead pack. Ideally, all trapped air bubbles should be removed from the system, but this is difficult to do in a system consisting of glass tubes that do not withstand high pressures. Other materials should be considered if further research is to be conducted. Lastly, the temperature in the lab should be kept constant not to affect the viscosity of the fluids.

Bibliography

Anfinsen, C. R., 2018. Identification of two phase flow regimes in three dimensional porous medium (specialization project).

Aursjø, O., Erpelding, M., Tallakstad, K. T., Flekkøy, E. G., Hansen, A., Måløy, K. J., 2014. Film flow dominated simultaneous flow of two viscous incompressible fluids through a porous medium. Frontiers in Physics 2, 63.

Avraam, D. G., Payatakes, A. C., 1995. Flow regimes and relative permeabilities during steady-state two-phase flow in porous media. Journal of Fluid Mechanics 293, 207236.

Bear, J., 2013. Dynamics of fluids in porous media. Courier Corporation.

Blunt, M. J., 2017. Multiphase Flow in Permeable Media: A Pore-Scale Perspective. Cambridge University Press.

Blunt, M. J., Bijeljic, B., Dong, H., Gharbi, O., Iglauer, S., Mostaghimi, P., Paluszny, A., Pentland, C., 2013. Pore-scale imaging and modelling. Advances in Water Resources 51, 197–216.

Datta, S. S., Dupin, J.-B., Weitz, D. A., 2014. Fluid breakup during simultaneous two-phase flow through a three-dimensional porous medium. Physics of Fluids 26 (6), 062004.
URL https://doi.org/10.1063/1.4884955

Fand, R., Kim, B., Lam, A., Phan, R., 1987. Resistance to the flow of fluids through simple and complex porous media whose matrices are composed of randomly packed spheres. Journal of fluids engineering 109 (3), 268–273.

Grøva, M., Hansen, A., 2011. Two-phase flow in porous media: power-law scaling of effective permeability. In: Journal of Physics: Conference Series. Vol. 319. IOP Publishing, p. 012009.

Husøy, J. K., 2018. Identification of the transition between two phase flow regimes in sphere packs (master thesis).

Lage, J., 1998. The fundamental theory of flow through permeable niedia from darcy to turbulence. Transport phenomena in porous media 1.

Lake, L. W., et al., 1989. Enhanced oil recovery.

Lindberg, 2005. Performance fluids. http://www.lindberg-lund.fi/files/Tekniskedatablad/EXXON-D60-TD.pdf.

McPhee, C., Reed, J., Zubizarreta, I., 2015. Core analysis: A best practice guide. Vol. 64. Elsevier.

Odsæter, L. H., Berg, C. F., Rustad, A. B., 2015. Rate dependency in steady-state upscaling. Transport in Porous Media 110 (3), 565–589.

Orkla, 2016. Safety data sheet.

Osoba, J., Richardson, J., Kerver, J., Hafford, J., Blair, P., et al., 1951. Laboratory measurements of relative permeability. Journal of Petroleum Technology 3 (02), 47–56.

Paar, A., 2019. Viscosity of water. https://wiki.anton-paar.com/en/water/.

Rassi, E. M., Codd, S. L., Seymour, J. D., 2011. Nuclear magnetic resonance characterization of the stationary dynamics of partially saturated media during steady-state infiltration flow. New Journal of Physics 13 (1), 015007.
URL http://stacks.iop.org/1367-2630/13/i=1/a=015007

Rassi, E. M., Codd, S. L., Seymour, J. D., 2014. Corrigendum: Nuclear magnetic resonance characterization of the stationary dynamics of partially saturated media during steady-state infiltration flow (2011 new j. phys. 13 015007). New Journal of Physics 16 (3), 039501.
URL http://stacks.iop.org/1367-2630/16/i=3/a=039501

Reynolds, C. A., Menke, H., Andrew, M., Blunt, M. J., Krevor, S., 2017. Dynamic fluid connectivity during steady-state multiphase flow in a sandstone. Proceedings of the National Academy of Sciences 114 (31), 8187–8192.
URL http://www.pnas.org/content/114/31/8187

Savani, I., Bedeaux, D., Kjelstrup, S., Vassvik, M., Sinha, S., Hansen, A., Feb 2017. Ensemble distribution for immiscible two-phase flow in porous media. Phys. Rev. E 95, 023116.
URL https://link.aps.org/doi/10.1103/PhysRevE.95.023116

Shumway, R. H., Stoffer, D. S., 2017. Time series analysis and its applications: with R examples. Springer.

Sinha, S., Bender, A. T., Danczyk, M., Keepseagle, K., Prather, C. A., Bray, J. M., Thrane, L. W., Seymour, J. D., Codd, S. L., Hansen, A., 2017. Effective rheology of two-phase flow in three-dimensional porous media: experiment and simulation. Transport in porous media 119 (1), 77–94.

Sinha, S., Hansen, A., 2012. Effective rheology of immiscible two-phase flow in porous media. EPL (Europhysics Letters) 99 (4), 44004.

Sinha, S., Hansen, A., Bedeaux, D., Kjelstrup, S., 2013. Effective rheology of bubbles moving in a capillary tube. Physical Review E 87 (2), 025001.

Swagelok, 2018. Swagelock. https://www.swagelok.com/en/catalog/Product/Detail?part=SS-4F-05.

Tallakstad, K. T., Løvoll, G., Knudsen, H. A., Ramstad, T., Flekkøy, E. G., Måløy, K. J., Sep 2009. Steady-state, simultaneous two-phase flow in porous media: An experimental study. Phys. Rev. E 80, 036308.
URL https://link.aps.org/doi/10.1103/PhysRevE.80.036308

VindumEngineering, 2018. Vindum vp-series metering pumps. https://https://vindum.com/high-pressure-pumps/.

Xu, X., Wang, X., 2014. Non-darcy behavior of two-phase channel flow. Physical Review E 90 (2), 023010.

Zhang, H., Ramakrishnan, T., Nikolov, A., Wasan, D., 2016. Enhanced oil recovery driven by nanofilm structural disjoining pressure: flooding experiments and microvisualization. Energy & Fuels 30 (4), 2771–2779.

Appendix A

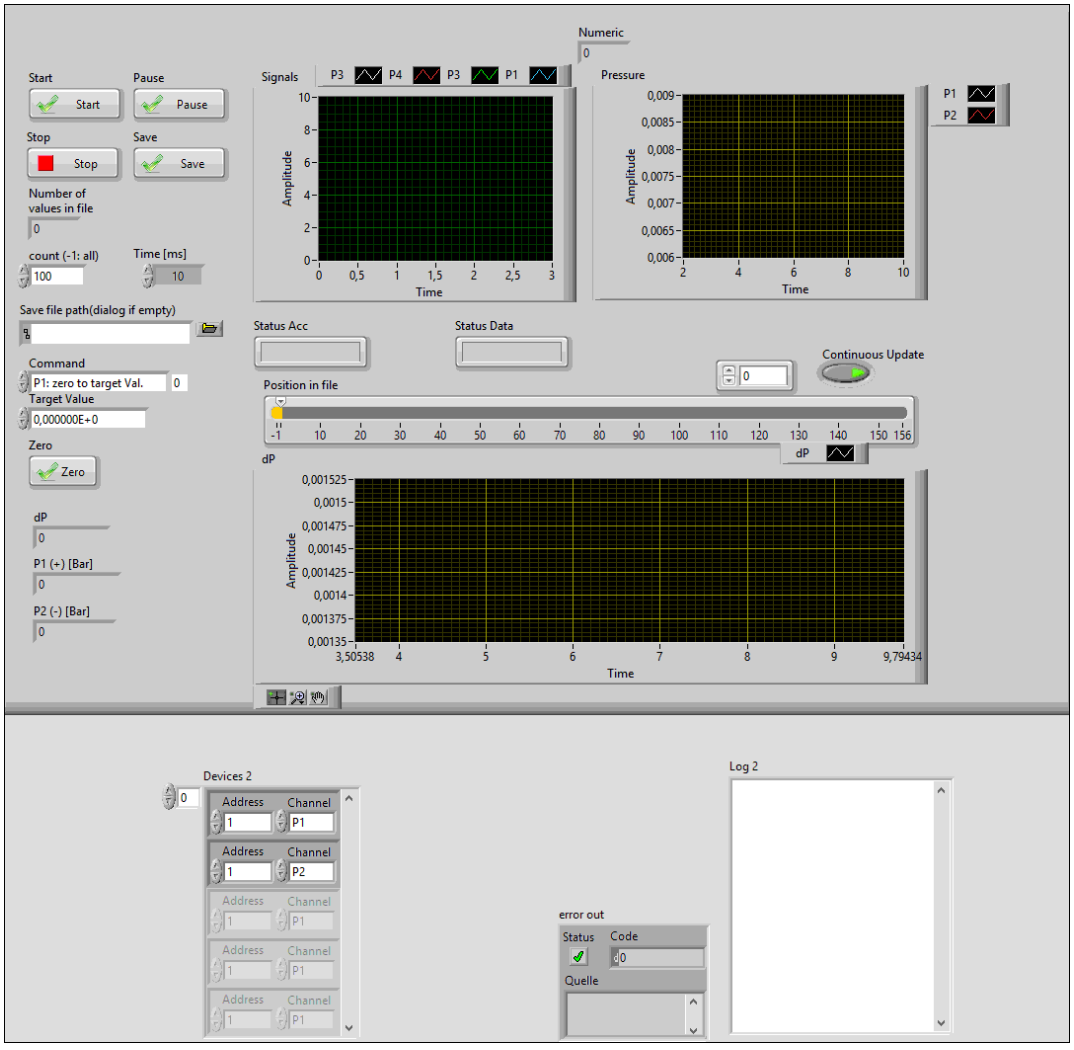

Figure 7.1: Labview front panel.

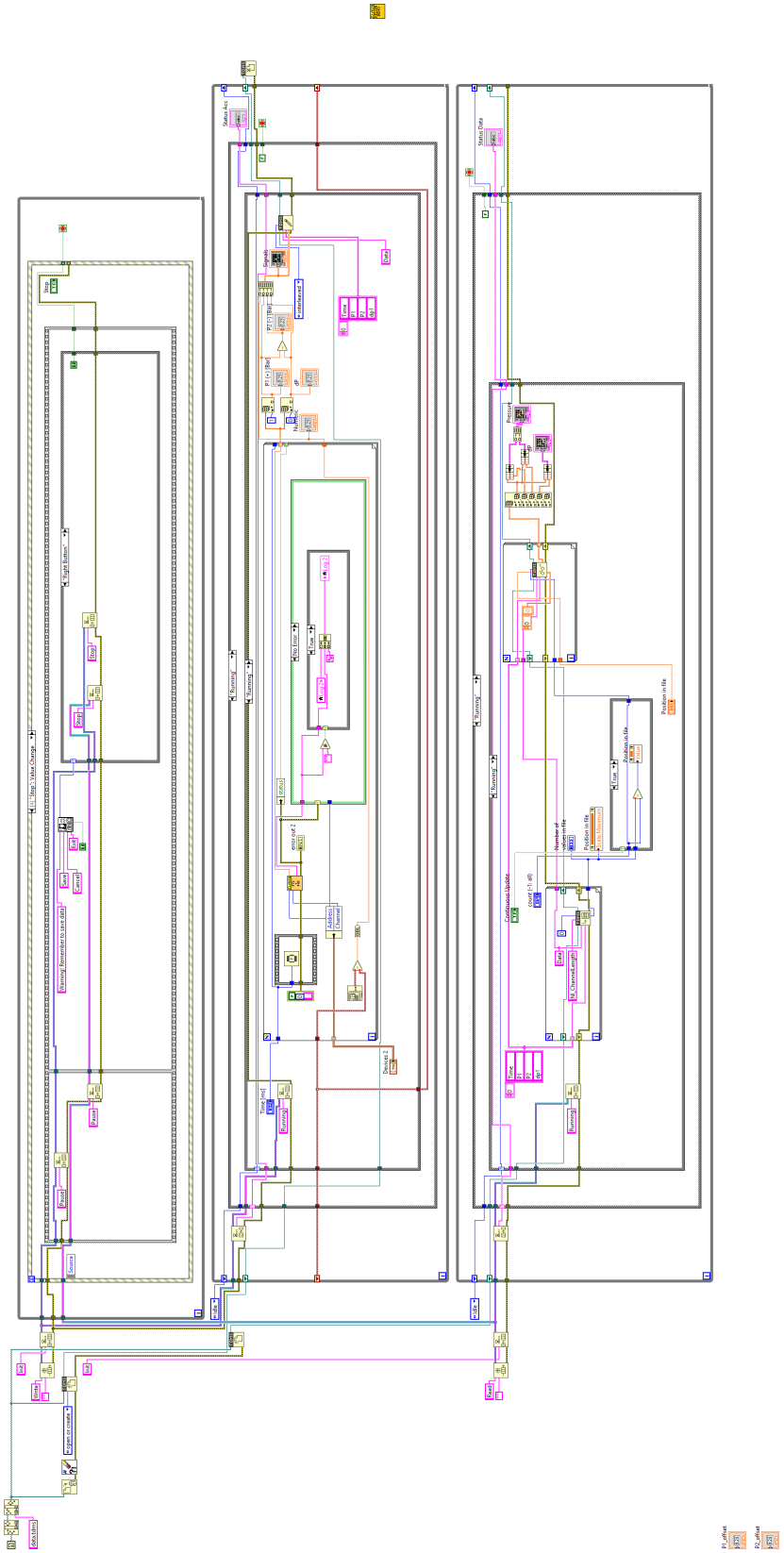

Figure 7.2: Labviw block diagram.

Appendix B

7.1 No Flow Case

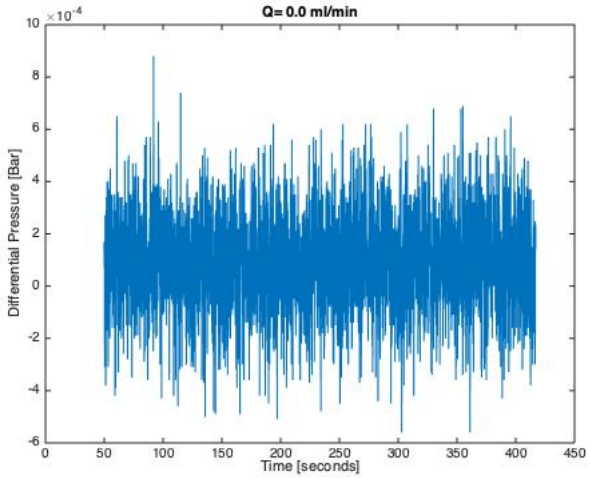

(a) UNIK 5000 for Q = 0.0 ml/min.

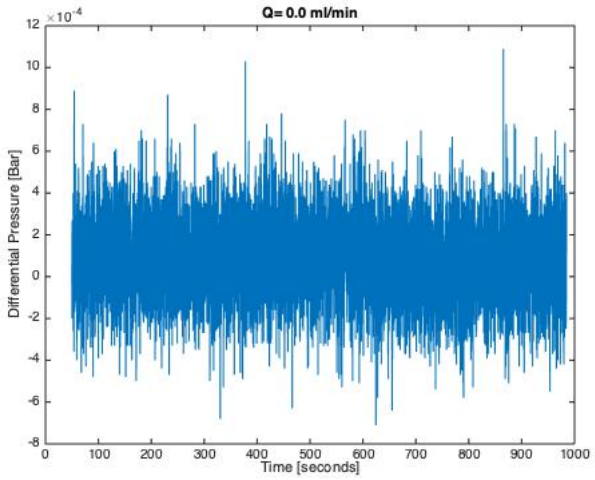

(b) PRD-33X Keller Q = 0.0 ml/min.

Figure 7.3: Pressure readings from UNIK 5000 and PRD-33X Keller differential pressure transducer, during $Q = 0.0ml/min$. Background noise is in the scale of about $\pm 0.0006bar$.

7.2 Steady state section for Single Phase Flow in LBP1

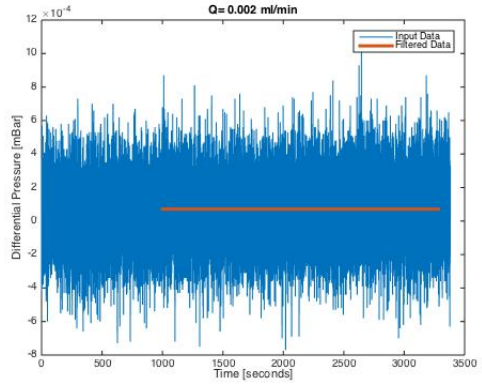

(a) Q = 0.002 ml/min

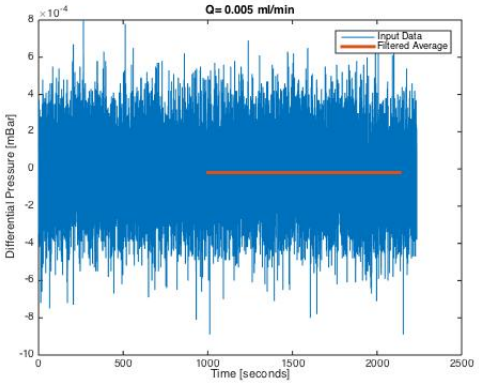

(b) Q = 0.005 ml/min

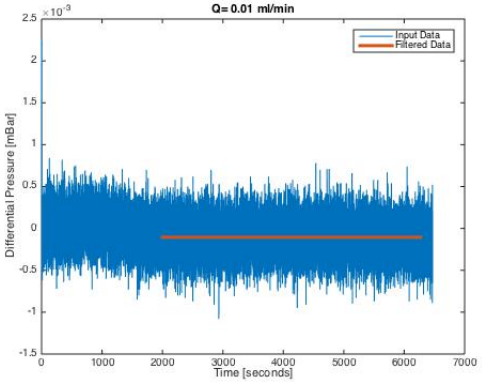

(c) Q = 0.01 ml/min

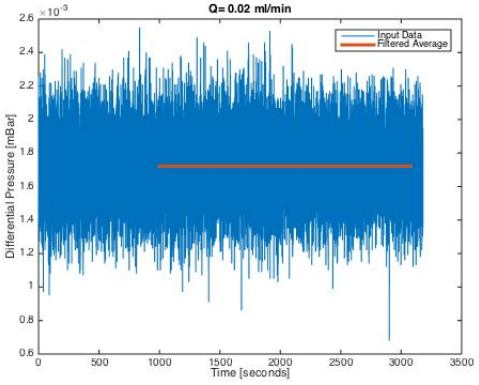

(d) Q = 0.02 ml/min

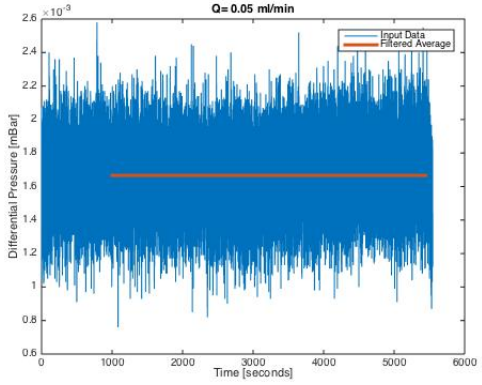

(e) Q = 0.05 ml/min

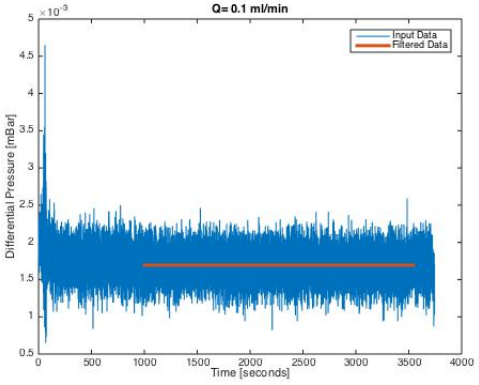

(f) Q = 0.1 ml/min

Figure 7.4: Steady state flow regime selection for single phase flow in LBP1. Variations in the measured pressure are in the rage of $\pm 0.0006 bar$, equal to the background noise found for $Q = 0.0 ml/min$. Larger "spikes" caused by noise from the pressure transducers and pumps, have been removed before calculating the average value.

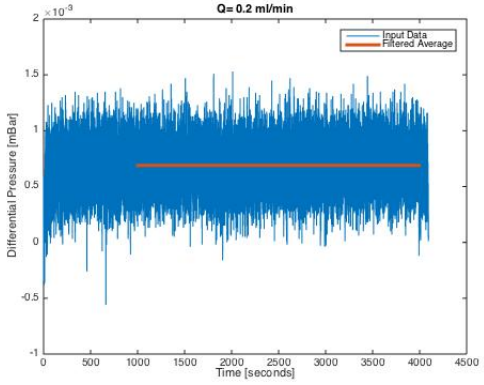

(g) Q = 0.2 ml/min

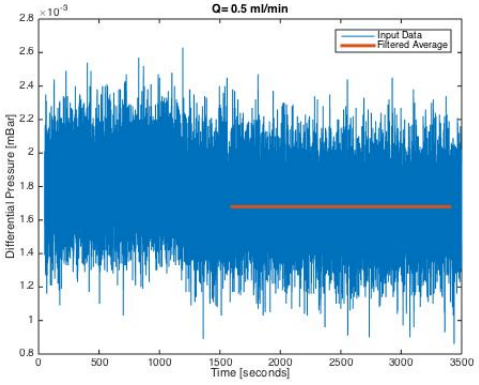

(h) Q = 0.5 ml/min

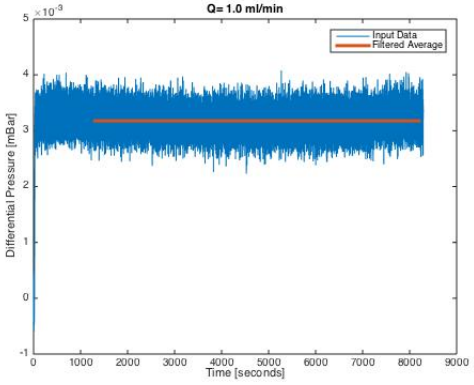

(i) Q = 1.0 ml/min

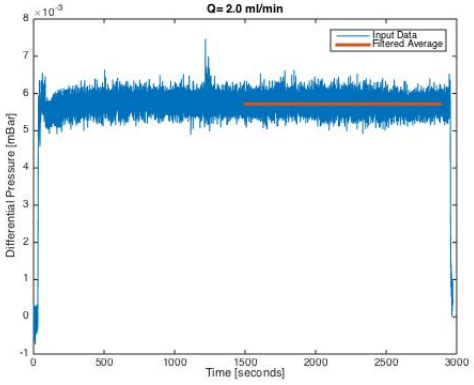

(j) Q = 2.0 ml/min

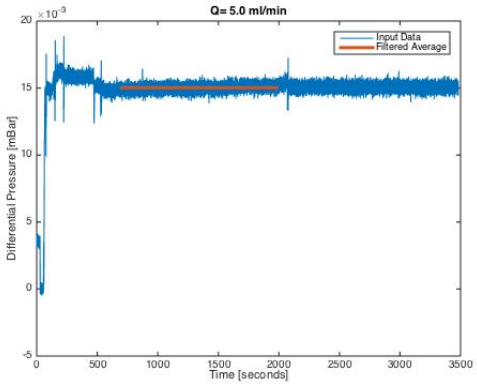

(k) Q = 5.0 ml/min

Figure 7.4: Steady state flow regime selection for single phase flow in LBP1. Variations in the measured pressure are in the rage of $\pm 0.0006bar$, equal to the background noise found for $Q = 0.0ml/min$. Larger "spikes" caused by noise from the pressure transducers and pumps, have been removed before calculating the average value.

7.3 Steady state section for Single Phase Flow in LBP2

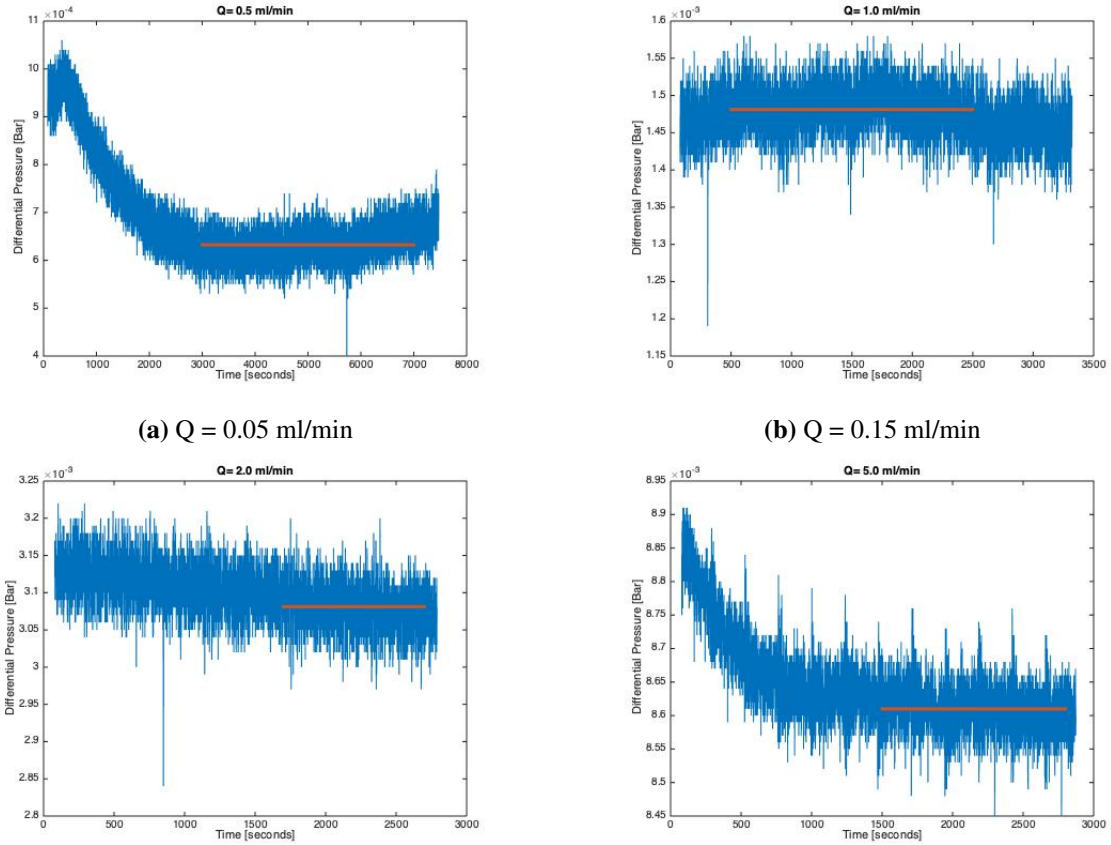

(a) Q = 0.05 ml/min

(b) Q = 0.15 ml/min

(c) Q = 0.2 ml/min

(d) Q = 0.5 ml/min

Figure 7.5: Steady state flow regime selection for single phase flow in LBP2. Variations in the measured pressure are in the rage of $\pm 0.0006 bar$, equal to the background noise found for $Q = 0.0 ml/min$. Larger "spikes" caused by noise from the pressure transducers and pumps, have been removed before calculating the average value.

7.4 Steady state section for Single Phase Flow in SBP

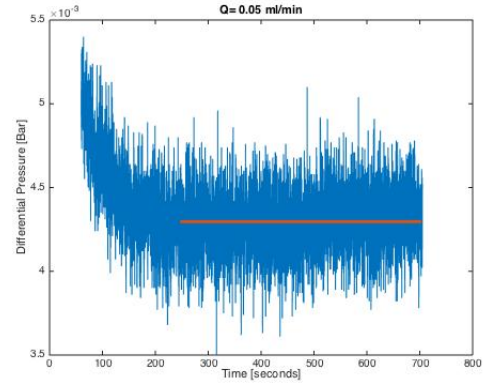

(a) Q = 0.05 ml/min

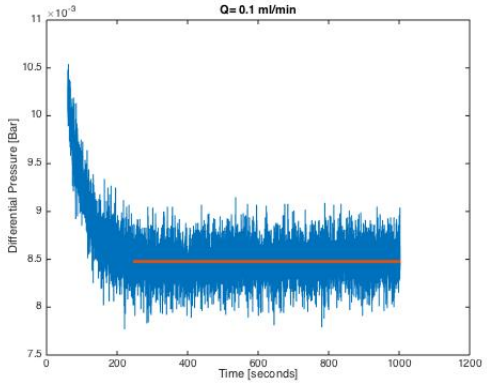

(b) Q = 0.15 ml/min

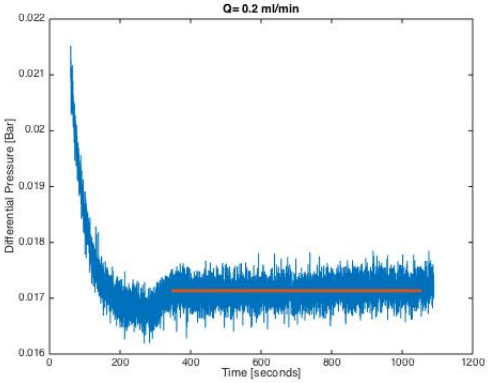

(c) Q = 0.2 ml/min

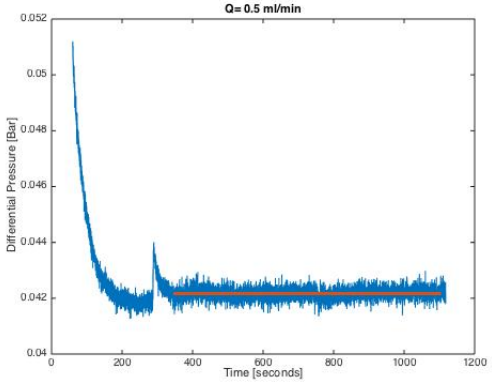

(d) Q = 0.5 ml/min

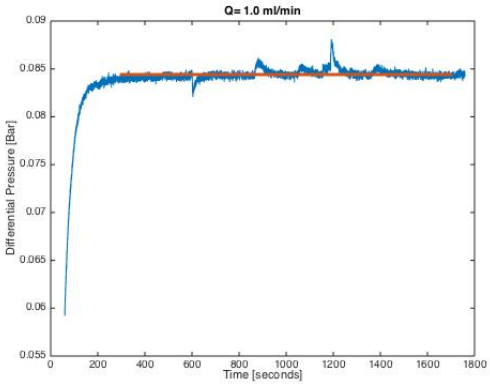

(e) Q = 1.0 ml/min

Figure 7.6: Steady state flow regime selection for single phase flow in SBP. Most variations in the measured pressure are in the rage of $\pm 0.0006bar$, equal to the background noise found for $Q = 0.0ml/min$. Larger "spikes" caused by noise from the pressure transducers and pumps, as seen for $Q = 1.0ml/min$, have been removed before calculating the average value.

7.5 Steady state section for Horizontal Two Phase Flow in LBP1 - Run 1

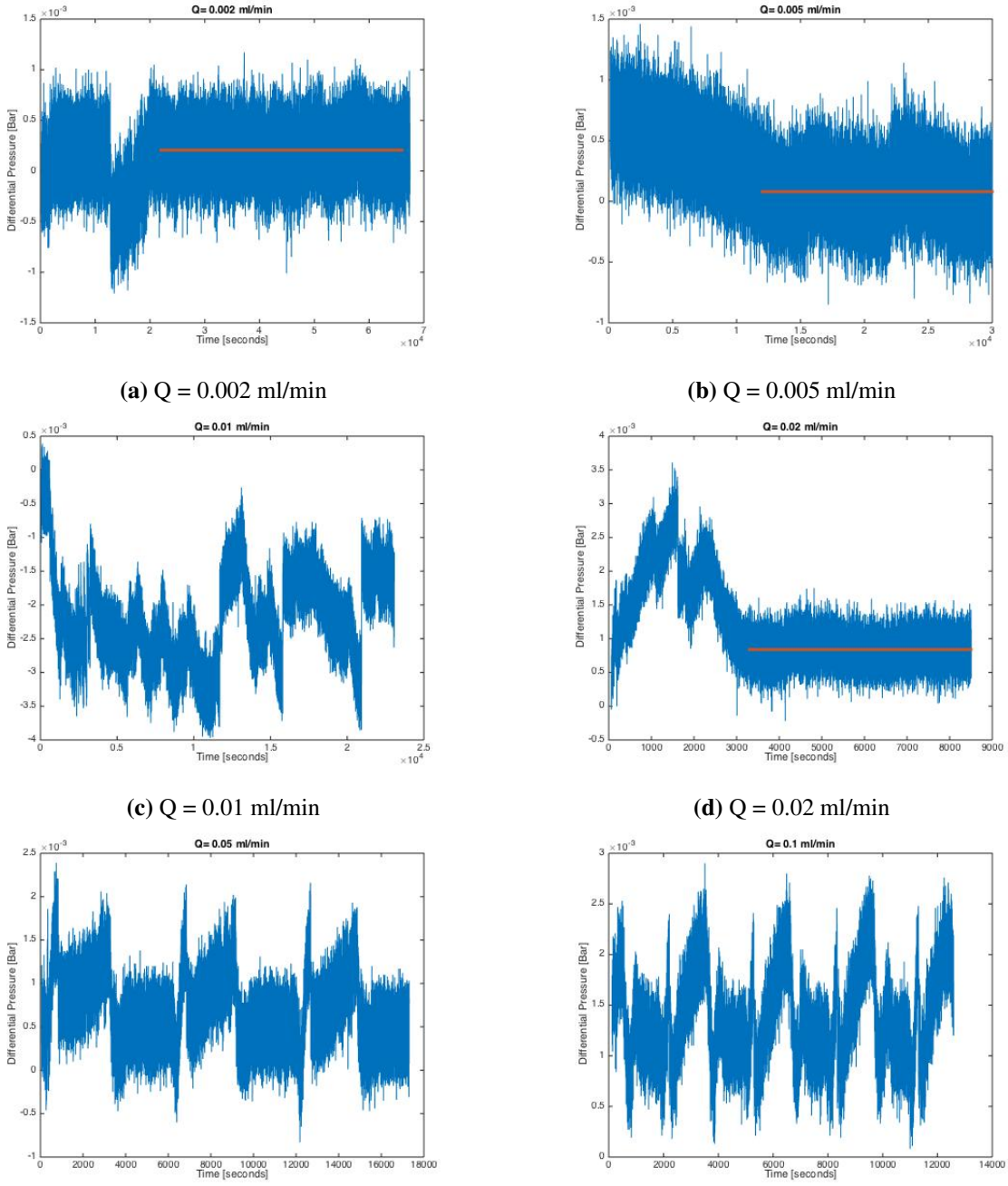

(a) Q = 0.002 ml/min

(b) Q = 0.005 ml/min

(c) Q = 0.01 ml/min

(d) Q = 0.02 ml/min

(e) Q = 0.05 ml/min

(f) Q = 0.1 ml/min

Figure 7.7: Steady state flow regime selection for two phase horizontal flow. Most variations of measured pressure in the steady state sections are in the rage of $\pm 0.0006 bar$, equal to the background noise found for $Q = 0.0 ml/min$. Larger "spikes" caused by noise from the pressure transducers and pumps, as seen in $Q = 0.2 ml/min$, have been removed before calculating the average value. If a steady state section is not indicated by a red line, the system is not considered stable and no average value was used for further analysis.

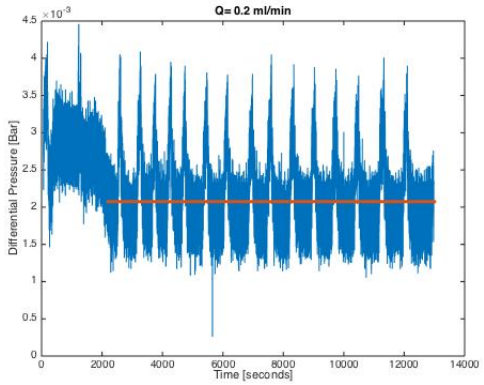

(g) Q = 0.2 ml/min

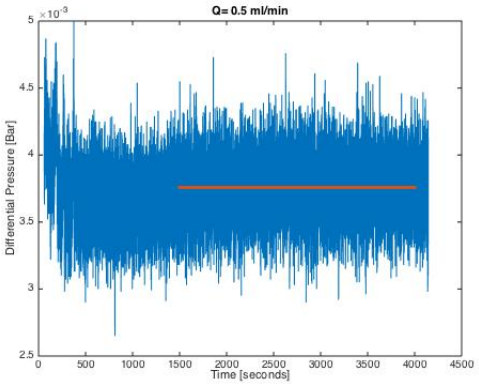

(h) Q = 0.5 ml/min

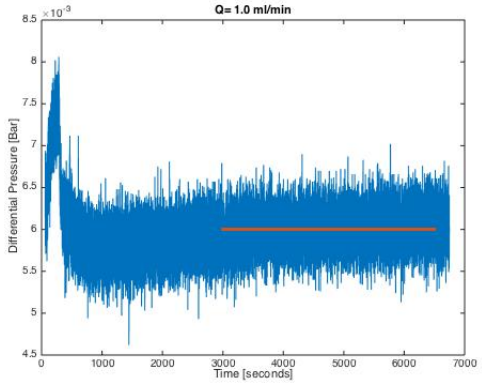

(i) Q = 1.0 ml/min

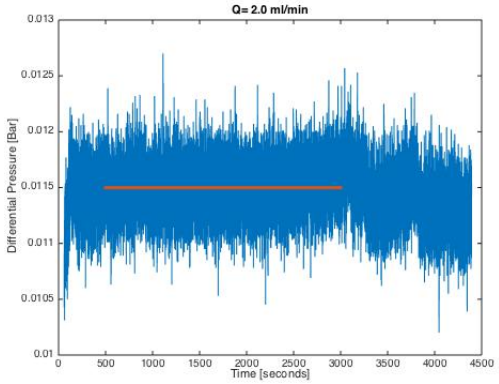

(j) Q = 2.0 ml/min

Figure 7.7: Steady state flow regime selection for two phase horizontal flow. Most variations of measured pressure in the steady state sections are in the rage of $\pm 0.0006 bar$, equal to the background noise found for $Q = 0.0 ml/min$. Larger "spikes" caused by noise from the pressure transducers and pumps, as seen for $Q = 0.2 ml/min$, have been removed before calculating the average value. If a steady state section is not indicated by a red line, the system is not considered stable and no average value was used for further analysis.

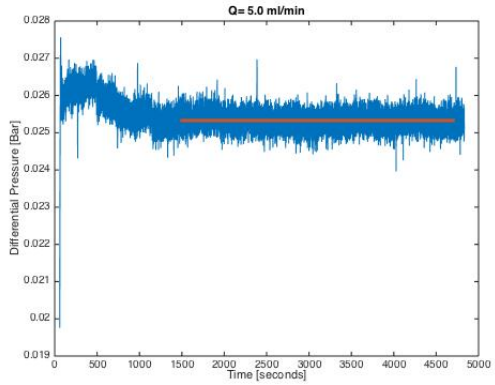

(k) Q = 5.0 ml/min

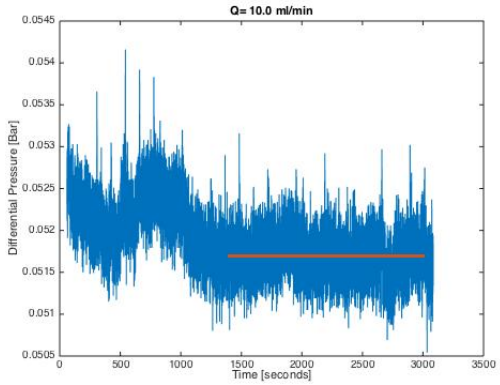

(l) Q = 10.0 ml/min

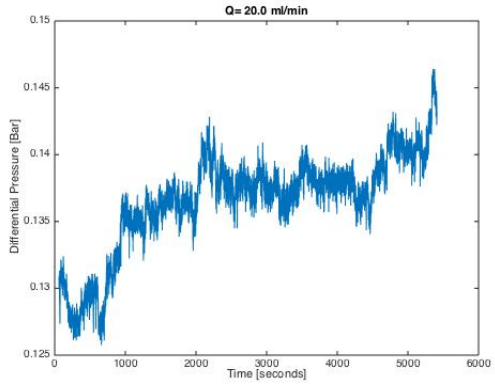

(m) Q = 20.0 ml/min

Figure 7.7: Steady state flow regime selection for two phase horizontal flow. Most variations of measured pressure in the steady state sections are in the rage of $\pm 0.0006bar$, equal to the background noise found for $Q = 0.0ml/min$. Larger "spikes" caused by noise from the pressure transducers and pumps, as seen for both $Q = 5.0ml/min$ and $Q = 10.0ml/min$, have been removed before calculating the average value. If a steady state section is not indicated by a red line, the system is not considered stable and no average value was used for further analysis.

7.6 Steady state section for Horizontal Two Phase Flow in LBP1 - Run 2

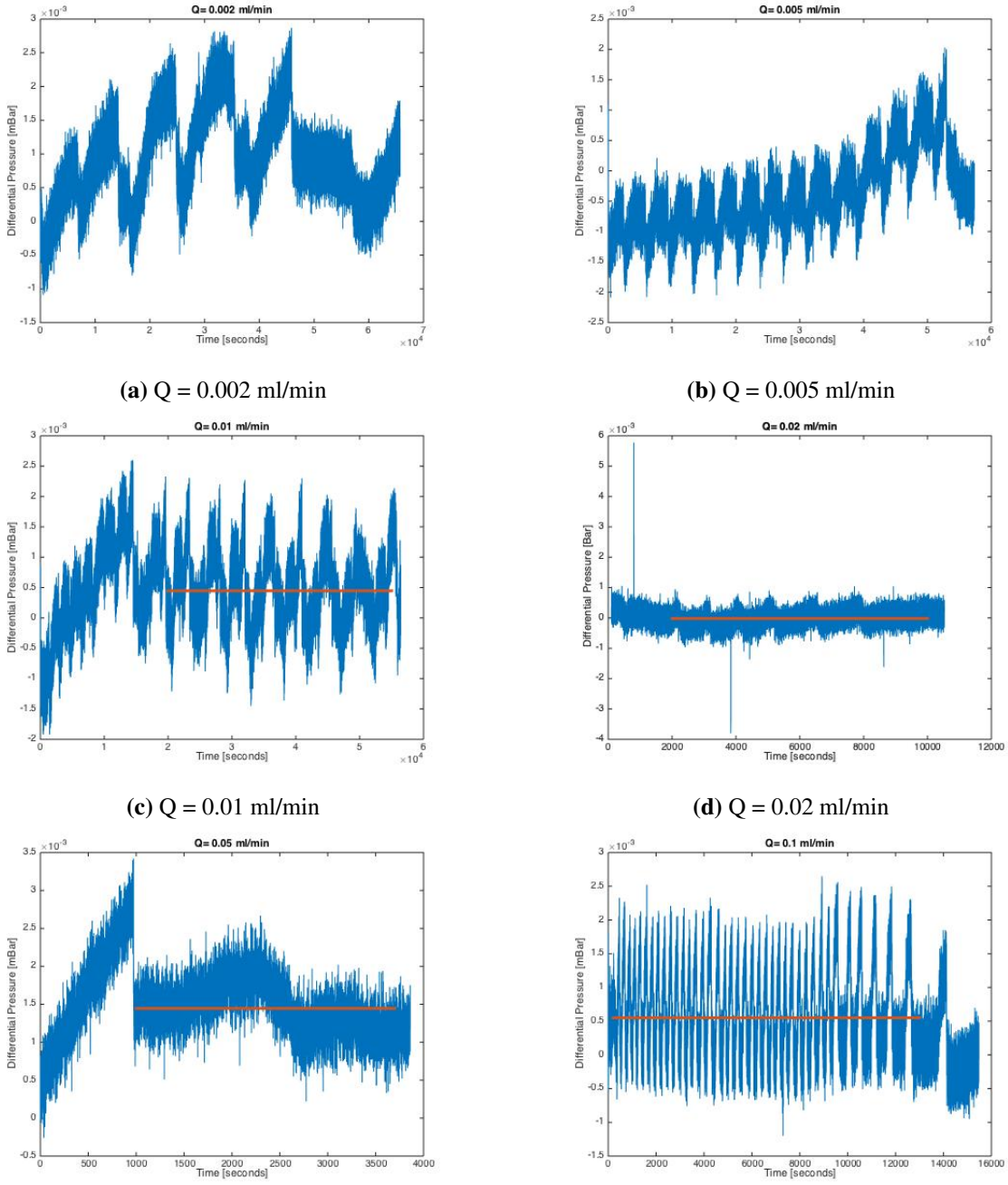

(a) Q = 0.002 ml/min

(b) Q = 0.005 ml/min

(c) Q = 0.01 ml/min

(d) Q = 0.02 ml/min

(e) Q = 0.05 ml/min

(f) Q = 0.1 ml/min

Figure 7.8: Steady state flow regime selection for two phase horizontal flow. Variations of measured pressure in the steady state sections are in the rage of $\pm 0.002 bar$. This is larger than the background noise found for $Q = 0.0 ml/min$. "Spikes" caused by noise from the pressure transducers and pumps have been removed before calculating the average value. If a steady state section is not indicated by a red line, the system is not considered stable and no average value was used for further analysis.

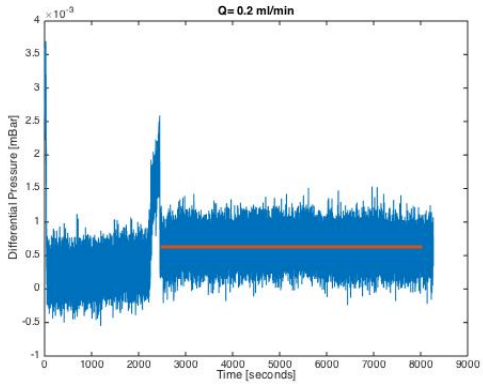

(g) Q = 0.2 ml/min

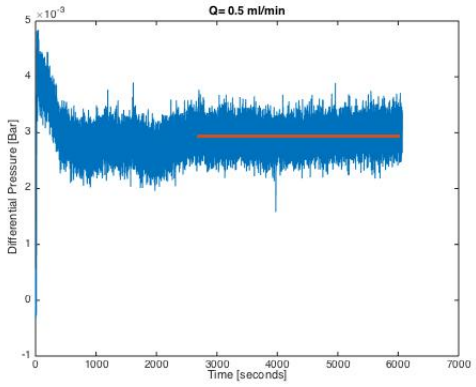

(h) Q = 0.5 ml/min

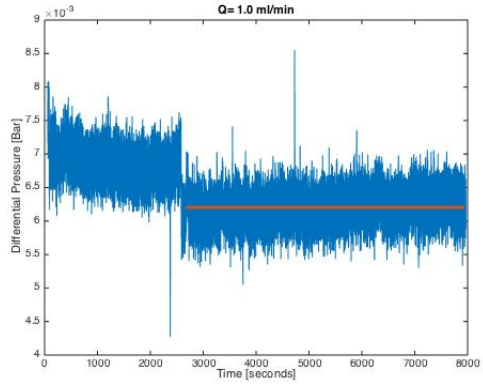

(i) Q = 1.0 ml/min

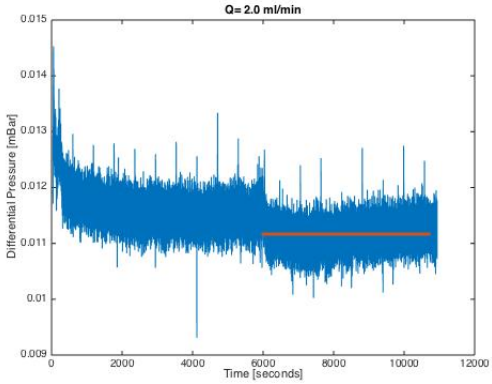

(j) Q = 2.0 ml/min

Figure 7.8: Steady state flow regime selection for two phase horizontal flow. Most variations of measured pressure in the steady state sections are in the rage of $\pm 0.0006 bar$, equal to the background noise found for $Q = 0.0 ml/min$. Larger "spikes" caused by noise from the pressure transducers and pumps have been removed before calculating the average value. If a steady state section is not indicated by a red line, the system is not considered stable and no average value was used for further analysis.

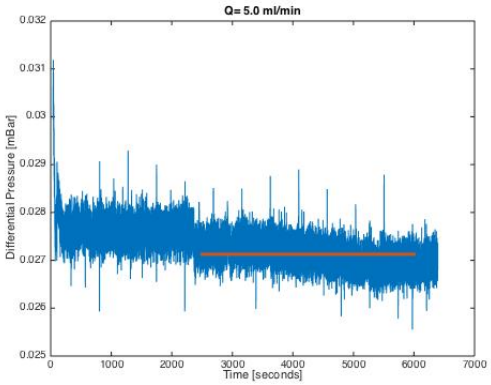

(k) Q = 5.0 ml/min

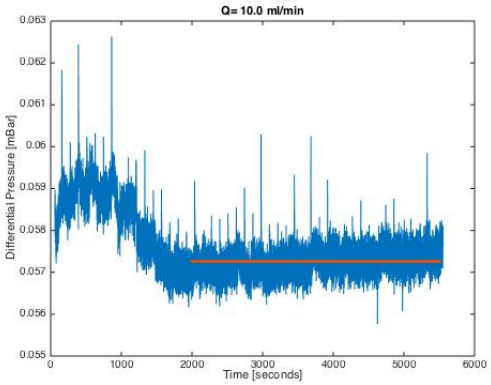

(l) Q = 10.0 ml/min

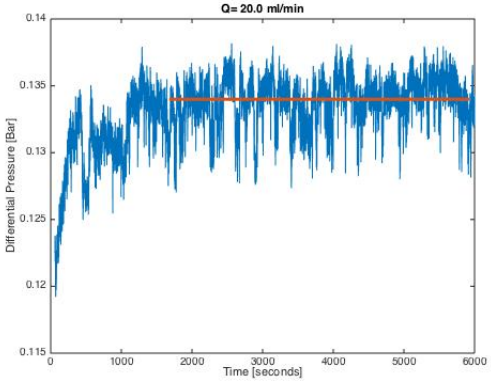

(m) Q = 20.0 ml/min

Figure 7.8: Steady state flow regime selection for two phase horizontal flow. Most variations of measured pressure in the steady state sections are in the rage of $\pm 0.0006bar$, equal to the background noise found for $Q = 0.0ml/min$. For $Q = 20.0mil/min$ variations are larger, possibly caused by the rapid change of pump piston. "Spikes" have been removed before calculating the average value. If a steady state section is not indicated by a red line, the system is not considered stable and no average value was used for further analysis.

7.7 Steady state section for Vertical Two Phase Flow in LBP - Run 1

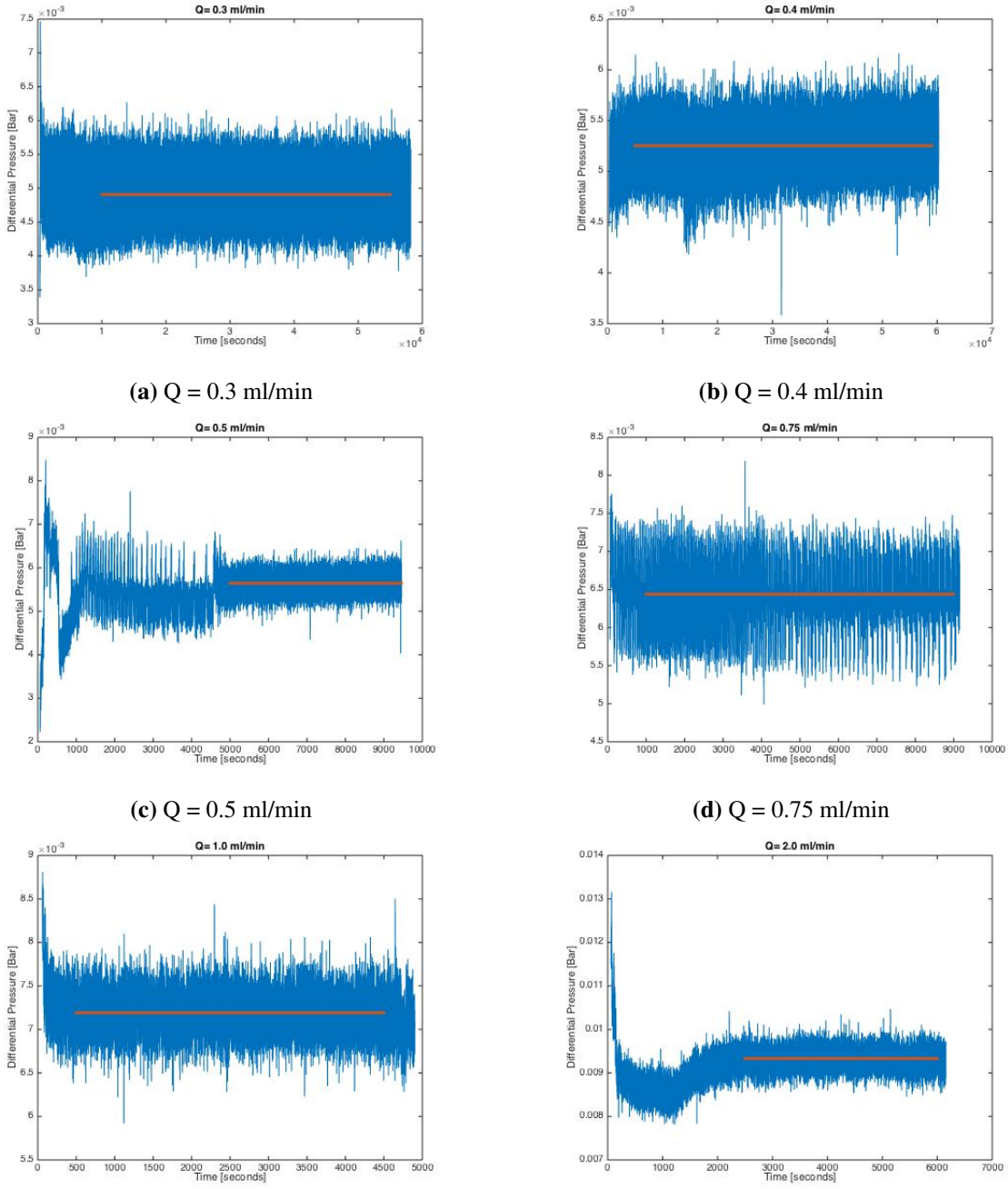

(a) Q = 0.3 ml/min

(b) Q = 0.4 ml/min

(c) Q = 0.5 ml/min

(d) Q = 0.75 ml/min

(e) Q = 1.0 ml/min

(f) Q = 2.0 ml/min

Figure 7.9: Steady state flow regime selection for two phase vertical flow. Most variations of measured pressure in the steady state sections are in the rage of $\pm 0.0006 bar$, equal to the background noise found for $Q = 0.0 ml/min$. Larger "spikes" caused by noise from the pressure transducers and pumps have been removed before calculating the average value. If a steady state section is not indicated by a red line, the system is not considered stable and no average value was used for further analysis.

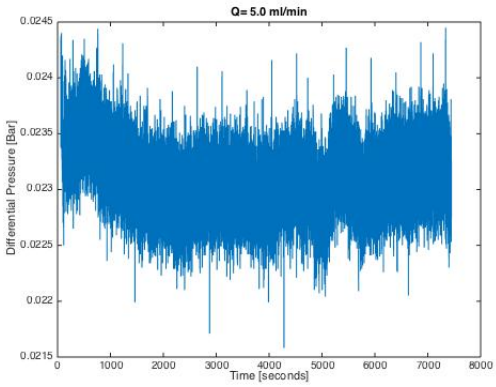

(g) Q = 5.0 ml/min

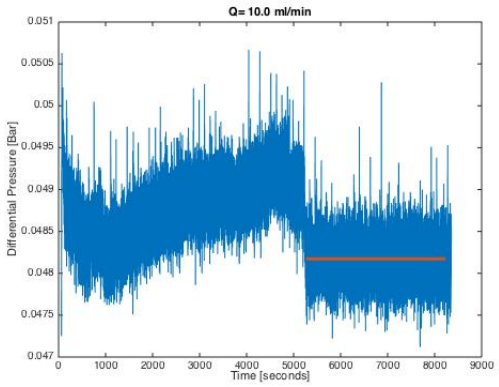

(h) Q = 10.0 ml/min

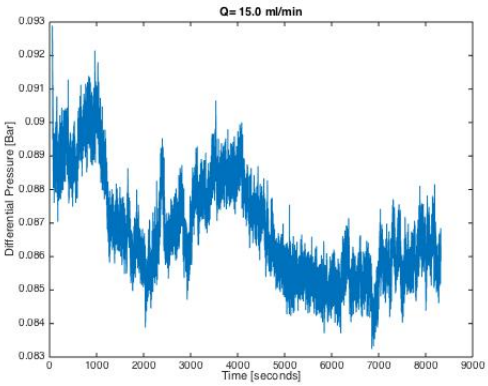

(i) Q = 15.0 ml/min

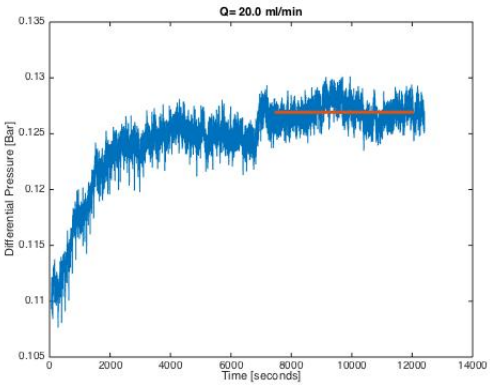

(j) Q = 20.0 ml/min

Figure 7.9: Steady state flow regime selection for two phase vertical flow. Variations in measured pressure in the steady state sections are larger than the bacgground noise of $\pm 0.0006 bar$ found for $Q = 0.0 ml/min$. "Spikes" have been removed before calculating the average value. If a steady state section is not indicated by a red line, the system is not considered stable and no average value was used for further analysis.

7.8 Steady state section for Vertical Two Phase Flow in LBP - Run 2

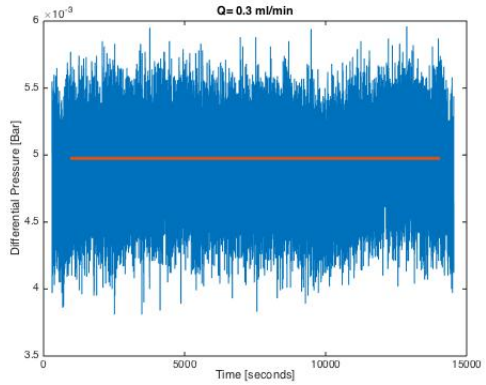

(a) Q = 0.3 ml/min

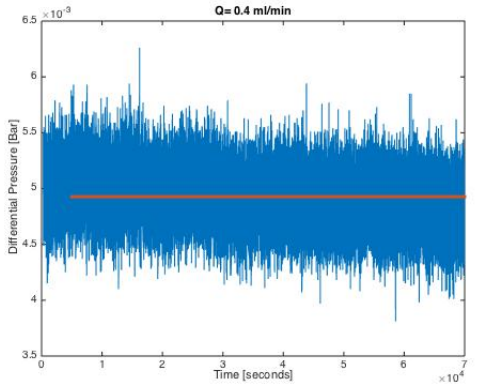

(b) Q = 0.4 ml/min

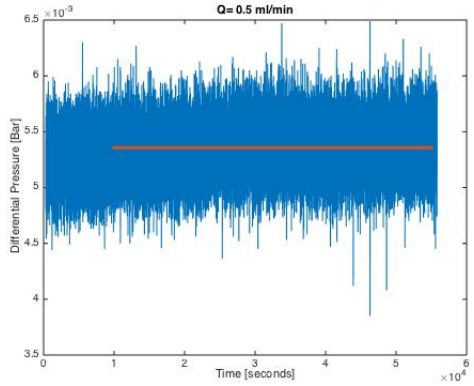

(c) Q = 0.5 ml/min

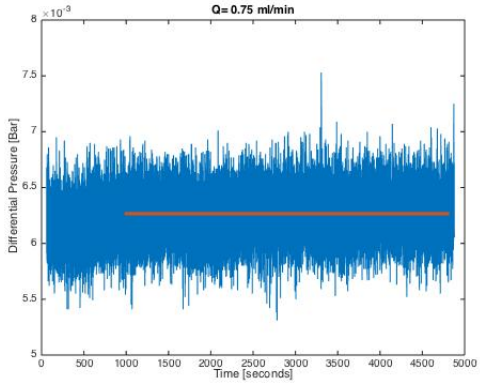

(d) Q = 0.75 ml/min

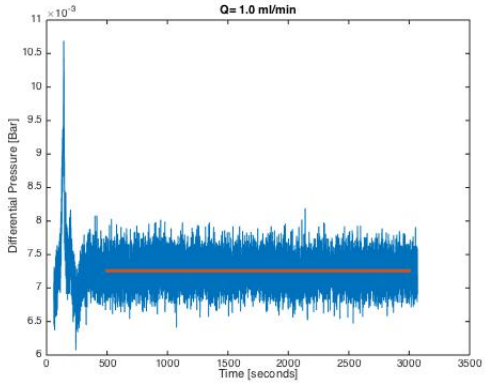

(e) Q = 1.0 ml/min

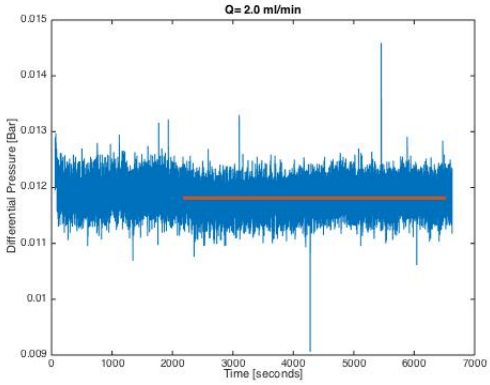

(f) Q = 2.0 ml/min

Figure 7.10: Steady state flow regime selection for two phase vertical flow. Most variations of measured pressure in the steady state sections are in the rage of $\pm 0.0006 bar$, equal to the background noise found for $Q = 0.0 ml/min$. Larger "spikes" caused by noise from the pressure transducers and pumps have been removed before calculating the average value. If a steady state section is not indicated by a red line, the system is not considered stable and no average value was used for further analysis.

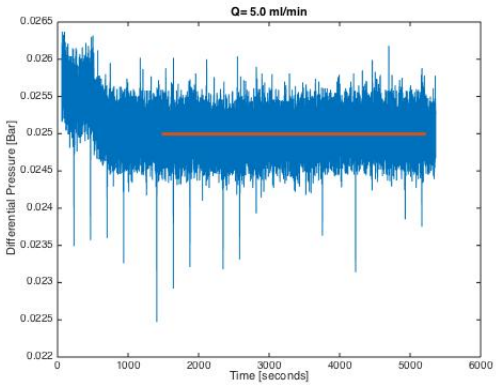

(g) Q = 5.0 ml/min

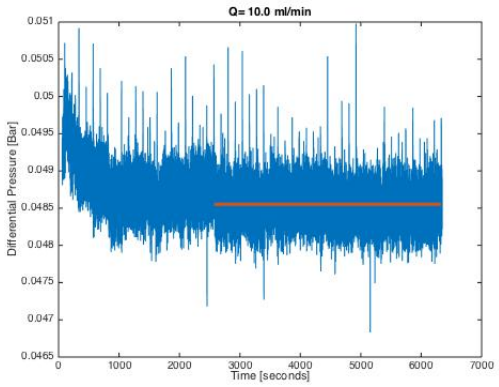

(h) Q = 10.0 ml/min

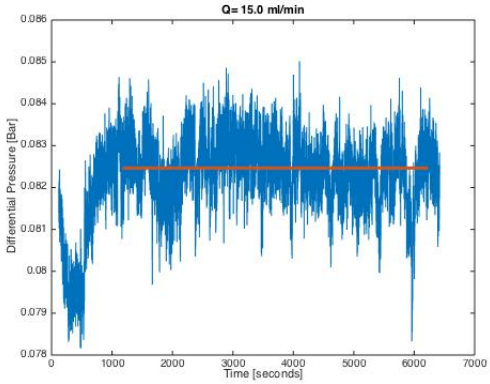

(i) Q = 15.0 ml/min

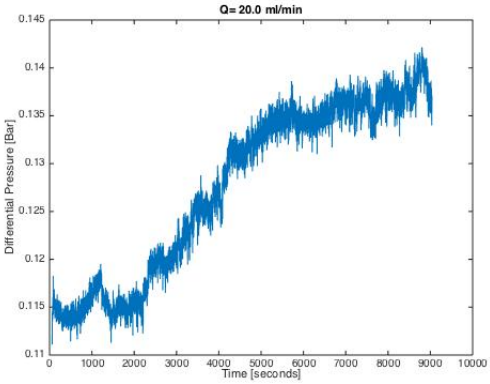

(j) Q = 20.0 ml/min

Figure 7.10: Steady state flow regime selection for two phase vertical flow. Variations in measured pressure in the steady state sections are larger than the background noise of $\pm 0.0006 bar$ found for $Q = 0.0 ml/min$. "Spikes" have been removed before calculating the average value. If a steady state section is not indicated by a red line, the system is not considered stable and no average value was used for further analysis.

7.9 Steady state section for Vertical Two Phase Flow in SBP - Run 1

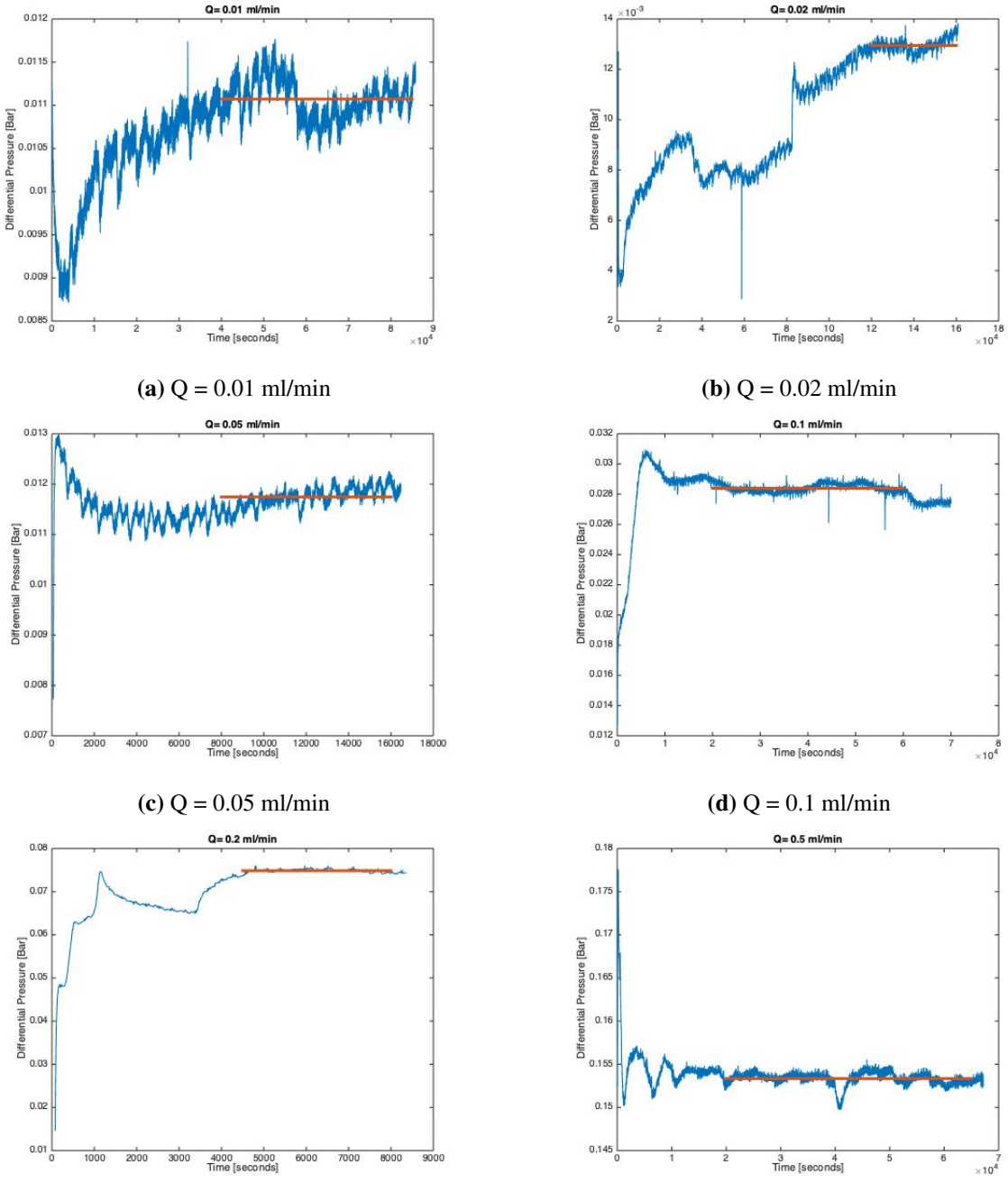

(a) Q = 0.01 ml/min

(b) Q = 0.02 ml/min

(c) Q = 0.05 ml/min

(d) Q = 0.1 ml/min

(e) Q = 0.2 ml/min

(f) Q = 0.5 ml/min

Figure 7.11: Steady state flow regime selection for two phase vertical flow. Variations in measured pressure in the steady state sections are larger than the background noise of $\pm 0.0006 bar$ found for $Q = 0.0 ml/min$. Thus, the variations most likely represent a real instability in pressure in the bead pack. Larger "spikes" caused by noise from the pressure transducers and pumps have been removed before calculating the average value. If a steady state section is not indicated by a red line, the system is not considered stable and no average value was used for further analysis.

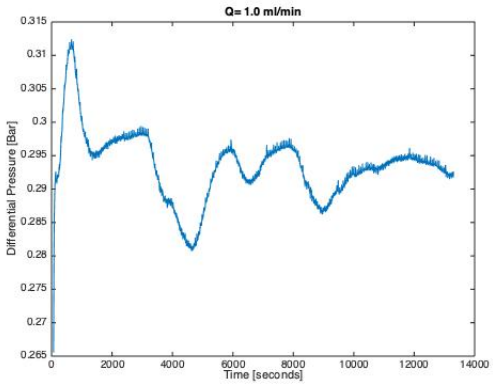

(g) Q = 1.0 ml/min

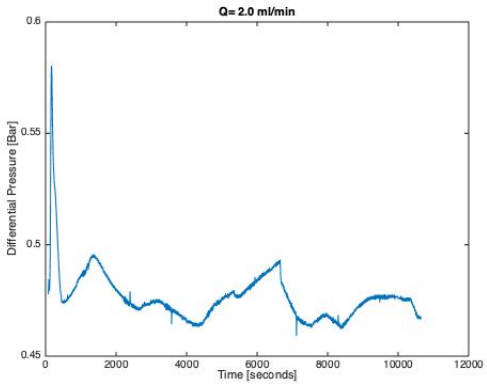

(h) Q = 2.0 ml/min

Figure 7.11: Steady state flow regime selection for two phase vertical flow. Variations in measured pressure in the steady state sections are larger than the background noise of $\pm 0.0006 bar$ found for $Q = 0.0 ml/min$. Thus, the variations most likely represent a real instability in pressure in the bead pack. Larger "spikes" caused by noise from the pressure transducers and pumps have been removed before calculating the average value. If a steady state section is not indicated by a red line, the system is not considered stable and no average value was used for further analysis.

7.10 Steady state section for Vertical Two Phase Flow in SBP - Run 2

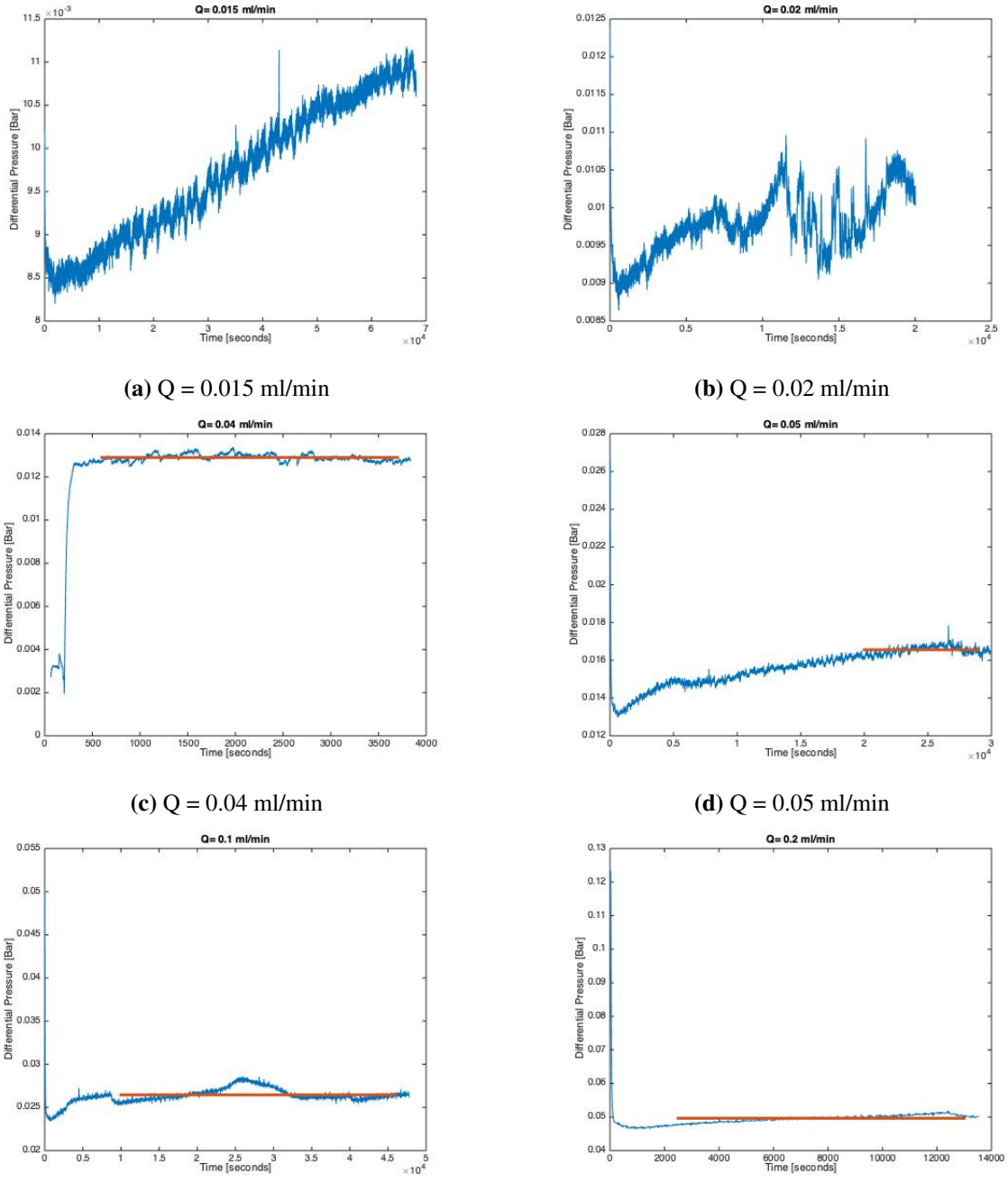

(a) Q = 0.015 ml/min

(b) Q = 0.02 ml/min

(c) Q = 0.04 ml/min

(d) Q = 0.05 ml/min

(e) Q = 0.1 ml/min

(f) Q = 0.2 ml/min

Figure 7.12: Steady state flow regime selection for two phase vertical flow. Variations in measured pressure in the steady state sections are larger than the background noise of $\pm 0.0006 bar$ found for $Q = 0.0 ml/min$. Thus, the variations most likely represent a real instability in pressure in the bead pack. Larger "spikes" caused by noise from the pressure transducers and pumps have been removed before calculating the average value. If a steady state section is not indicated by a red line, the system is not considered stable and no average value was used for further analysis.

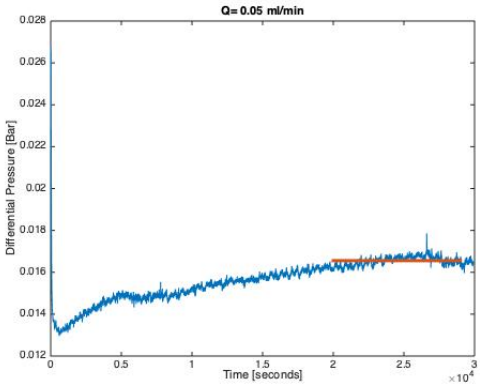

(g) Q = 0.5 ml/min

Figure 7.12: Steady state flow regime selection for two phase vertical flow. Variations in measured pressure in the steady state sections are larger than the background noise of $\pm 0.0006 bar$ found for $Q = 0.0 ml/min$. Thus, the variations most likely represent a real instability in pressure in the bead pack. Larger "spikes" caused by noise from the pressure transducers and pumps have been removed before calculating the average value. If a steady state section is not indicated by a red line, the system is not considered stable and no average value was used for further analysis.

7.11 Steady state section for Vertical Two Phase Flow w/Zalo - Run 1

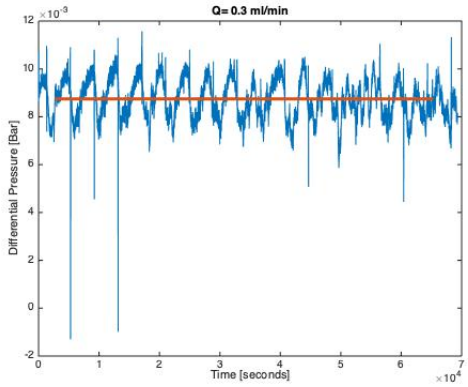

(a) Q = 0.3 ml/min

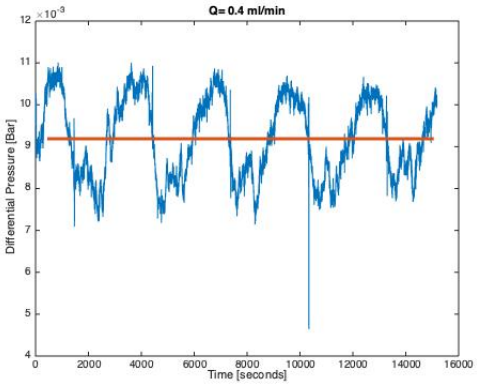

(b) Q = 0.4 ml/min

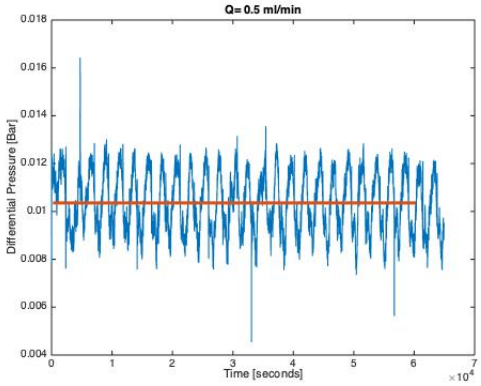

(c) Q = 0.5 ml/min

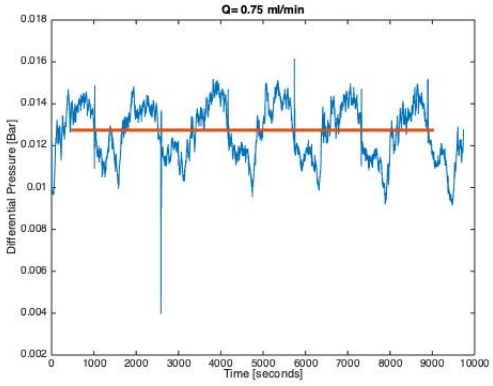

(d) Q = 0.75 ml/min

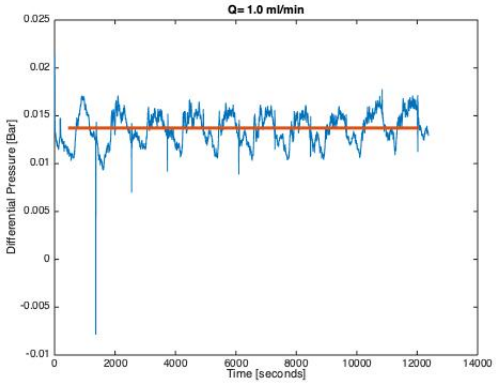

(e) Q = 1.0 ml/min

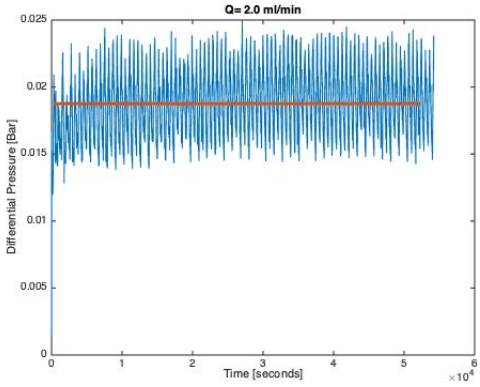

(f) Q = 2.0 ml/min

Figure 7.13: Steady state flow regime selection for two phase vertical flow. Variations in measured pressure in the steady state sections are larger than the background noise of $\pm 0.0006 bar$ found for $Q = 0.0 ml/min$. Thus, the variations most likely represent a real instability in pressure in the bead pack. These variations are found for all surfactant pressure readings. An average value has been used for analysis. If a steady state section is not indicated by a red line, the system is not considered stable and no average value was used for further analysis.

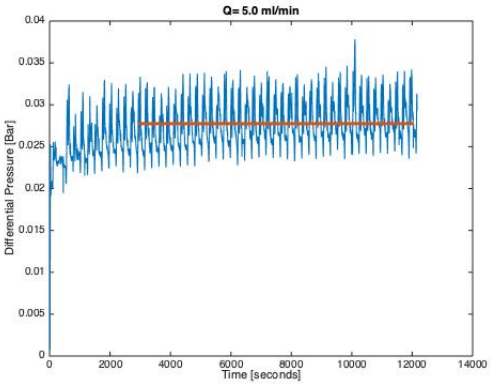

(g) Q = 5.0 ml/min

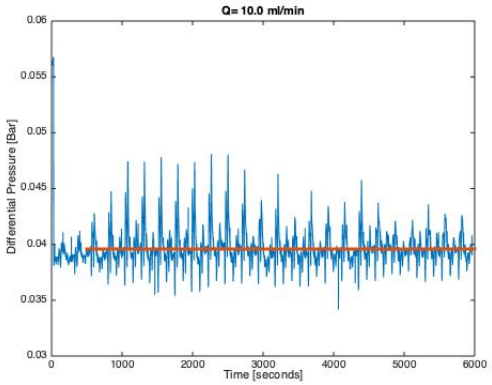

(h) Q = 10.0 ml/min

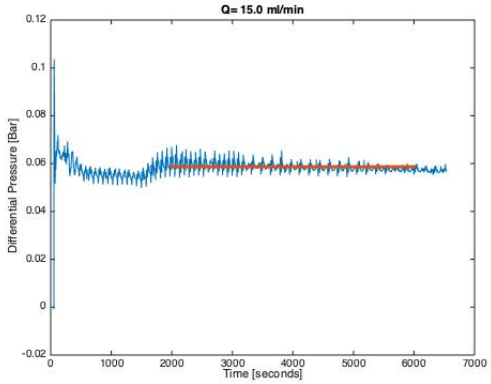

(i) Q = 15.0 ml/min

Figure 7.13: Steady state flow regime selection for two phase vertical flow. Variations in measured pressure in the steady state sections are larger than the background noise of $\pm 0.0006 bar$ found for $Q = 0.0 ml/min$. Thus, the variations most likely represent a real instability in pressure in the bead pack. These variations are found for all surfactant pressure readings. An average value has been used for analysis. If a steady state section is not indicated by a red line, the system is not considered stable and no average value was used for further analysis.

7.12 Steady state section for Vertical Two Phase Flow w/Zalo - Run 2

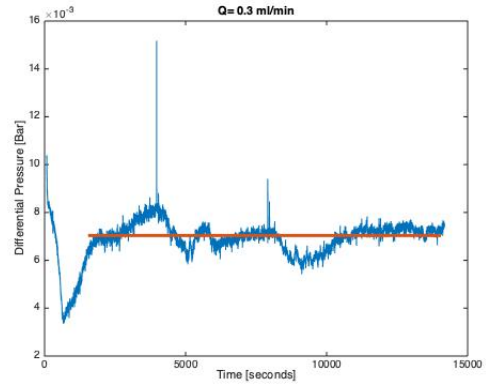

(a) Q = 0.3 ml/min

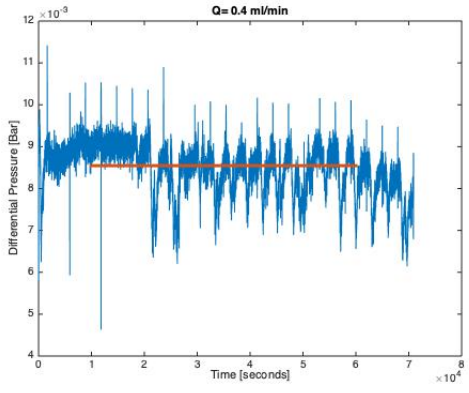

(b) Q = 0.4 ml/min

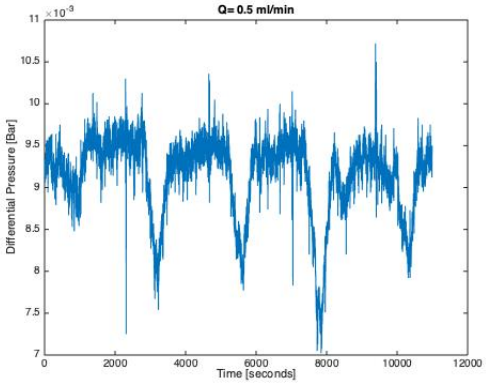

(c) Q = 0.5 ml/min

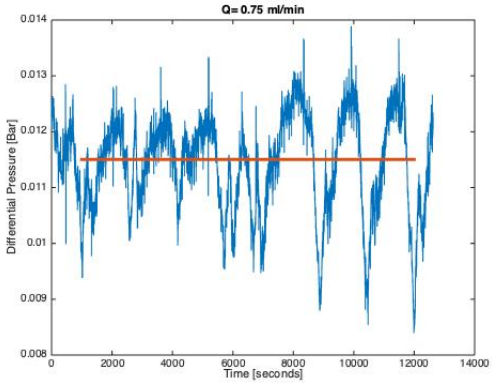

(d) Q = 0.75 ml/min

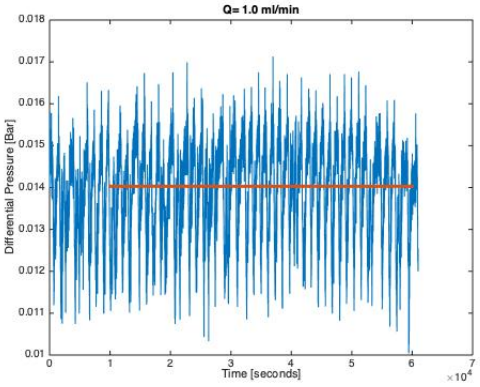

(e) Q = 1.0 ml/min

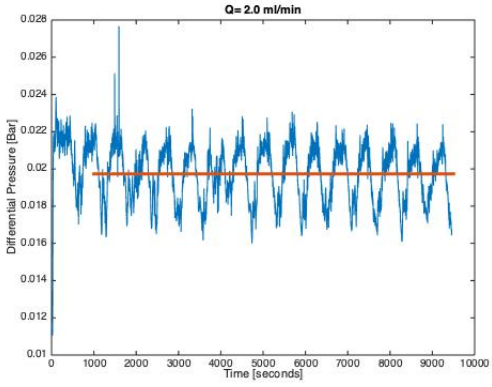

(f) Q = 2.0 ml/min

Figure 7.14: Steady state flow regime selection for two phase vertical flow. Variations in measured pressure in the steady state sections are larger than the background noise of $\pm 0.0006 bar$ found for $Q = 0.0 ml/min$. Thus, the variations most likely represent a real instability in pressure in the bead pack. These variations are found for all surfactant pressure readings. An average value has been used for analysis. If a steady state section is not indicated by a red line, the system is not considered stable and no average value was used for further analysis.

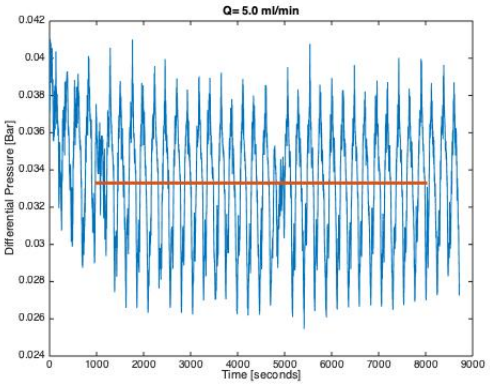

(g) Q = 5.0 ml/min

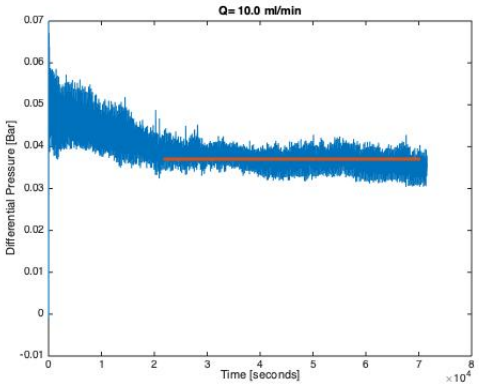

(h) Q = 10.0 ml/min

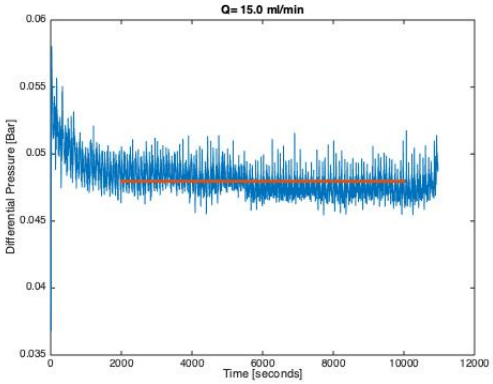

(i) Q = 15.0 ml/min

Figure 7.14: Steady state flow regime selection for two phase vertical flow. Variations in measured pressure in the steady state sections are larger than the background noise of $\pm 0.0006 bar$ found for $Q = 0.0 ml/min$. Thus, the variations most likely represent a real instability in pressure in the bead pack. These variations are found for all surfactant pressure readings. An average value has been used for analysis. If a steady state section is not indicated by a red line, the system is not considered stable and no average value was used for further analysis.

7.13 Steady state section for Vertical Two Phase Flow w/SDS - Run 1

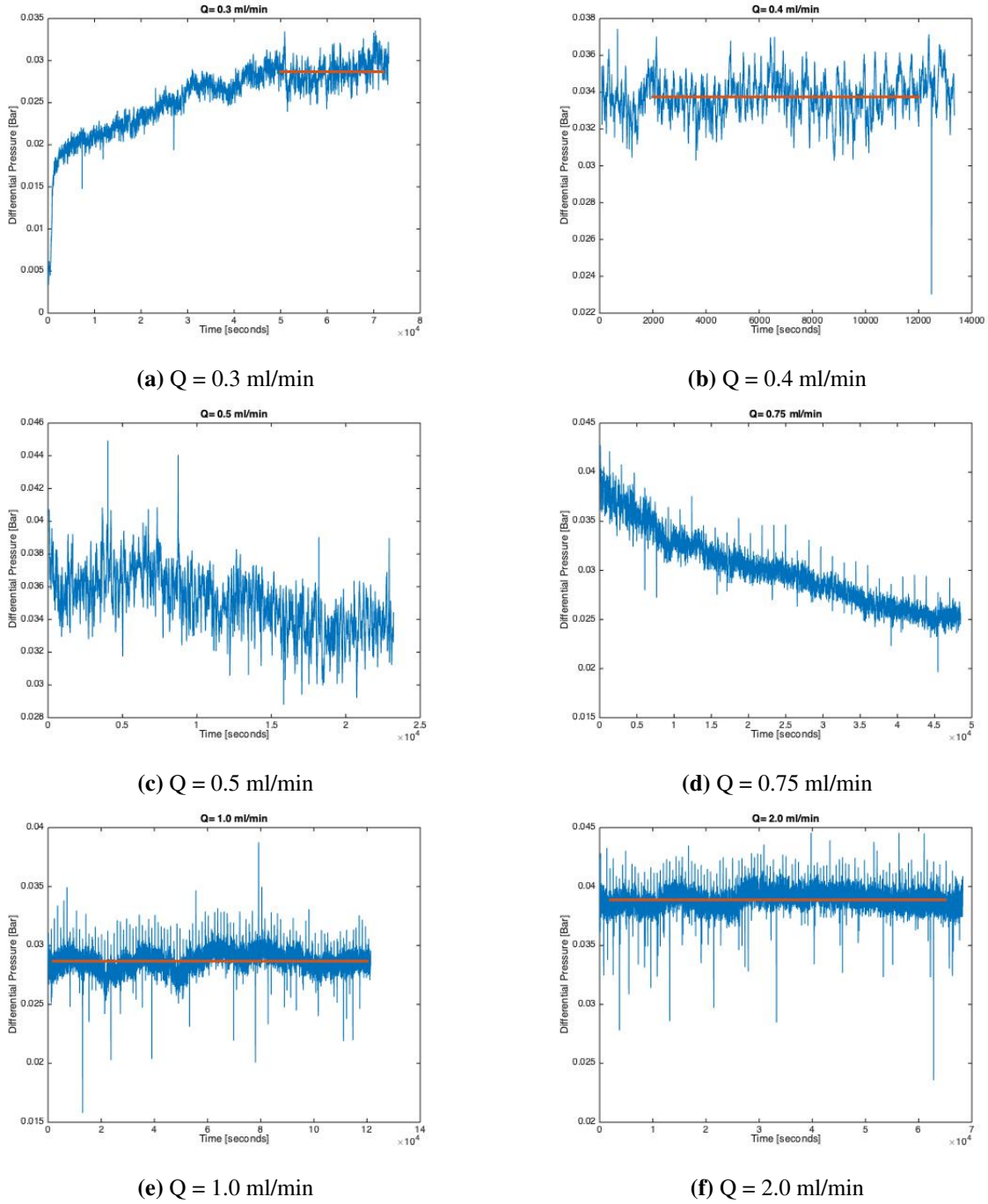

(a) Q = 0.3 ml/min

(b) Q = 0.4 ml/min

(c) Q = 0.5 ml/min

(d) Q = 0.75 ml/min

(e) Q = 1.0 ml/min

(f) Q = 2.0 ml/min

Figure 7.15: Steady state flow regime selection for two phase vertical flow. Variations in measured pressure in the steady state sections are larger than the background noise of $\pm 0.0006 bar$ found for $Q = 0.0 ml/min$. Thus, the variations most likely represent a real instability in pressure in the bead pack. These variations are found for all surfactant pressure readings. An average value has been used for analysis. If a steady state section is not indicated by a red line, the system is not considered stable and no average value was used for further analysis.

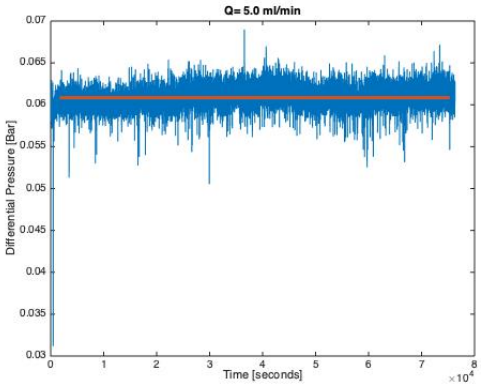

(g) Q = 5.0 ml/min

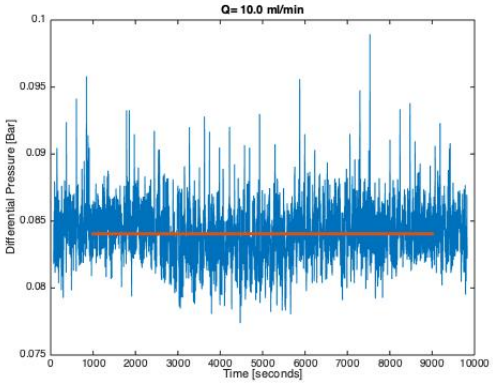

(h) Q = 10.0 ml/min

Figure 7.15: Steady state flow regime selection for two phase vertical flow. Variations in measured pressure in the steady state sections are larger than the background noise of $\pm 0.0006 bar$ found for $Q = 0.0 ml/min$. Thus, the variations most likely represent a real instability in pressure in the bead pack. These variations are found for all surfactant pressure readings. An average value has been used for analysis. If a steady state section is not indicated by a red line, the system is not considered stable and no average value was used for further analysis.

7.14 Steady state section for Vertical Two Phase Flow w/SDS - Run 2

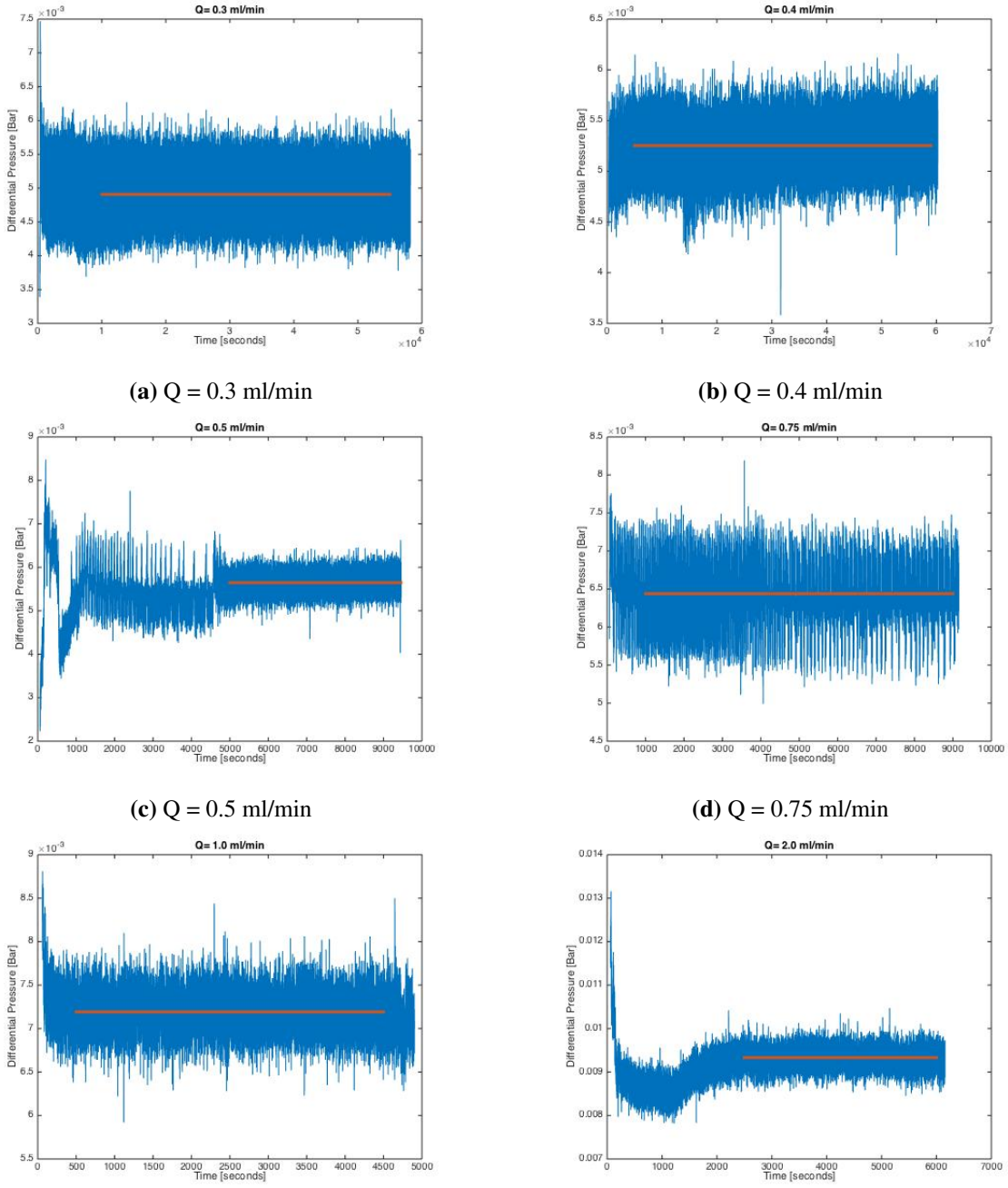

(a) Q = 0.3 ml/min

(b) Q = 0.4 ml/min

(c) Q = 0.5 ml/min

(d) Q = 0.75 ml/min

(e) Q = 1.0 ml/min

(f) Q = 2.0 ml/min

Figure 7.16: Steady state flow regime selection for two phase vertical flow. Variations in measured pressure in the steady state sections are larger than the background noise of $\pm 0.0006 bar$ found for $Q = 0.0 ml/min$. Thus, the variations most likely represent a real instability in pressure in the bead pack. These variations are found for all surfactant pressure readings. An average value has been used for analysis. If a steady state section is not indicated by a red line, the system is not considered stable and no average value was used for further analysis.

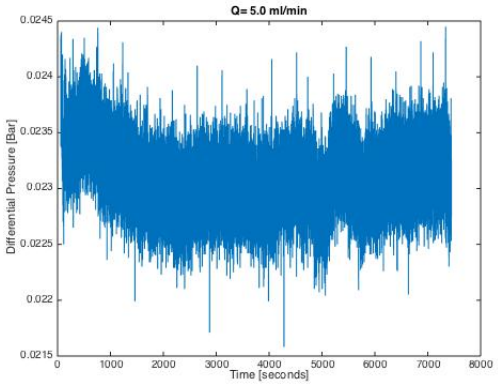

(g) Q = 5.0 ml/min

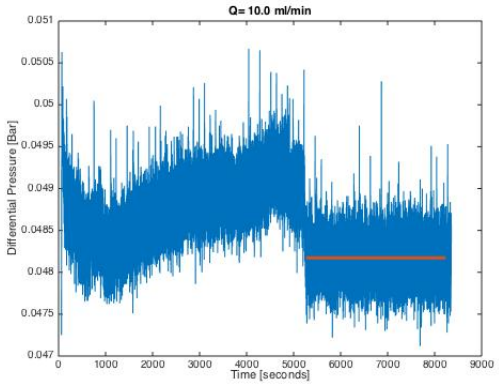

(h) Q = 10.0 ml/min

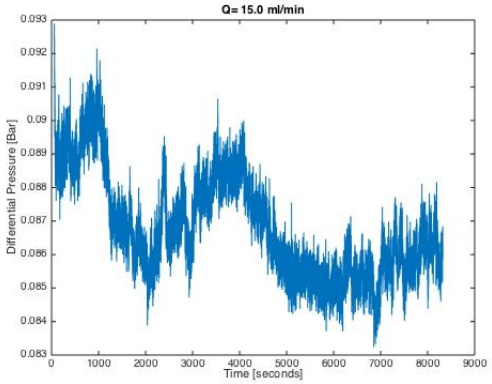

(i) Q = 15.0 ml/min

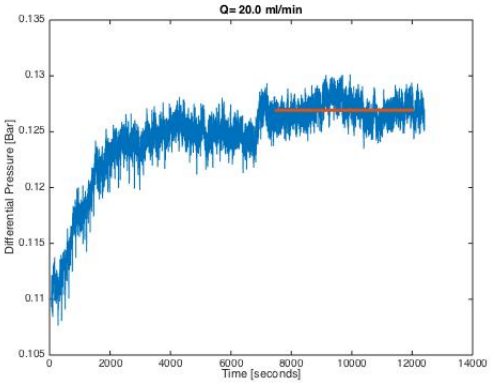

(j) Q = 20.0 ml/min

Figure 7.16: Steady state flow regime selection for two phase vertical flow. Variations in measured pressure in the steady state sections are larger than the background noise of $\pm 0.0006 bar$ found for $Q = 0.0 ml/min$. Thus, the variations most likely represent a real instability in pressure in the bead pack. These variations are found for all surfactant pressure readings. An average value has been used for analysis. If a steady state section is not indicated by a red line, the system is not considered stable and no average value was used for further analysis.

Appendix C

7.15 Pressure Gradients

Table 7.1 presents the pressure gradient, ∇P, for vertical flow in LBP1 and SBP, Sinha et al. (2017) results, and Husøy (2018) results. Results from Husøy (2018) is chosen for caparison instead of Anfinsen (2018), because both a LBP and a SBP has been tested by Husøy (2018).

Table 7.1: Pressure gradient for vertical flow in LBP1 and SBP, Sinha et al. (2017) results, and Husøy (2018) results.

	$log_{10}Ca$ [$-$]	∇P [Pa/m	$log_{10}\nabla P$ [-]
Sinha et al. (2017)	-5,43	142 857	5,154901526
	-4,75	228571	5,359021128
	-4	500000	5,698970004
Husøy (2018)-LBP	-2,899	20637	4,314646564
	-3,598	2171	3,336659823
	-5,297	228,7	2,359266165
	-6,598	90,27	1,955543442
Husøy (2018)-SBP	-2,846	2289000	6,359645793
	-3,846	215400	5,333245699
	-4,544	46550	4,667919685
	-5,026	15450	4,188928484
LBP1	-4,9652	2475	3,393575203
	-4,8403	2550	3,40654018
	-4,7434	2750	3,439332694
	-4,5673	3175	3,50174373
	-4,4423	3625	3,559308011
	-4,1413	5275	3,722222464
	-3,7434	12000	4,079181246
	-3,4423	24200	4,383815366
	-3,2662	42000	4,62324929
	-3,1413	65975	4,819379399
SBP	-6,2136	5000	3,698970004
	-6,0887	4500	3,653212514
	-5,7877	6450	3,809559715
	-5,6908	8300	3,919078092
	-5,3897	13250	4,122215878
	-5,0887	24800	4,394451681
	-4,6908	61150	4,786396461
	-4,3897	146800	5,166726056
	-4,0887	236700	5,374198258

Christina Rong Anfinsen

Experimental Investigation of Pressure Versus Rate Correlation for Two Phase Flow in Bead Packs

NTNU
Norwegian University of
Science and Technology